THE USE OF THIN POLYMERIC COATINGS TO PREVENT FRETTING CORROSION AND METALLIC CONTACT IN STEEL-ON-STEEL SYSTEMS

by

Kent Allen Day

Thesis submitted to the Faculty of the
Virginia Polytechnic Institute and State University
in partial fulfillment of the requirements for the degree of

MASTER OF SCIENCE

in

Mechanical Engineering

APPROVED:

M. J. Furey, Chairman

N. S. Eiss, Jr.

H. H. Mabie

March, 1986
Blacksburg, Virginia

THE USE OF THIN POLYMERIC COATINGS TO PREVENT FRETTING CORROSION AND METALLIC CONTACT IN STEEL-ON-STEEL SYSTEMS

by

Kent Allen Day

(ABSTRACT)

A fundamental study was conducted to investigate the ability of thin polymeric coatings to prevent metallic contact and fretting corrosion in steel-on-steel systems. Ten polymer types were chosen for study: polymethylmethacrylate (PMMA), polytetrafluoroethylene (PTFE), polyimide (PI), polyvinylidene fluoride (PVDF), polyvinylidene chloride (PVDC), polyvinyl chloride (PVC), low-density polyethylene (LDPE), high-density polyethylene (HDPE), polysulfone (PSO) and polystyrene (PS). These polymers were applied as thin films to a steel disk which was in turn fretted by a normally-loaded steel sphere.

The experimental investigation consisted of two phases. In the first phase, the lives of the ten polymer types were evaluated over a range of normal loads from 11.1 to 44.5 N. In the second phase, optical and electron microscopy were used to document the fretting process at the sphere-film interface as a function of time.

ACKNOWLEDGEMENTS

I would like to express my gratitude to the following people for their assistance throughout this research:

Dr. M. J. Furey for his guidance and advice throughout the past year. It is through him that I have learned the proper techniques and methods of scientific research. I would also like to thank Dr. Furey for his support, help and comments in the preparation of this thesis.

Dr. N. S. Eiss, Jr. and Dr. H. H. Mabie for serving on my advisory committee and providing valuable advice and assistance during the past year.

and Boyd Coatings Research Company, Incorporated for preparing several of the coatings used in this work.

for his advice concerning the behavior of polymers studied in this research.

for encouraging me to attend graduate school.

for preparing polymer solutions and her assistance with the coating of test specimens.

for his assistance with the scanning electron microscope.

The Army Research Office for sponsoring this study.

, my parents, who have provided enormous support throughout my education and have made this entire experience possible.

TABLE OF CONTENTS

TABLE OF CONTENTS (cont'd)

TABLE OF CONTENTS (cont'd)

LIST OF FIGURES

LIST OF FIGURES (Cont'd)

LIST OF FIGURES (Cont'd)

LIST OF FIGURES (Cont'd)

LIST OF FIGURES (Cont'd)

LIST OF TABLES

LIST OF TABLES (Cont'd)

LIST OF TABLES (Cont'd)

1.0 INTRODUCTION

Fretting corrosion is a complex wear phenomenon that occurs between contacting surfaces having small amplitude relative motion. Both mechanical and chemical factors are assumed to play significant roles in the process, although the nature of each is not completely understood. Fretting corrosion can result in severe surface damage to the contacting bodies along with the production of abrasive metallic oxide particles (in metal systems).

Practically any mechanical system which has close tolerances and is subject to vibration can be suspected to undergo some damage due to fretting corrosion. Typical examples are: shrink fits, bolted and riveted connections, splined connections and bearing-housing interfaces. The surface damage caused in the process can change the tolerances of the system resulting in excessive vibration and loss of fit. Pits or grooves in the surface can also be the source of fatigue crack initiation, causing eventual failure of the assembly.

Since 1981, research at VPI&SU has centered on gaining a better understanding of the fretting process in realistic field-like situations and investigating possible methods to prevent fretting corrosion. Work funded by the Naval Research Office investigated a problem existing with ship motor-generator sets (1). Fretting corrosion was found to occur at the interface of two bearing-cartridge assemblies which support the electrical rotor, causing excessive noise and vibration. Results of the experimental investigation show that load, frequency of vibration, amplitude of vibration and the presence of grease all have a significant effect on the fretting process at the bearing-cartridge interface.

In work at VPI&SU sponsored by the Army Research Office, initiated in 1983, an investigation was begun to study the use of thin polymeric coatings to prevent fretting corrosion (2). In an initial study, Sweitzer (3) investigated four different polymer types: polyvinyl chloride (PVC), low-density polyethylene (LDPE), polytetrafluorethylene (PTFE) and polysulfone (PSO). These polymers were applied as thin films to a steel ball which was then fretted against a flat steel plate. All of the films, with the exception of PVC, were found to fret the steel plate. The problem, general approach, and examples of initial results were described in a paper by Furey, et al. (4).

Beginning in 1984, fretting corrosion research at VPI&SU (sponsored by the Army Research Office) continued in two primary areas. The first was further investigation of the apparent ability of chlorinated polymers (e.g., polyvinyl chloride and polyvinylidene chloride) to prevent fretting corrosion. Working with polyvinyl chloride and polyvinylidene chloride, Puzio (5) considered the possible chemical processes occurring at the interface between the polymer and steel. In another investigation, Rorrer (6) studied the effect of various experimental parameters (e.g., sliding amplitude, load, environment, etc.) on the fretting behavior of polyvinyl chloride coatings. The second area of investigation, presented in this thesis, considered the use of a wide variety of polymeric films, many of which had not been previously investigated.

In this thesis, ten different types of polymer films were studied as a method to prevent metallic contact and fretting corrosion in steel-on-steel systems. In considering the use of polymeric coatings as a

preventive measure against fretting corrosion, two requirements are necessary: the film must be able to prevent metal-metal contact (under the loading and vibration) and the film itself must not fret the steel. It is then the intent of the following work to gain an understanding of the factors which determine the life of polymeric coatings under fretting conditions and their ability to prevent fretting damage to the steel countersurface. For all of the work presented in this thesis, the contact geometry chosen was sphere-on-flat. Polymer coatings were applied to a steel flat which was fretted by a steel sphere.

In summary, the objectives of this research were as follows:

1. To provide fundamental information concerning the use of polymeric films to prevent fretting corrosion.

2. To investigate a wide variety of polymer types exhibiting a large range of chemical and physical properties.

3. To study the effect of normal load on the life of these films at constant sliding amplitude and frequency.

4. To study the fretting process at the sphere-film interface as a function of time for each of the polymer films, using both optical and electron microscopy. This study was conducted at one normal load and constant sliding amplitude and frequency.

5. To determine whether or not each of the polymer types can fret steel by examination of the photographic data obtained from the fretting experiments mentioned above.

2.0 LITERATURE REVIEW

This review is divided into three sections. In the first, an overview of existing mechanisms developed to explain fretting and fretting corrosion will be presented. The second section will discuss the work that has been done on the fretting of steel by polymers. In the final section, a survey of the work that has been done on the properties and behavior of thin polymer films on rigid substrates will be given.

2.1 Mechanisms of Fretting and Fretting Corrosion

Before presenting various mechanisms to explain fretting and fretting corrosion, a definition of both types of behavior will be given. The OECD (Organization for Economic Cooperation and Development) glossary of tribological terms (7) defines fretting and fretting corrosion as:

> Fretting is a "wear phenomena occurring between two surfaces having oscillatory relative motion of small amplitude;"
>
> Fretting Corrosion is a "form of fretting in which chemical reaction predominates."

It should also be noted that fretting corrosion can result in the production of metallic oxide particles which are abrasive and can accelerate the wear process.

Since the first published work on fretting corrosion in 1927 by Tomlinson, a wide variety of mechanisms have been proposed to explain the phenomena. To date, there is no consensus as to a precise mechanism to explain fretting corrosion. Much of the controversy seems to be over the role that both mechanical and chemical factors play in the wear process. Several investigators have attempted to explain the process by

purely mechanical means, while others present theories which account for an interaction between the two factors. For comprehensive reviews on fretting and fretting corrosion, works by Hurricks (8) and Waterhouse (9) are suggested to the reader.

Tomlinson (10) was the first investigator to study the causes and mechanisms of fretting corrosion. Tomlinson notes that after machined steel surfaces have been in contact and subjected to vibration, there is a marked production of oxide; furthermore, the surfaces are pitted and have a corroded appearance. Explaining the phenomena, Tomlinson believed that the effect was due to molecular cohesion between the two bodies.

Feng and Rightmire (11) attribute the cause of fretting to "ordinary" wear. In the initial stage of the process, wear particles are generated by the plastic contact and shear of asperities. Then, due to the oscillatory nature of fretting, the wear process becomes one of abrasion in which metal and metallic oxide particles are trapped in the interface.

Uhlig (12) was one of the first investigators to suggest that fretting included both chemical and mechanical factors. Uhlig proposes that as the contacting bodies slide across each other, asperities remove existing surface films, exposing clean metal. Gases from the atmosphere then quickly adsorb on the clean, active surfaces, possibly producing a layer of metallic oxide. Based on this model, Uhlig develops an expression for the weight loss of a specimen undergoing fretting:

$$W \text{ (total)} = (K_o L^{1/2} - K_1 L)\ C/F + K_2 l\ L\ C$$

where: W is the specimen weight loss.

L is the load.

F is the frequency.

l is the slip amplitude.

K_o , K_1 and K_2 are experimentally determined constants.

C is the number of cycles.

The first term of the expression is a chemical factor; the second, a mechanical factor.

Due to the requirement of slip as a prerequisite for fretting, Johnson (13) has investigated the mechanics of microslip for contacting metal surfaces. Working with normally loaded, spherical surfaces in contact, Johnson finds fretting damage confined to an outer annulus of the circular contact area once an oblique or tangential oscillating force is applied to one of the bodies. An increase in the oscillating load results in an increase in the size of the annular region. The reason for this behavior lies in the distribution of traction forces at the interface. Due to a non-uniform distribution of normal pressures over the contact zone, certain regions (corresponding to the annulus) will have insufficient traction to prevent microslip for even the smallest oblique or tangential forces.

Bethune and Waterhouse (14) have studied the electrochemical nature of the contact zone under fretting conditions. Experimenting with a wide variety of copper and aluminum alloys in electrolytic solutions,

they monitored the corrosion current of the contacting interface as a function of cycles of fretting. Results indicate that at the onset of fretting, a sharp increase in corrosion current occurs which is primarily attributed to the disruption of oxide films on the surface.

Investigating possible mechanisms of fretting wear, Stowers and Rabinowicz (15) conclude that the fretting wear process resembles that of unidirectional adhesive wear. Contradicting previous work, they find that wear coefficient is independent of slip amplitude and load and that wear volume can be simply determined by Archard's wear equation (16). In this equation, the predicted weight loss is directly proportional to the wear coefficient, load and sliding distance; and inversely proportional to the hardness of the softer material.

Waterhouse and Taylor (17) have investigated the mechanisms of debris formation during fretting. They find the wear behavior to be consistent with the delamination theory of wear as proposed by Suh (18). In fretting, the production of wear particles is found to be primarily due to the propagation of subsurface cracks. Further fretting of the debris results in a higher content of metallic oxide. Waterhouse (19) also states that in the early stages of fretting, the process is governed by adhesion. This adhesion results in the initiation of fatigue cracks, leading to the later stage in which the wear process is governed by delamination.

Sproles and Duquette (20) also propose that the formation of debris in fretting is a two-stage process. In the initial stage, the contacting surfaces are heavily cold-worked, exhausting their ductility. Brittle cracks then form on the surfaces resulting in debris formation.

In his work on the role of oxidation in the fretting process, Bill (21) notes three different types of behavior due to oxidative processes. First, during the fretting process, thin oxide films are stripped from the surface with each cycle. Second, oxidation occurs at sites of fatigue damage. Third, the continual formation of oxide films on the surfaces limits the amount of fretting damage. Bill also notes that at low temperatures the role of oxidation is primarily of an interactive nature with fatigue mechanisms, with an increase in interfacial temperature he states that oxidative processes play an increasingly significant role.

2.2 Fretting of Steel by Polymers

A survey of the literature reveals that although some work has been done on the fretting of steel against "bulk" polymers, little has been done on the use of polymer coatings to prevent fretting corrosion.

In their 1964 paper on the mechanics of fretting, Johnson and O'Connor (22) propose the use of a thin elastic coating applied to one of the contacting bodies to eliminate the occurrence of microslip. In a preliminary analysis, they theoretically develop the problem for the two-dimensional contact of cylinders with an elastic layer. Two geometries were then chosen for experimental investigation: a flat circular contact between two bodies which are loaded in shear and torsion; and an idealized lap joint.

Results of the theoretical development show that for contact between cylinders (cylinder-cylinder) and spheres (sphere-sphere), bonding of an elastic layer to one of the contacting bodies cannot eliminate

slip at the interface due to the existence of zero pressure at the edges of the contact area. The only method that would allow no microslip in such a case would be to bond the film to both surfaces.

For the first experimental setup, an epoxy resin was used to coat one of the steel surfaces. A steady normal load and a twisting moment ($\pm M$), less than that required to cause gross sliding, were applied to the contact system. For films of 7.62 to 152.4 μm, fretting damage was prevented up to a ratio of the applied moment to the moment required to cause gross sliding of 0.85. This is more than twice the ratio determined for uncoated surfaces. Similar results were obtained for the lap joint in which rubber films from 63.5 to 317.5 μm were used. The results of both experiments show that the use of an elastic layer between the contacting surfaces eliminates concentrated shear stresses and hence microslip.

Several interesting conclusions are presented which would be useful in designing an elastic film to prevent fretting:

1. The method will be successful in preventing microslip if the pressure between the contacting surfaces is at no place zero.

2. The thickness should be small compared to the contact area diameter, primarily to limit the compliance of the joint.

3. A compromise must be made between the rigidity of the film and the allowed compliance of the joint.

4. The resistance of a joint to fretting can be increased with higher coefficients of friction.

5. The ratio of the fatigue strength of the polymer to its elastic modulus should be large.

The fretting of carbon fiber reinforced plastics (CFRP) against mild steel has been investigated by Ohmae, Kobayashi and Tsukizoe (23). They find that for both the CFRP and the steel specimens, wear is increased with increasing slip amplitude. Due to the oriented nature of the CFRP specimens, the direction of sliding was also found to be an important factor. Minimum damage was found when the sliding direction coincided with the orientation of the fibers.

The most extensive work on the fretting of steel on polymers was published in a series of papers by Higham, Bethune and Stott (24,25). Nine different polymer types: polytetrafluorethylene (PTFE), polyethylene (PE), polyvinylidene fluoride (PVDF), polylchlorotrifluorethylene (PCTFE), polysulfone (PSO), polyvinyl chloride (PVC), polymethylmethacrylate (PMMA), polycarbonate (PC) and nylon 66 were investigated. The polymer specimens were obtained from commercially available sheet films 3 mm thick. These were fretted against hot rolled steel with a composition of 0.18% C, 0.73% Mn, 0.23% Si, 0.17% Ni and 0.13% Cr. The steel counterface was in the form of a hemisphere with 4 mm radius. A range of loads (130-330 μg), amplitudes (3-10 μm) and frequencies (30-60 Hz) was studied.

Several trends were evident from the experimental work:

1. It has been shown that a number of polymers can cause fretting damage to a steel surface, the damage taking the form of transfer of α-Fe_2O_3 to the polymer surface.

2. Under a given set of experimental conditions the amount of wear of steel increases as the polymer countersur-

face is changed in the order PTFE and PE, PVDF, PCTFE, PSO, PVC, PMMA, PC, nylon 66.

3. An incubation period in which no wear of the steel takes place occurs for all the polymers. The length of this period depends on the polymer countersurface and decreases in the order PTFE, PE, PVDF, PCTFE, PVC, PMMA, PC, and nylon 66.

4. No metal wear is observed when the countersurface is PTFE, while it only occurs with PE when the fretting amplitude is greater than 7 μm. The other polymers produce metal wear at amplitudes of 3 μm and above although metal wear does not occur with PVDF at amplitudes greater than 8 μm.

5. Wear to the polymer during fretting against steel takes the form of fibre formation for PS, PVC, PC, nylon 66 and, to a small extent, PE. It takes the form of a transfer of polymer film to the metal for PTFE and PVDF. No polymer wear is observed for PCTFE and PMMA, nor for PVDF at amplitudes below 8 μm.

6. There is a close correlation between the amount of metal wear and the surface energetics (in terms of the critical surface tension and coefficient of friction) of the polymer.

7. It appears that any property of a polymer that indicates its adhesive properties or surface energetics should provide a useful criterion for determining the amount of fretting damage inflicted on a metal by the polymer.

Investigating the role of experimental conditions on the fretting of steel by polycarbonate (26), the authors find:

1. It has been shown that polycarbonate can cause fretting damage to a steel surface during sliding in laboratory air, the damage involving transfer of α-Fe_2O_3 to the polymer surface.

2. The plots of wear against number of cycles show three stages of damage: (a) an incubation period during which no wear of the steel takes place, (b) a running in period during which the rate of wear decreases with number of cycles and (c) a steady state period during which the rate of wear is fairly constant.

3. The air-formed film originally present protects the steel during the incubation period, but this film eventually breaks down and wear of the steel commences.

4. The length of the incubation period increases with decreasing amplitude of slip in the range 14-4 μm and becomes infinitely long at an amplitude of about 2 μm. It also increases with increasing frequency of vibration in the range of 10-60 Hz.

5. During the running in period the initial annulus of slip on the polycarbonate becomes increasingly covered with transferred α-Fe_2O_3 debris, while in the steady state period the contact area between the two surfaces increases in size, thus increasing the area over which transfer of the debris can take place.

6. In general the amount of metal wear after a given number of cycles increases with increasing amplitude of slip, with decreasing frequency of vibration and with decreasing applied load in the range 830-130 g.

7. The presence of water vapor is a necessary requirement for wear of the metal surface. The amounts of wear in moist oxygen, moist argon and moist nitrogen are greater than that in laboratory air, while very little wear occurs in dry oxygen, dry argon or dry nitrogen.

Bethune, Stott and Higham propose several mechanisms (27) for the formation of α-Fe_2O_3 debris. One is the possible oxidation of the metal due to frictional heating. A second mechanism is the possible dehydration of a hydrated oxide such as α-FeO·OH. This would require the presence of oxygen and water vapor. This mechanism is consistent with the observed results in that both oxygen and water vapor are required to cause metal damage. A final mechanism is that the metal surface becomes chemically active enough to become pyrophoric. A pyrophoric process can be caused by the metal not being able to dissipate its heat of oxidation fast enough. In this process a local temperature rise will occur, possibly resulting in the formation of metallic oxide.

2.3 Behavior of Thin Polymeric Films on Rigid Substrates

Amuzu, Briscoe, Tabor, and Smith (28,29) have studied the frictional behavior and shear strength of thin polymeric films deposited on rigid substrates such as glass. The authors find that the shear strength of the area in contact is dependent on the contact pressure, temperature and sliding velocity. The dependency of shear strength on contact pressure is given by:

$$\tau = \tau_o + \alpha P$$

where: τ = shear strength

P = contact pressure

τ_o, α = constants which depend on the polymer type for a constant temperature and sliding velocity

This relationship has been used to predict the frictional behavior (e.g., coefficient of friction) for a wide variety of polymeric films. Experimental work shows close agreement between the predicted and measured values at high loads and low sliding speeds. The relationship has also been modified to consider the viscoelastic nature of the polymeric films, accounting for the experimentally observed dependence of the shear strength of the film on sliding velocity.

Solvent and thermal history has also been shown to be a factor in the frictional behavior of polymeric films (30). The quality of the solvent is found to significantly affect the mechanical properties of polymeric films. Poor solvents promote less crystallinity causing the

film to be more ductile. This results in lower interfacial shear strength, an hence lower friction. Good solvents lead to more extensive crystallization, resulting in more brittle behavior and higher friction. Thermal history can also cause changes in degree of crystallinity and therefore the frictional behavior of polymeric films.

Theoretical development of the problem of a rigid indentor in contact with an elastic layer on a rigid substrate has received considerable attention in the literature. Alexsandrov and Vorovich (31,32) have formulated the problem for a cylindrical indentor with its axis parallel to a flat, layered substrate. The development is complex and will not be presented here. However, some considerations used in the formulation will be mentioned:

1. The contact between the die and elastic layer is generally considered to be frictionless; outside the contact zone the layer is unloaded.

2. The elastic layer is either rigidly bonded to the substrate or it rests freely upon it without friction.

3. The solution for forces, moment and contact pressures acting on the layer is approximate in nature and has received little experimental verification.

4. The solution is a function of the material properties of the layer and its thickness.

Matthewson (33) has investigated the contact of axisymmetric bodies (spheres, cones and a "general" axisymmetric profile) with flat, layered substrates both theoretically and experimentally.

For the case of a spherical indentor, several considerations are used in the formulation: 1. the elastic modulus of the film is much less than that of the substrate and indentor; 2. the thickness of the layer is small compared to the contact radius and the characteristic dimension of the indentor; 3. the film is rigidly bonded to the substrate; and 4. there is no friction between the indentor and the coating. Although Matthewson does not present a complete solution for the problem (sphere-on-layered flat) for values of Poisson's ratio less than 0.5, he states that experimental work was required to empirically determine several constants used in the expressions for stresses and strains in the layer.

The three components of stress and strain (radial, circumferential and normal) are evaluated as a function of the contact area radius (a), layer properties (elastic modulus and Poisson's ratio) and film thickness (h). All stress and strain values are averaged throughout the coating thickness. Results of the development show that all strains and stresses are very sensitive to Poisson's ratio of the coating. As an example, shear stresses can vary by as much as a factor of six as Poisson's ratio goes from 0.3 to 0.5, the higher stresses corresponding to the higher values of Poisson's ratio. A similar change in shear stresses occurs when a/h varies from 2.5 to 5.0, with higher stresses at higher a/h values. In comparison with Hertzian theory (which does not account for the layer thickness), the proposed theory indicates at small thicknesses ($a/h > 6$) the actual contact area is about 60% of the Hertzian value. For a/h values less than 1, the problem can be solved by the Hertzian theory with the indentor acting on the bulk coating.

An experimental apparatus was developed by Matthewson to determine contact areas. A spherical indentor was loaded against silicone rubber films (1.15 - 2.15 mm in thickness) which were deposited on roughened glass. Ink was then deposited around the contact area, allowing better identification of the edges of the contact zone when viewed through an optical microscope. The ink also served as a lubricant to minimize friction between the sphere and coating. Once contact areas were measured, they could be used in the theory to calculate unknown constants in the expressions for stress and strain. From these expressions, relationships between the applied normal load and the amount of penetration were developed. These could then be compared with the experimentally measured loads and penetrations. Results show that the theory is increasingly accurate with increasing values of a/h, about 10% for $a/h > 2$ and less than 3% for $a/h > 5$.

Conway and Engle (34) have developed numerical methods to solve for stress distributions over the contact area. Two contact geometries are considered, contact of an elastic layer between two spheres and contact of an elastic layer between two cylinders. Development is similar to that of Matthewson with the exception that rough indentors are considered. The roughness is considered to be sufficient enough to cause full adherence of the layer to the indentor. As might be expected, this condition causes significant shear stresses to be developed within the layer that in a practical case might cause film failure or debonding from the substrate.

3.0 EXPERIMENTAL WORK

This work had two primary goals. The first was to expand our knowledge of the ability of thin polymeric films to prevent fretting corrosion and metallic contact by evaluating a wide variety of polymer types. The second goal was to document the fretting process between the polymer-steel interface as a function of run time.

In order to study the fretting process for the various film types, a normal load and test run times had to be determined. This was done in the first phase of experimentation in which the effect of normal load on polymer film life was investigated. Data from the first phase was used to select both normal load and test run times for the second phase. In the second phase, optical macroscopy and scanning electron microscopy (SEM) were used to study the fretting process as a function of time.

3.1 Preparation of Test Specimens

To complete both the first and second phases of experimentation for each polymer film, sixteen 52100 steel balls and four 1045 disks were required. Three to five "wear" scars were generated on each of the disks depending on the experimental phase. One scar was generated on each ball. Both components (ball and disk) required extensive cleaning prior to use. Additional surface preparation was needed for the disks before they could be coated with the polymer films.

3.1.1 Contact Geometry

The contact geometry chosen for this work is shown in Figure 3-1. A 52100 steel ball (15.875 mm in diameter) is loaded in contact with a

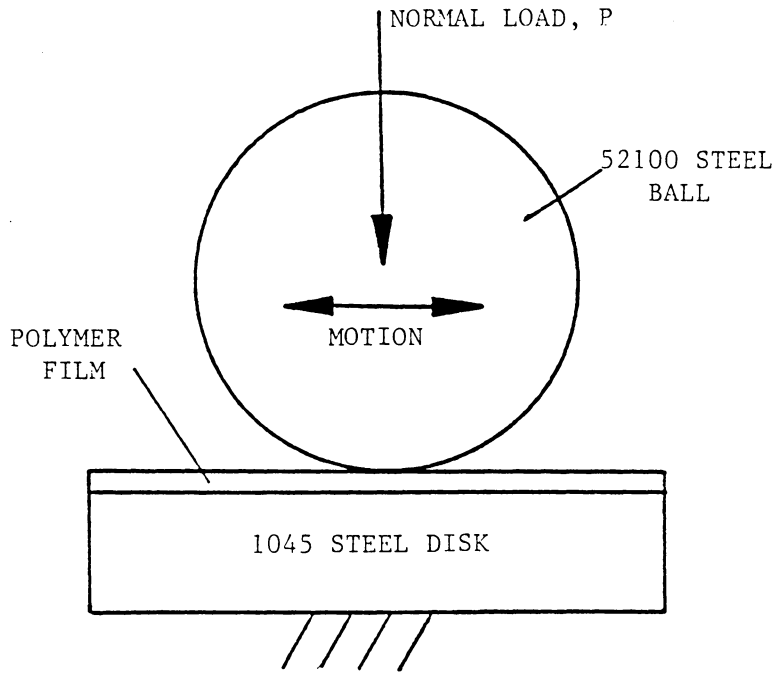

FIGURE 3-1. Contact Geometry.

polymer coated 1045 steel disk. Small amplitude reciprocating motion is then introduced through the ball.

3.1.2 Disk Surface Preparation and Marking

The 1045 steel disks required surface preparation prior to coating. The disks were 24.8 mm in diameter and 7.9 mm thick. They were cut from 25.4 mm diameter bar stock. After cutting, one side of the disk was ground to approximately 1.0 μm Ra. The disks were then marked, using a punch so that after they were coated the original lay of the surface grinding marks could be determined. After grinding, the disks were sandblasted resulting in a final roughness of 1.5± μm Ra.

Figure 3-2 is a scanning electron micrograph of the disk surface after preparation. The area shown is 2.3 mm by 1.8 mm which is approximately the size of most of the scar areas which will be presented in the next chapter. It can be seen that the surface is fairly random in nature.

3.1.3 Cleaning

Both uncoated disks and balls were cleaned by the same procedure. The disks were cleaned after all of the surface preparation work was completed. The balls were cleaned as received.

The procedure involves five steps and is as follows:

1. Clean disk and ball in a 1% (by weight) aqueous solution of Na_3PO_4 in an ultrasonic cleaner for five minutes. This step removes most of the bulk organic contamination.

2. Clean disk and ball in distilled water in an ultrasonic cleaner

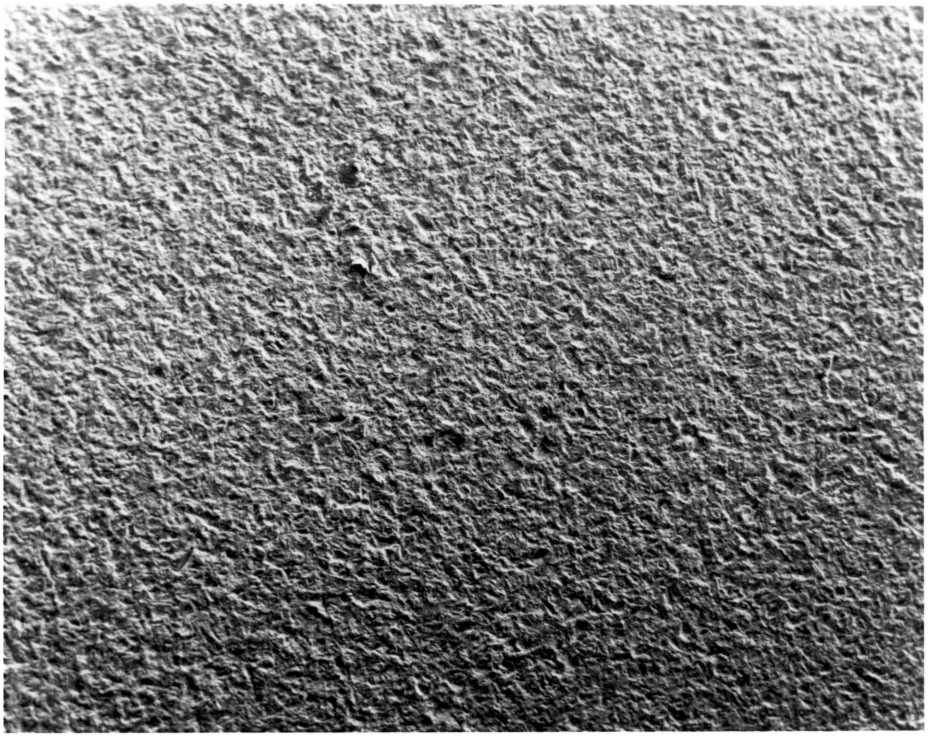

FIGURE 3-2. Scanning Electron Micrograph of an Uncoated Disk Surface.

for five minutes. This removes most inorganic contaminants and any of the remaining Na_3PO_4.

3. Clean disk and ball in methanol for five minutes in an ultrasonic cleaner. This removes the distilled water.

4. Evaporation/condensation cleaning in methanol. The disks or balls are suspended in a wire mesh over boiling methanol. As the methanol evaporates and comes in contact with the metal surfaces (which are much cooler), it condenses and returns to the boiling liquid. This process was continued for five minutes to remove any remaining organic contamination.

5. Evaporation/condensation cleaning in hexane. This step is exactly the same as the previous, with the exception that hexane is used instead of methanol.

After cleaning, the disks and balls were stored in sealed petri dishes, each containing a small packet of $CaCl_2$. The $CaCl_2$ was used as a desiccant to prevent rusting of the clean metal surfaces.

3.1.4 Polymer Selection

Ten different polymers were chosen for investigation. Of the ten, four of the polymer types were coated at VPI&SU (PVDC, PVC, PSO and PS). The remaining six were prepared at Boyd Coatings Research Company Incorporated in Hudson, Massachusetts under the direction of Dr. Pedro Diaz. The polymers chosen represent a wide variety of mechanical, thermal and structural properties. Table 3-1 shows the polymer types and their structure (35,36,37). Table 3-2 summarizes some pertinent mechanical and thermal properties (38). As can be seen, a wide range of

TABLE 3-1 Polymer Types Chosen for Investigation

Polymer	Abbreviation	Structure
polymethylmethacrylate	PMMA	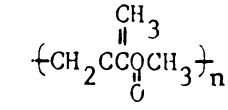
polytetrafluoroethylene	PTFE	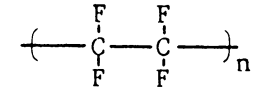
polyimide	PI	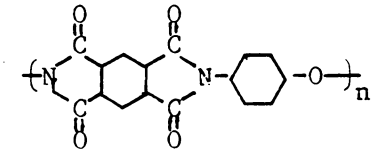
polyvinylidene fluoride	PVDF	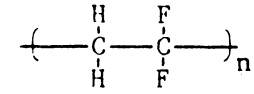
polyvinylidene chloride	PVDC	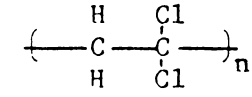
low-density polyethylene	LDPE	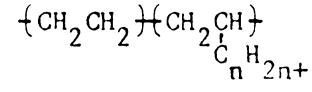
polyvinyl chloride	PVC	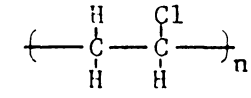
polysulfone	PSO	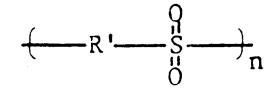
polystyrene	PS	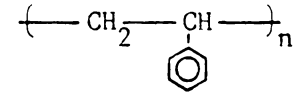
high-density polyethylene	HDPE	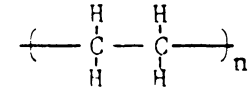

TABLE 3-2 Polymer Properties[a]

Property	Polymer Type									
	PMMA	PTFE	PI	PVDF	PVDC	LDPE	PVC	PSO	PS	HDPE
Melt Temperature (Crystalline) (°C)	-	327	-	164-178	160	106-115	-	-	-	130-137
Glass Transition Temperature (Amorphous)(°C)	90-105	-	310-365		0-2	-	75-105	190	100-105	-
Tensile Strength at Break (MPa)	48.3-75.9	13.8-34.5	72.4-117.9	24.8-49.7	19.3	8.3-31.4	41.4-51.7	-	35.9-51.7	22.1-31.0
Tensile Yield Strength (MPa)	-	-	86.2	43.4-56.6	-	8.9-14.5	55.2-89.7	70.3	-	26.2-33.1
Compressive Yield Strength (MPa)	72.4-124.1	11.7	206.8-275.8	36.5-95.1	13.8-18.6	-	55.2-89.6	275.8	82.7-89.6	18.6-24.8
Shear Strength (MPa)	27.6-43.4	8.3-20.0	49.7	14.5-29.0	11.0	4.8-17.9	24.1-29.7	40.7	20.7-29.7	12.4-17.9
Young's Modulus (GPa)	2.2-3.1	0.4	2.1	1.0-2.9	0.34-0.55	0.17-0.28	2.4-4.1	2.5	2.3-3.3	1.1
Poisson's Ratio	0.35	0.46	0.35	0.34	0.35	0.46	0.35	0.37	0.35	0.46
Elongation at Break (%)	2-10	200-400	8-10	12-400	350-400	100-650	40-80	50-100	1.2-1.5	10-1200
Thermal Conductivity (W/m·K)	1700-2500	2500	960-1100	1000-1700	1300	3300	1500-2100	2600	1300	4600-5000

[a] Source: Reference (38).

mechanical properties exist. For example: If we consider compressive yield strength, its value can range from as low as 11.7 MPa for PTFE to as high as 275.8 MPa for polyimide. The melt or glass transition temperature also varies significantly with polymer type. For the crystalline polymers, the melting temperature can be as low as 106°C for LDPE to over 300°C for PTFE. A similar range exists for the amorphous polymers--PVC having the lowest glass transition temperature (75°C) and polyimide the highest (365°C).

Polymethylmethacrylate is an amorphous, linear atactic thermoplastic. It is characterized by excellent mechanical properties such as high tensile strength (62 MPa) and high impact strength. PMMA is also favored for its optical clarity. However, it has low resistance to abrasion (39). Bulk PMMA (obtained from 3mm films) has been shown to fret steel (24).

Polytetrafluoroethylene is a highly linear crystalline polymer. This linear structure accounts for its low friction but poor wear behavior, since in the absence of branching and crosslinking chains of the polymer are free to slide across one another (40).

Polyimides have been the subject of some tribological investigation (37,41) primarily because of their excellent strength properties and thermal stability. Both fatigue and adhesive mechanisms are believed to be important factors in wear of the polymer. Generally polyimides are amorphous and are often used to coat metals because of their superior dielectric properties. At their decomposition point they do not melt but crumble into fine powder.

Polyvinylidene fluoride is a crystalline polymer, similar to PTFE in structure with the exception that two of the fluorine atoms are replaced by hydrogen. It also has higher yield strength than PTFE. PVDF has been shown to wear steel along with thin film transfer under fretting conditions at sliding amplitudes less than 8 μm (24).

The chlorinated polymers, PVDC and PVC are the most thermally unstable of all of the polymers tested. Both thermally decompose by the evolution of HCl, accompanied by chain scission and the formation of conjugated double bonds (42). PVC has superior strength properties compared to PVDC and tends to be less crystalline. Bethune, Higham and Stott (24) have shown bulk PVC to fret steel, whereas Sweitzer and Puzio (3,5), working with PVC coatings found that the polymer did not cause fretting damage.

Low-density polyethylene is partially crystalline (50-60%) and contains branched chains. Its counterpart, high-density polyethylene (or linear polyethylene), is highly crystalline (greater than 90%). The difference in mechanical properties is due to this difference in structure. HDPE tends to be much stiffer (E = 1.1 GPa) than LDPE (E = 0.23 GPa) and has greater tensile strength and hardness (43). Polyethylene has been shown to fret steel at slip amplitudes greater than 7 μm (24).

Polysulfone is an amorphous polymer with excellent thermal stability. The R group in its structure is an aryl-oxygen linkage. PSO also has excellent mechanical properties (tensile strength = 70.3 MPa; shear strength = 40.7 MPa). PSO has also been shown to fret steel (24).

Polystyrene is a linear, amorphous polymer. Very little tribologi-

cal work has been done with polystyrene, possibly because of its brittle nature (elongation at break = 1.5%). Polystyrene also has a low distortion temperature of 85°C at which it softens and losses its structural integrity. At elevated temperatures it degrades into a mixture of styrene and other low molecular weight compounds (44).

3.1.5 Application of Polymer Films

Table 3-3 shows the method by which each polymer coating was applied to the steel disk. As was previously stated, four of the films were coated at VPI&SU while the remaining six were prepared at Boyd Coatings in Hudson, Massachusetts. See Appendix B for detailed coating procedures.

3.1.6 Film Thickness Measurement

Polymer film thickness was determined by the use of an Elektro Physik model F102 Minitest Coating Thickness Gauge which operates on the basis of eddy current. The device consisted of a spring-mounted probe approximately 1 mm in diameter which was placed directly on the film to be measured. The probe sensor was electrically connected to a metering device which indicated the film thickness in thousandths of an inch. Prior to measurement, the device was calibrated using films of known thickness that were supplied with the gauge. For each coated disk, five film thickness measurements were taken across the area of the disk in which the testing was to be conducted.

3.2 Testing Equipment

The testing device used in this work, known as the Mark IIIB fret-

TABLE 3-3 Polymer Types: Method of Application

Polymer Type	Method of Application	Where Prepared
PMMA	Solvent Deposition	Boyd Coatings
PTFE	Aqueous Emulsion	Boyd Coatings
PI	Solvent Deposition	Boyd Coatings
PVDF	Electrostatic Powder	Boyd Coatings
PVDC	Solvent Deposition	VPI&SU
LDPE	Electrostatic Powder	Boyd Coatings
PVC	Solvent Deposition	VPI&SU
PSO	Solvent Deposition	VPI&SU
PS	Solvent Deposition	VPI&SU
HDPE	Electrostatic Powder	Boyd Coatings

ting corrosion device, was originally developed to study fretting corrosion at a bearing-cartridge interface (1). The device can be easily adapted to study three different contact geometries: 1. cylinder-in-cylinder; 2. sphere-in-cylinder; and 3. sphere-on-flat. For the sphere-on-flat geometry, which is used in this work, two contact systems can be run simultaneously. The device also allows measurement of friction force on the ball and electrical contact between the ball and disk.

3.2.1 Mark IIIB Overview

Detailed description of Mark IIIB characteristics have been presented elsewhere (1,3); therefore, only a brief overview will be given here. Figure 3-3 is a schematic drawing showing the major components of the Mark IIIB. Reciprocating motion is provided by a shaker table which in turn is driven by a variable speed motor. The vertical motion of the shaker table is then converted to horizontal motion by the drive linkage. This conversion results in a reduction of amplitude by a factor of five. The ball specimen holders are attached to the drive linkage. The disk holders are mounted on a piece of angle iron attached to the base plate. The contact system (ball and disk) is loaded by hanging weights through a pulley system across the ball holder. The specimen holders are enclosed in a Plexiglas chamber allowing different environments to be investigated.

Figure 3-4 shows a more detailed view of the ball and disk holders. The ball is secured by tightening a threaded cylindrical holder. Set-screws tapped in the disk holder secure the disk. Strain gauges, mounted in the ball strain arm, allow continuous monitoring of friction

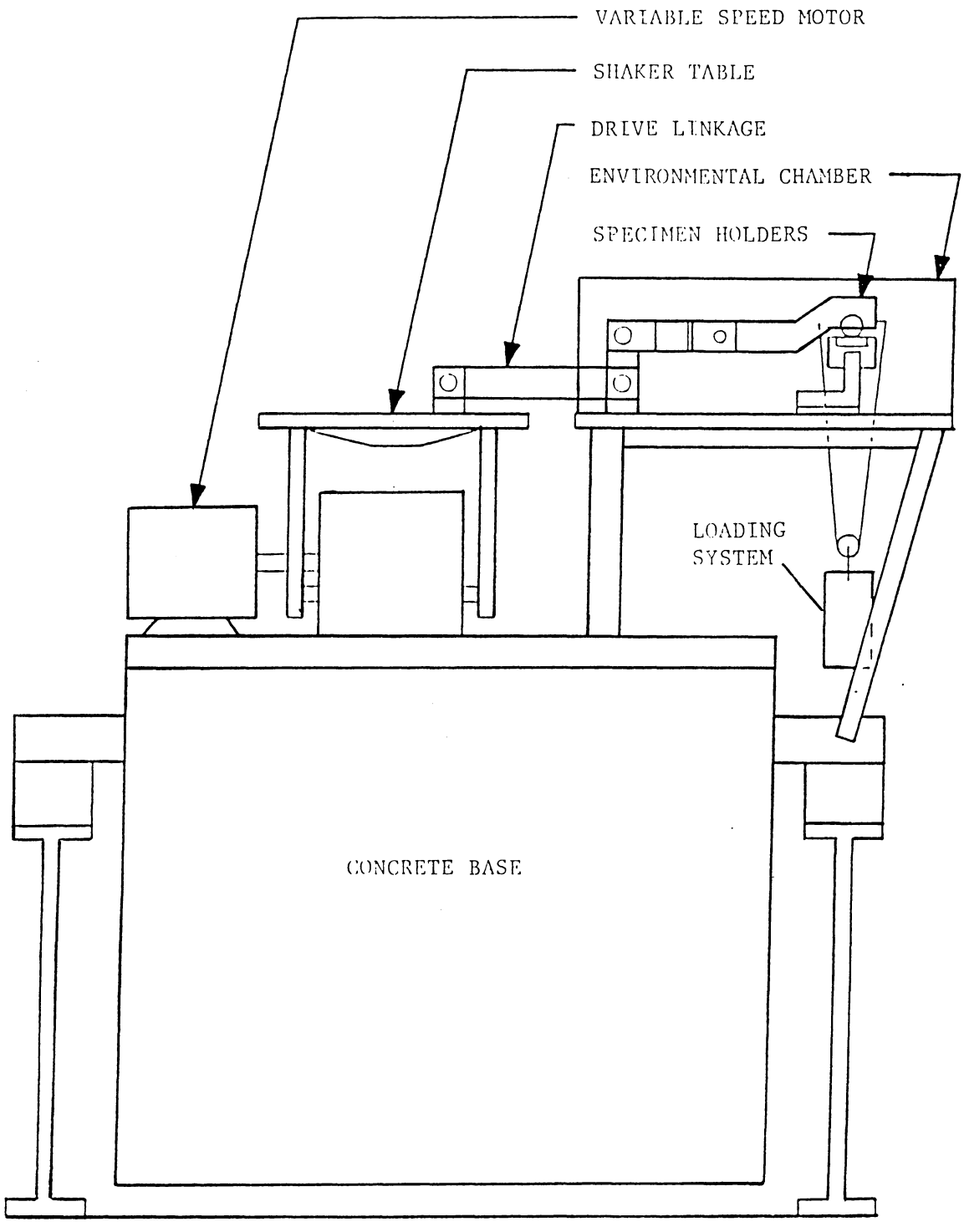

FIGURE 3-3. Mark IIIB Fretting Corrosion Device.

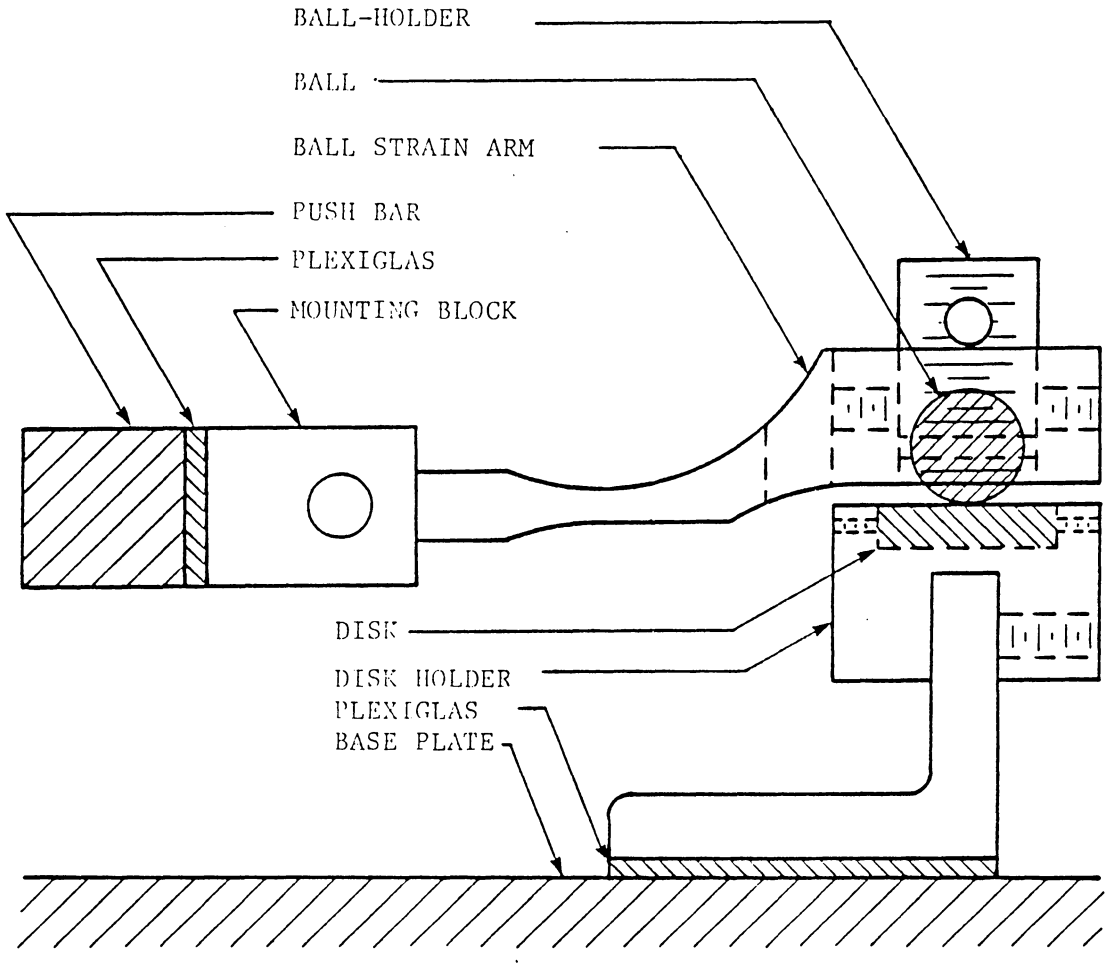

FIGURE 3-4. Ball and Disk Specimen Holders.

forces through a strip chart recorder. A voltage divider circuit is used to place a 15 mV potential across the contacting ball and coated disk. This potential is also monitored by a strip chart recorder. When the polymer film breaks through and metal-metal contact occurs, the potential across the interface goes to zero (0 resistance) which is registered on the recorder as a contact spike. By this method (45), the occurrence of metallic contact can be determined.

Prior to running experiments, both the strain gauge circuitry and electrical contact circuitry require calibration. The friction force was calibrated by hanging known weights through a pulley cable system incorporated on the environmental chamber. This process results in a tension force of known magnitude on the ball strain arm, which in turn causes a corresponding deflection of the strip chart recorder pen. By using a range of loads a calibration chart could be developed. A typical friction force calibration chart is presented in Figure 3-5. Changes in the recorder pen deflection for a given load could be adjusted by changing the sensitivity of the recorder.

The electrical contact circuitry was calibrated so that no-metallic contact and metallic contact behavior could be monitored. A typical calibration chart is shown in Figure 3-6. The ball strain arm was electrically insulated from the disk holder and then electrical contact was simulated by short circuiting the ball and disk holders. The corresponding deflection on the recorder could then be adjusted by changing the strip chart recorder sensitivity.

Table 3-4 summarizes the capabilities of the Mark IIIB fretting

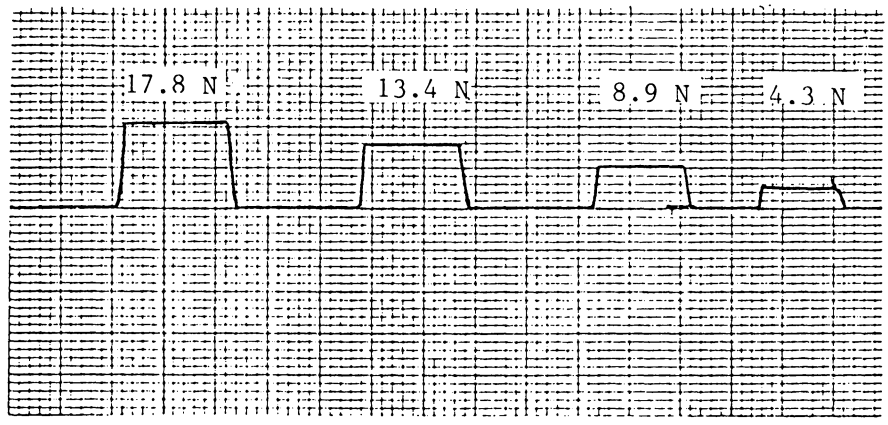

FIGURE 3-5. Friction Force Calibration Chart.

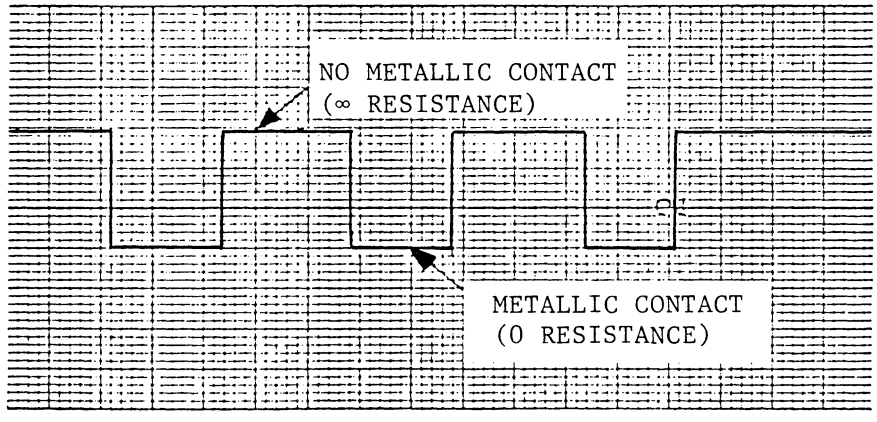

FIGURE 3-6. Metallic Contact Calibration Chart.

TABLE 3-4 Mark IIIB Capabilities

Number of test positions	Five (maximum)
Normal load	0-200 N
Amplitude of vibration	0-500 μm
Frequency of vibration	10-100 Hz
Test specimen geometry	Sphere-on-flat Sphere-in-cylinder Cylinder-in-cylinder
Test specimen material	Metals, Polymers, Ceramics
Temperature	Ambient
Environment	Controlled (e.g., room air, dry nitrogen and other gases)

corrosion device.

3.2.2 Mark IIIB Operation

Running of fretting tests involved a four-step procedure. It was as follows:

1. Both ball and disk were mounted in their respective holders. The disk was mounted so that the original lay of the grinding marks (prior to sandblasting) was perpendicular to the sliding direction.

2. All instrumentation was then activated: strip chart recorders, bridge amplifiers and the variable speed motor.

3. The normal load was then applied to the ball strain arm.

4. Thirty seconds after Step 3, the shaker table was engaged and set at the desired test frequency.

To terminate a test, the above procedure was followed in reverse order.

3.3 Procedure

The experimental work consisted of two phases. The first phase was to study the load-life behavior of the various polymer types. The second phase characterized the fretting process at the polymer-steel interface for the ten polymer types.

3.3.1 Load-Life Behavior

To conduct phase two of the experimental work, a normal load and test run times had to be determined. A range of normal loads was selected to determine the lives of the polymer films being evaluated. The loads were chosen based on past experience with testing polymeric films

at VPI&SU and were 11.1 N, 22.3 N, and 44.5 N. Table 3-5 summarizes the test conditions for phases one and two of the experimental work.

Initially, one test, consisting of two ball-disk contact systems run in parallel, was conducted for each polymer at each load. This resulted in two life values for each polymer at each of the three test loads. Based on these data, a load and test run times for phase two were determined. Results of this process are described in the next chapter, Sections 4.2.1 and 4.2.2.

After selection of the load and run times for phase two, an additional test was run at each of the other two loads (those not selected for phase two) to supplement the life data obtained from the first tests. The additional tests were run in the same fashion as the first, and on the same disks. This resulted in four life data points at each of the loads not chosen for phase two for each of the polymers.

3.3.2 Characterizing the Fretting Process

After selecting the load for phase two, a series of run times had to be determined to illustrate the fretting process. It was decided to run three tests for each polymer with varying run times to show the process. These run times are presented in the next chapter; Section 4.2.2.

Each of these tests consisted of two ball-disk systems run in parallel on the Mark IIIB. One of the ball-disk setups from each of the tests was used for macroscopic and SEM observation. Contact and frictional data from both disks was used to supplement the life data at the phase two load.

TABLE 3-5 Experimental Test Conditions

Number of test positions	2
Normal load	Phase 1: 11.1 N, 22.3 N and 44.5 N Phase 2: 22.3 N
Amplitude of vibration	300 μm (peak-to-peak)
Frequency of vibration	20 Hz
Test specimen geometry	Sphere-on-flat (15.875 mm ball diameter)
Temperature	~21°C
Environment	Room air ~ 55% R.H.

After the tests were run, each corresponding ball and disk scar were photographed using a Wild 420 Macroscope equipped with a Wild MPS 55/512 Photo Automat and shutter piece connected to a Leitz 35 mm film carrier loaded with Kodak ASA 200 Ektachrome film. The macroscope was also equipped with a rotatable quarterwave plate which provided the ability to change the contrast of the scars being photographed. For all of the photographs, quartz halogen coaxial incident illumnation was used, being directed along the viewing path. For each of the ball and disk scars from each of the three tests, a standard set of magnifications was used: 7.4X, 10X, 12.8X, 16X and 25.6X. No attempt was made to remove any of the polymer debris on either the ball or disk scars.

After macroscopic observation was completed, the disk specimens were sputter-coated with Au-Pd and observed with a AMR 900 Model J3 scanning electron microscope. As with the macroscope, a standard set of magnifications was used for each polymer. These were 20X, 50X, 200X and 1000X. The two lower magnifications were used to provide an overall view of the scar. Both 200X and 1000X magnifications were used to photograph the details of the scar at the ends of the sliding path, the edges parallel to the sliding path, and the center of the scar. Only Test 1 and Test 3 (see section 4.2.2 in the next chapter) disk scars were observed with SEM.

4.0 RESULTS

The results of this work are presented in two sections corresponding to phase one and phase two of the experimental work described in the previous chapter. In the first section, all of the life and friction data are presented. The second section presents the macroscope and SEM work that was done to characterize the fretting process.

4.1 Load-Life Behavior

To evaluate the life of the polymeric films at each load (11.1, 22.3, and 44.5 N) at least one test, resulting in two life values, was run at each load. A test was terminated either when the film had failed (as determined by electrical contact measurement) or after one hour of run time.

4.1.1 Coating Thickness

Table 4-1 shows the thickness of the polymer films chosen for investigation. Each mean and range is the result of the twenty thickness measurements that were taken on the four coated disks used for each polymer type (see Appendix C). Also note that Table 4-1 divides the films into four groups based on similar thicknesses. The life and frictional data will be presented in the same groups.

4.1.2 Evaluating Polymer Film Life

After the load-life tests were completed, analysis of the contact data showed three possible measurements of polymer film life. Figure 4-1 shows the first two. Time A indicates the time at which there is the first deviation from no metallic contact. Time B indicates the time at

TABLE 4-1 Polymer Film Thickness
(μm)

Group	Polymer	Mean	Range
I	PMMA	7.10	6.10-8.13
I	PTFE	10.1	8.64-12.7
I	PI	11.6	10.9-12.7
II	PVDF	25.3	20.3-30.5
II	PVDC	27.3	22.9-33.0
III	LDPE	46.6	33.0-63.5
III	PVC	60.0	59.8-71.1
III	PSO	62.6	61.0-67.3
IV	PS	86.0	81.3-91.4
IV	HDPE	111.8	99.1-132.1

which the first full metallic contact spike occurs. Time C, shown in Figure 4-2, is the time when full metallic contact occurs.

All three times were tabulated and Time B, the time when the first full metallic contact spike occurs, was chosen as the measure of film life. Time B was chosen because it was the most consistent measure from test to test. Furthermore, photographic evidence of the disk scars showed that the film had broken through. Appendix D contains all the polymer life data.

Figures 4-3 through 4-7 summarize the results of the load-life tests. Figure 4-3 is a plot of average polymer film life versus mean film thickness (reported in Table 4-1) and polymer type for each of the three test loads; 11.1, 22.3 and 44.5 N. Note that for each of the test loads there is a large range of average life. For example: at 11.1 N normal load, average film life varies from as low as 76 seconds for PMMA to over 3600 seconds for PVC, PSO, PS and HDPE. Also note that at the 44.5 N test load all of the films, with the exception of HDPE, have failed in less than 300 seconds. It is also evident that film life is not only a function of film thickness--independent of polymer type. At 22.3 N, PI films had an average life 900 seconds greater than films that were two to four times as thick (PVDF, PVDC and LDPE).

Figures 4-4 through 4-7 illustrate the effect of normal load on average polymer film life. As can be seen, there is a tendency for average life to decrease with increasing normal load. It should also be noted that several of the polymer films (PVC, PSO, PS and HDPE) had lives which exceeded the maximum one hour test period at least one of

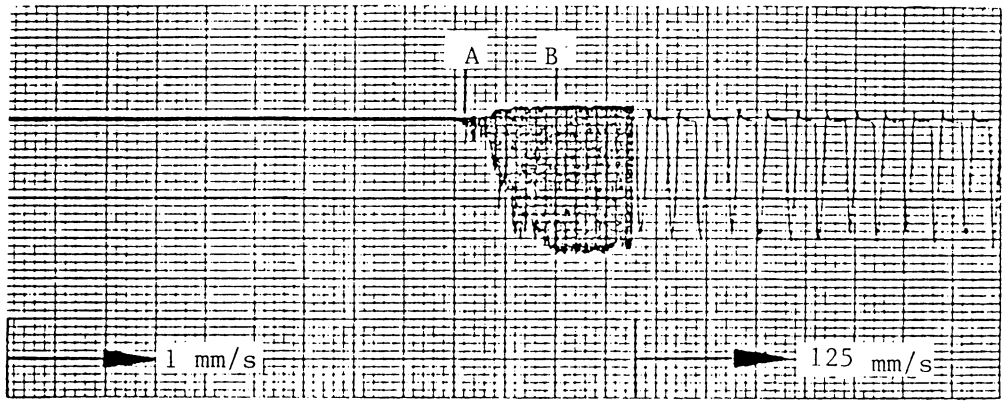

FIGURE 4-1. Possible Measurements of Polymer Film Life. LDPE Contact Data at 11.1 N Normal Load. A: Time at which First Deviation from No Metallic Contact Occurs. B: Time at which First Full Metallic Contact Spike Occurs.

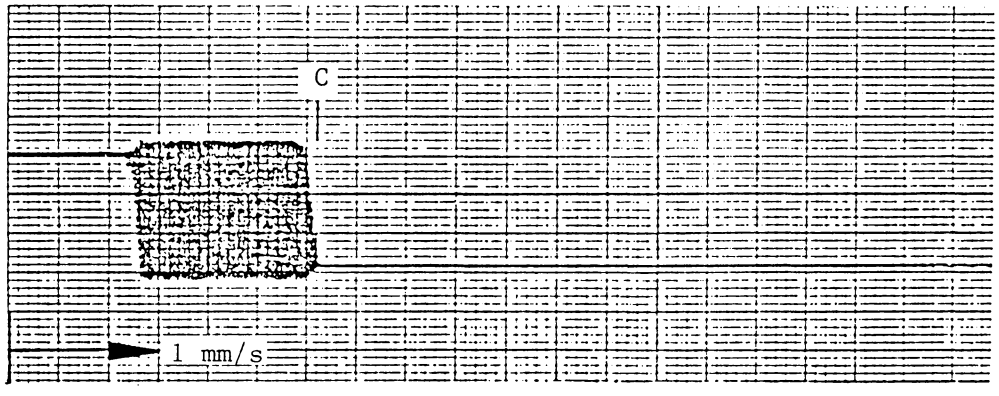

FIGURE 4-2. Possible Measurements of Polymer Film Life. LDPE Contact Data at 11.1 N Normal Load. C: Time Until Full Metallic Contact.

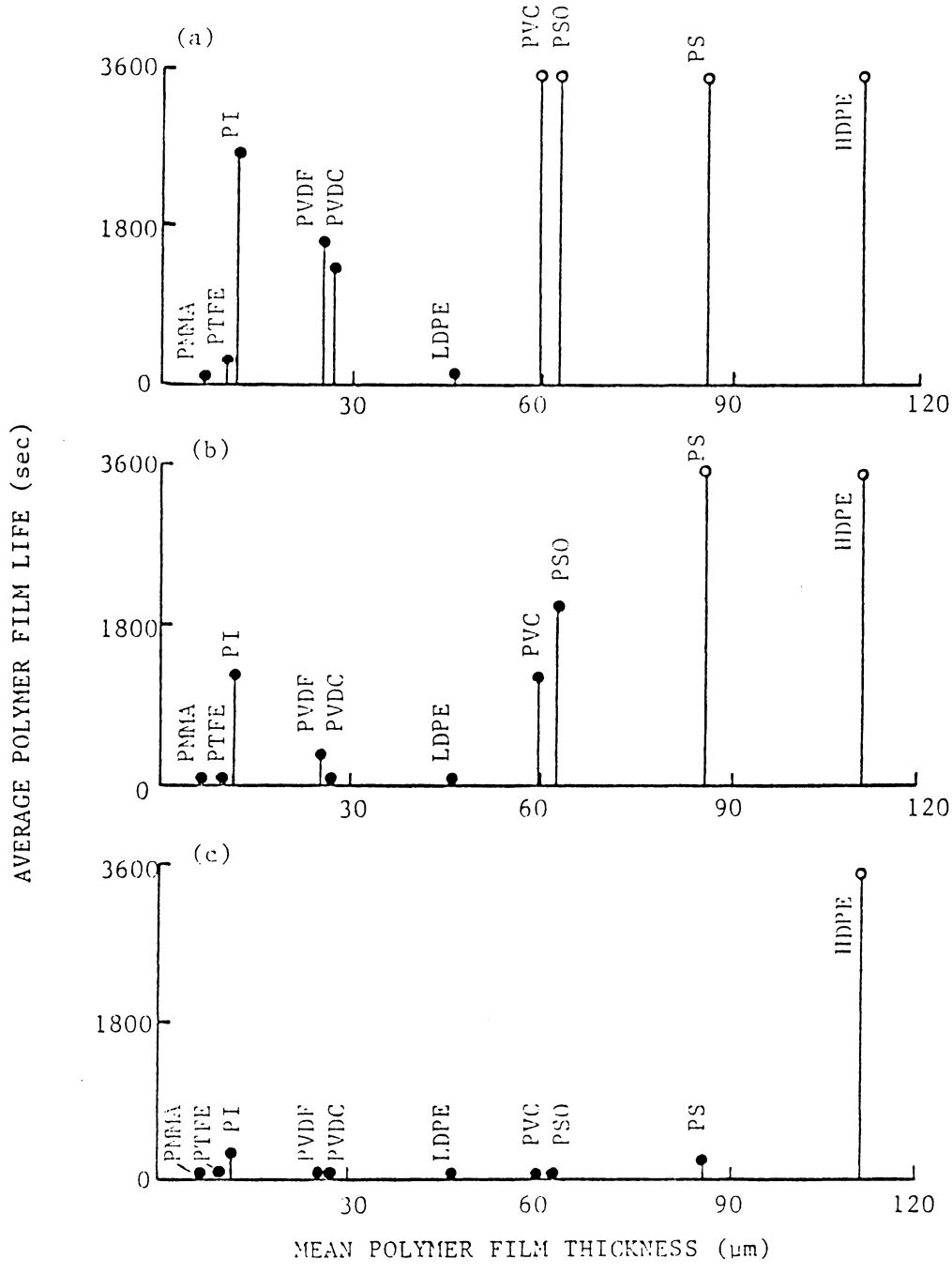

o Indicates Life Exceeds 3600 Seconds.

FIGURE 4-3. Average Polymer Life Versus Film Type and Thickness: (a) 11.1 N Normal Load; (b) 22.3 N Normal Load; (c) 44.5 N Normal Load.

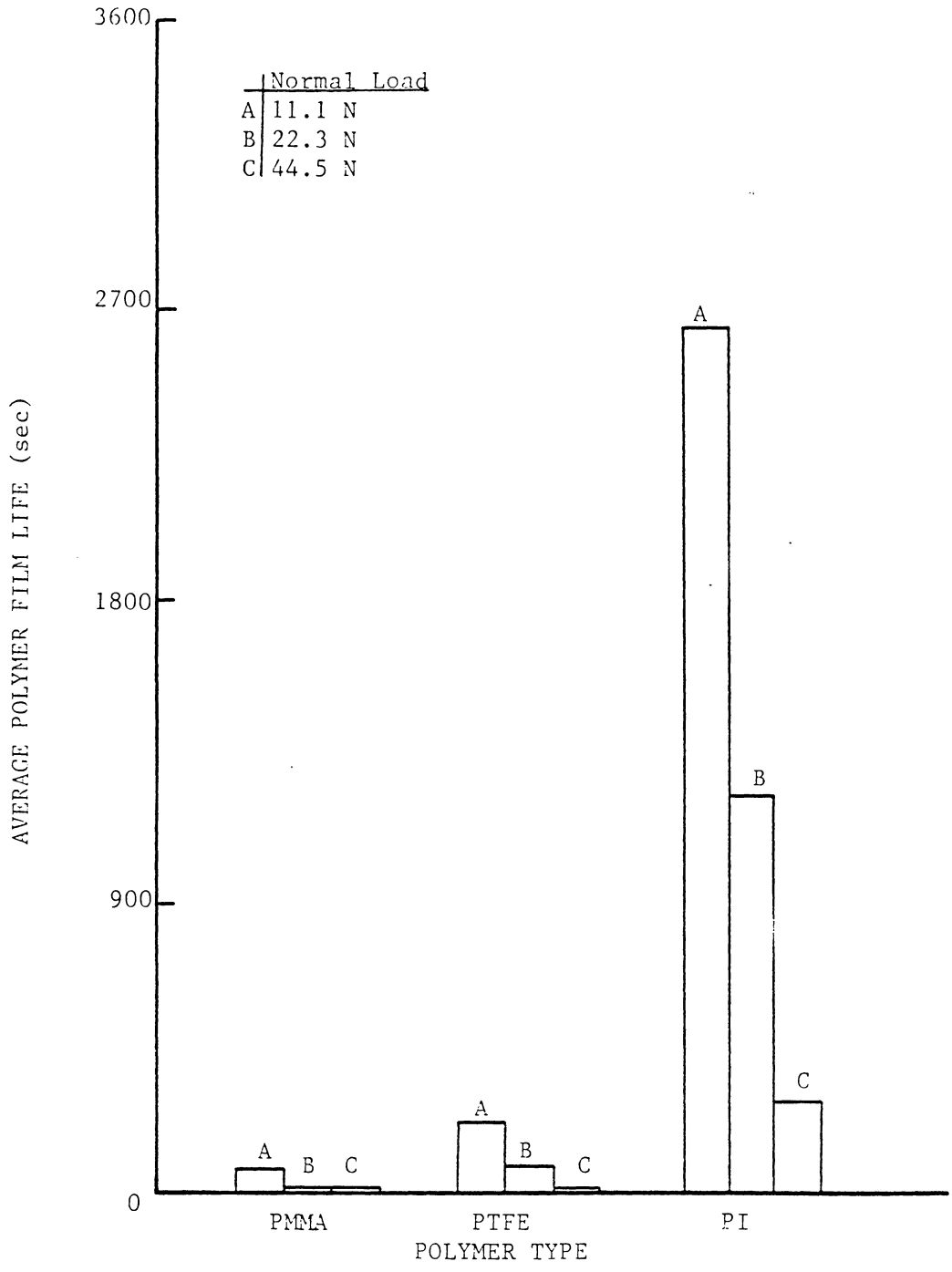

FIGURE 4-4. Average Polymer Film Life: Group I Films.

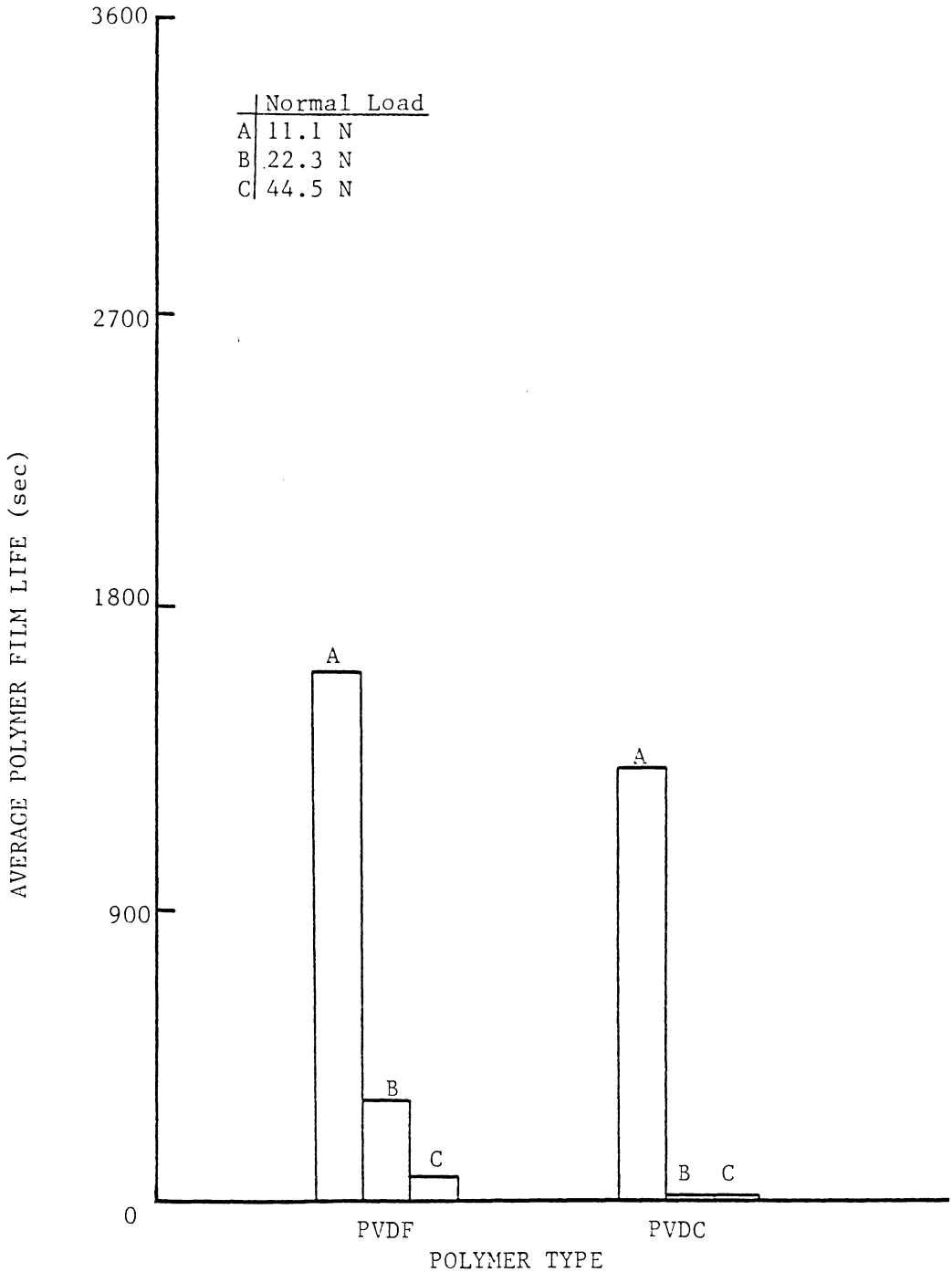

FIGURE 4-5. Average Polymer Film Life: Group II Films.

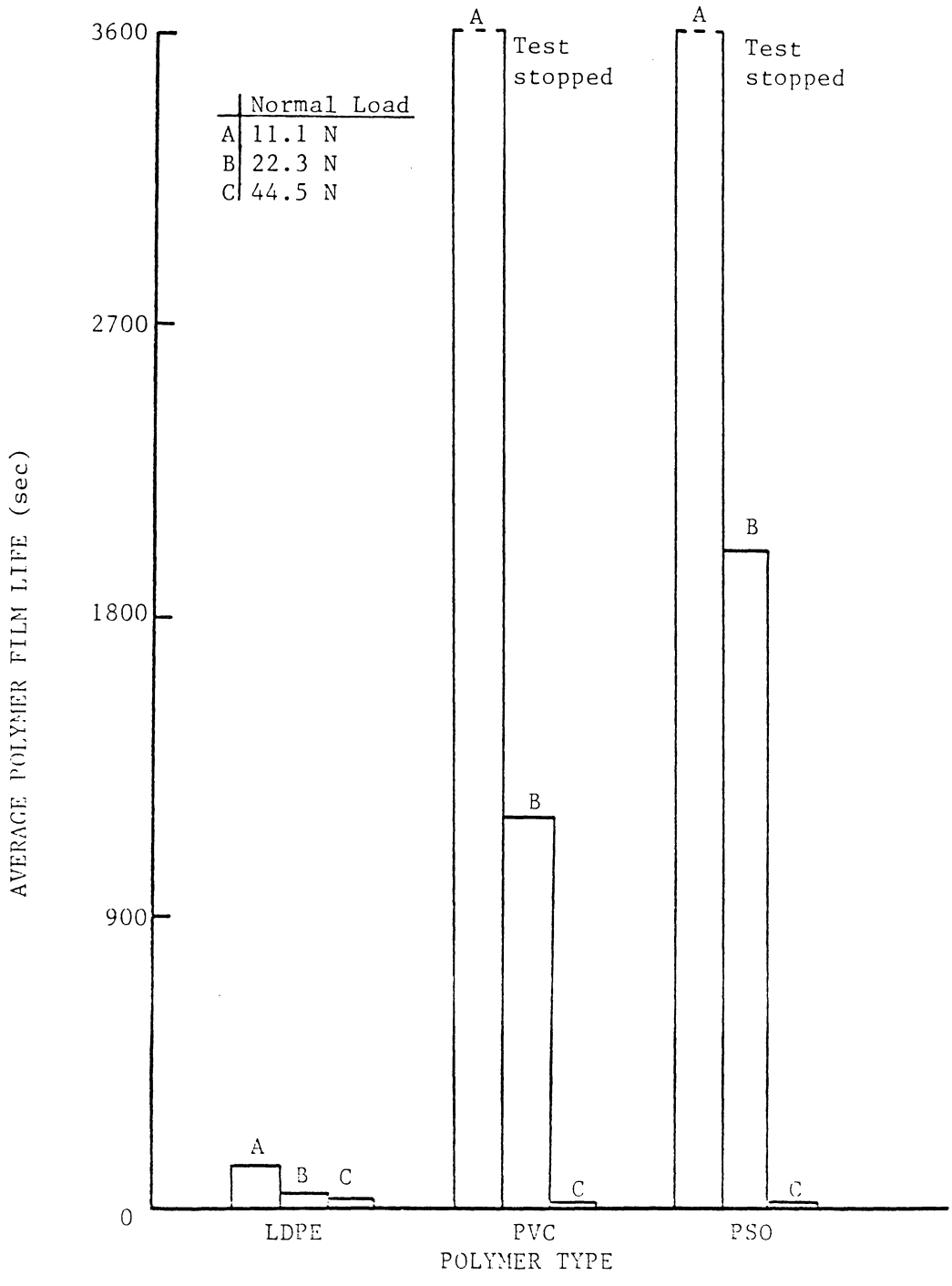

FIGURE 4-6. Average Polymer Film Life: Group III Films.

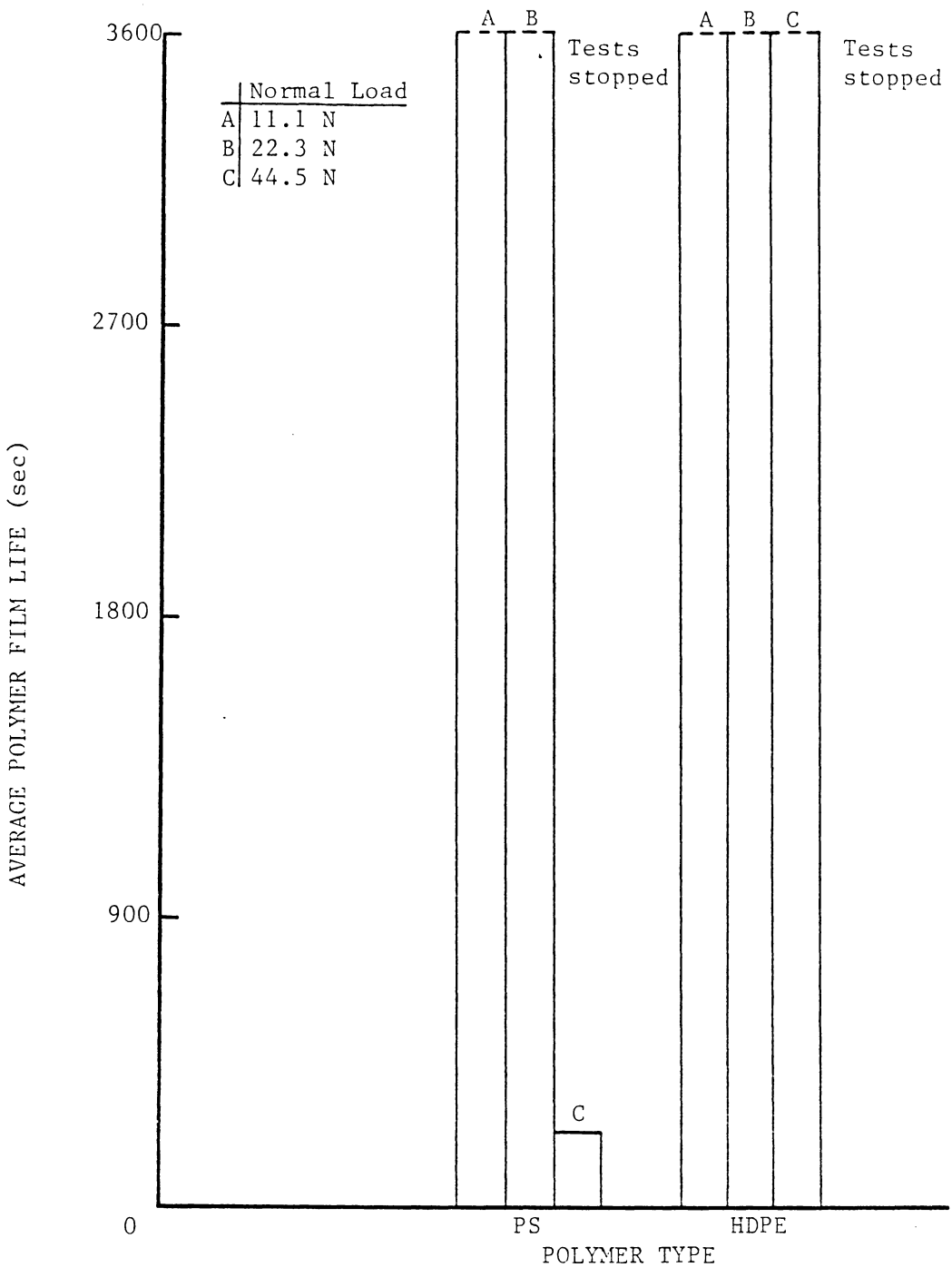

FIGURE 4-7. Average Polymer Film Life: Group IV Films.

the three test loads. Analysis of variance was used for those polymers for which the three life means were known (PMMA, PTFE, PI, PVDF, PVDC and LDPE) to determine whether the decrease in life with increasing normal load was statistically significant. Results of this analysis (presented in Appendix F) show that for PTFE, PI, PVDF and PVDC, the trend is statistically verified. For PMMA and LDPE, no conclusion could be made as to a variation in average life for the range of normal loads tested. Both PVC and PSO had lives at 11.13 N that were greater than 3600 seconds; therefore, a simple t-test was used on the 22.3 and 44.5 N life means. Results of this analysis (also presented in Appendix F) show that for PVC and PSO, there is a statistically significant decrease in film life as normal load is increased from 22.3 N to 44.5 N. For PS and HDPE, at least two of the three life means were greater than 3600 seconds; therefore no conclusion could be made as to the effect of load on life.

4.1.3 Load-Friction Behavior

For the load-life experiments, both initial and final coefficients of friction were tabulated prior to film failure (see Appendix E). A typical friction chart is shown in Figure 4-8. The chart speeds are 1 mm/s and 125 mm/s. Run time increases from left to right. The bandwidth shown represents the frictional forces between the steel ball and coated disk for both directions of motion during each cycle of fretting. Frictional forces can be easily obtained at any time during the fretting experiment by measuring the bandwidth in Figure 4-8, dividing the resulting measurement by two and then comparing to a calibration

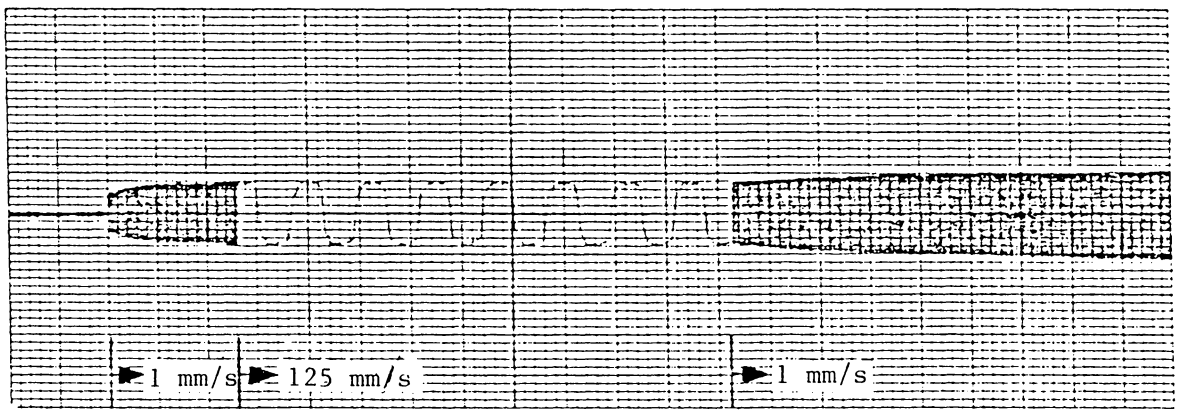

FIGURE 4-8. Typical Friction Data. PVDF at 11.1 N Normal Load.

chart. For the chart shown, 1 mm of bandwidth represents 1.8 N of friction force.

Figures 4-9 thru 4-12 illustrate the range of initial and final coefficients of friction for each of the polymers investigated at each of the three test loads prior to film failure. Each initial and final value is obtained from an average of the observations reported in Appendix E. It can be seen that the coefficient of friction can vary greatly during a fretting test. For example, at 11.1 N the coefficient of friction for PSO can range from as low as 0.48 to as high as 1.2. There are also large differences in frictional behavior among the polymer types. PSO, PVC and PVDC all have mean final coefficients of friction greater than 1.0 while PTFE has the lowest coefficient (ca. 0.1) of friction of any of the films tested.

Figures 4-13 thru 4-22 are characteristic plots of coefficient of friction as a function of run time for each of the ten polymer types. Each plot is developed from one test at 22.3 N (the phase two test load; see Section 4.2.1). Note that for all but two of the polymers (PTFE and HDPE), the coefficient of friction is at its minimum value at the beginning of the test and at its maximum just prior to film failure. For PTFE and HDPE, the coefficient of friction remains constant throughout the test. Also note that several of the films (PI, PVC, PSO and PS) show abrupt changes in friction coefficient during the beginning of the test.

4.2 Characterizing the Fretting Process

Using life data presented in section 4.1.2, both load and test run

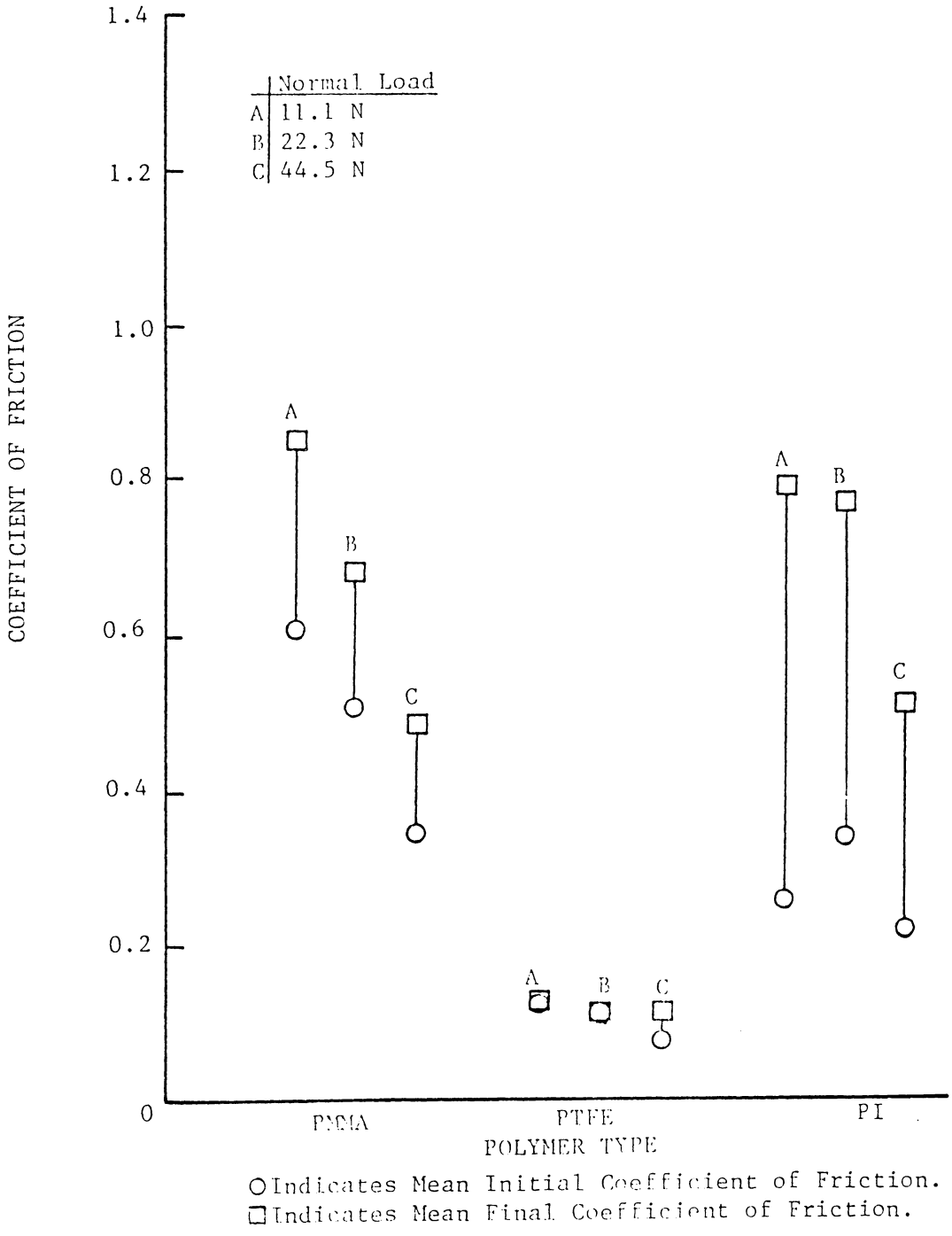

FIGURE 4-9. Range of Coefficient of Friction Prior to Film Failure: Group I Films.

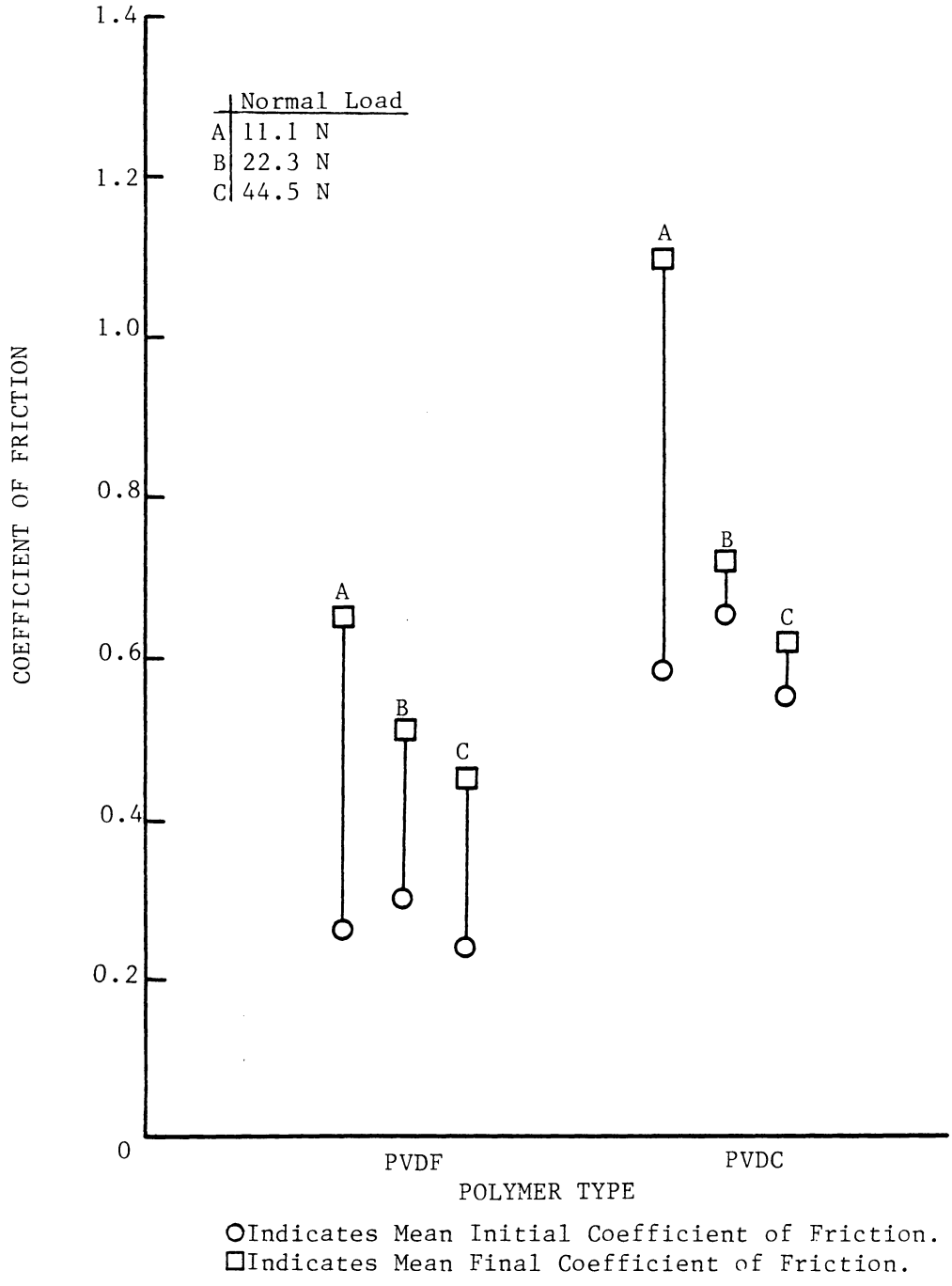

FIGURE 4-10. Range of Coefficient of Friction Prior to Film Failure: Group II Films.

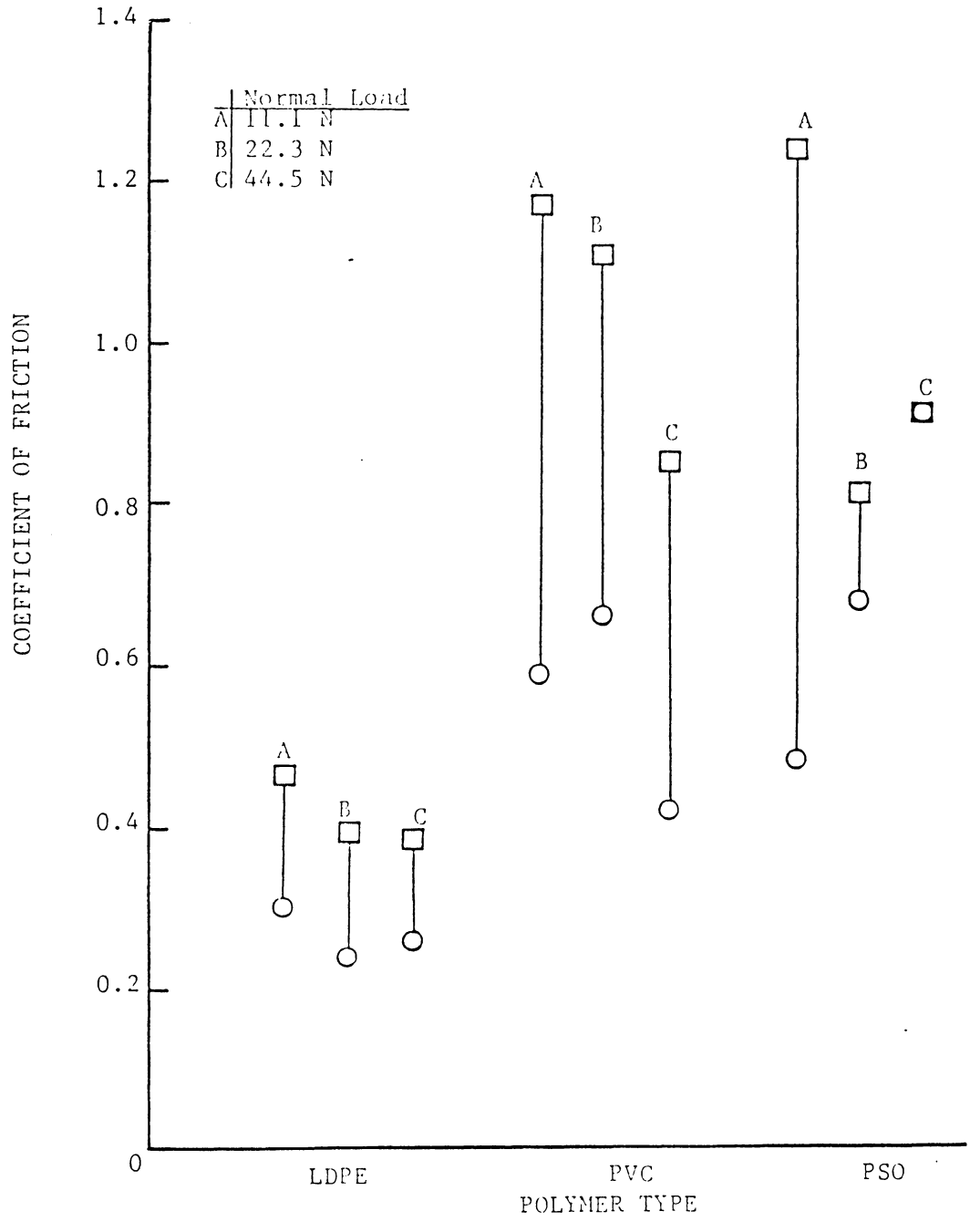

FIGURE 4-11. Range of Coefficient of Friction Prior to Film Failure: Group III Films.

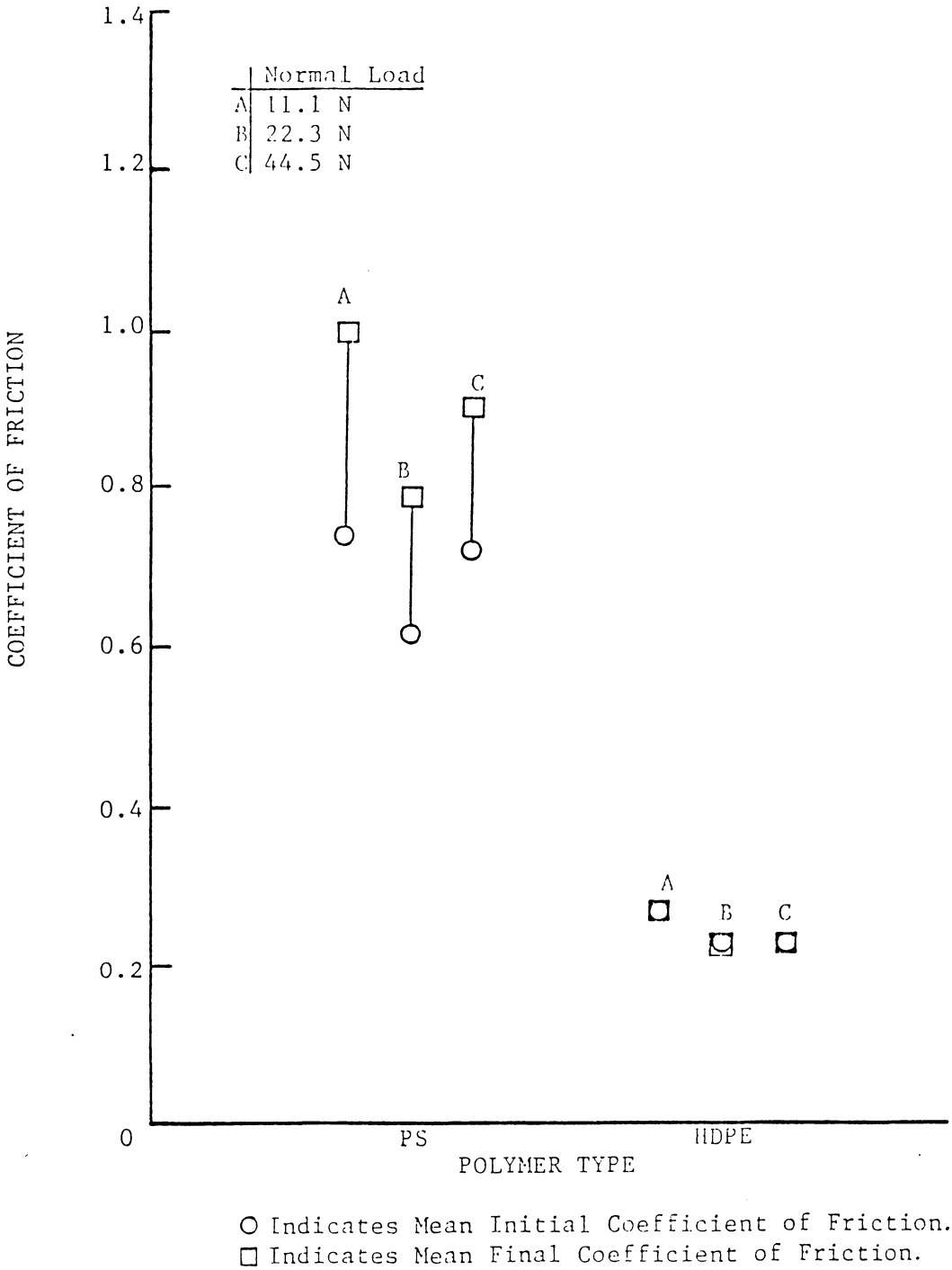

FIGURE 4-12. Range of Coefficient of Friction Prior to Film Failure: Group IV Films.

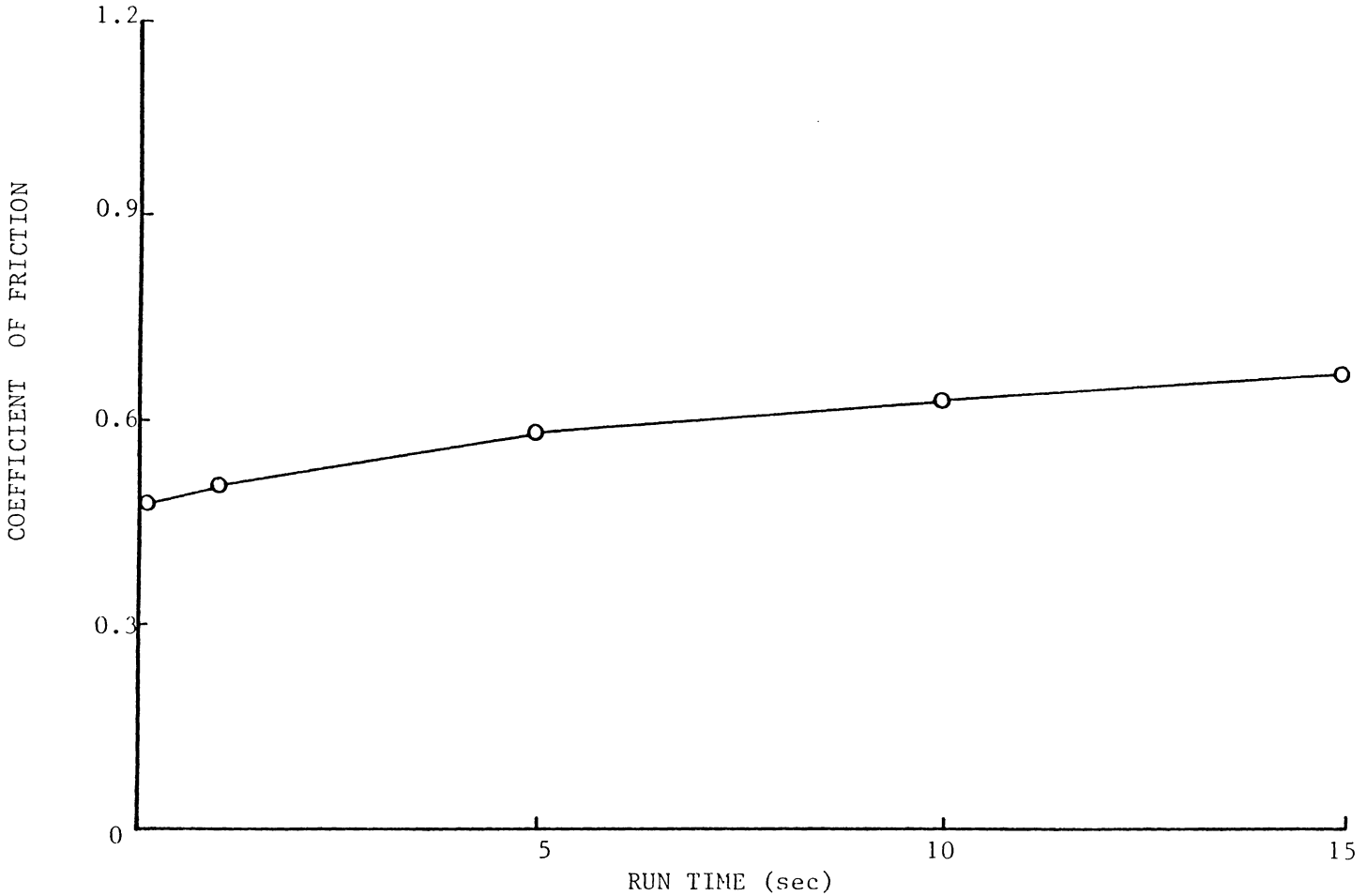

FIGURE 4-13. Frictional Behavior of PMMA at 22.3 N Normal Load.

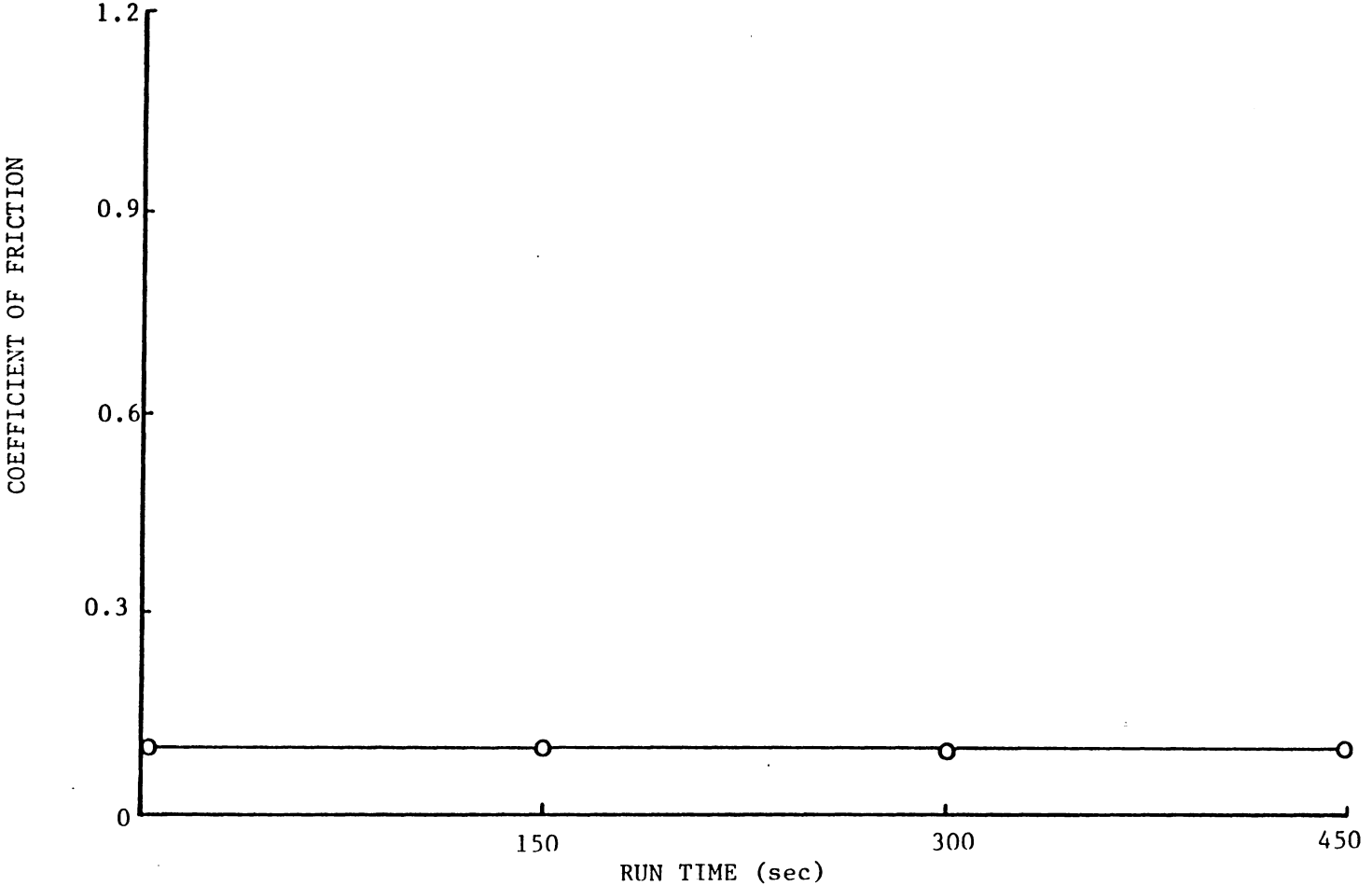

FIGURE 4-14. Frictional Behavior of PTFE at 22.3 N Normal Load.

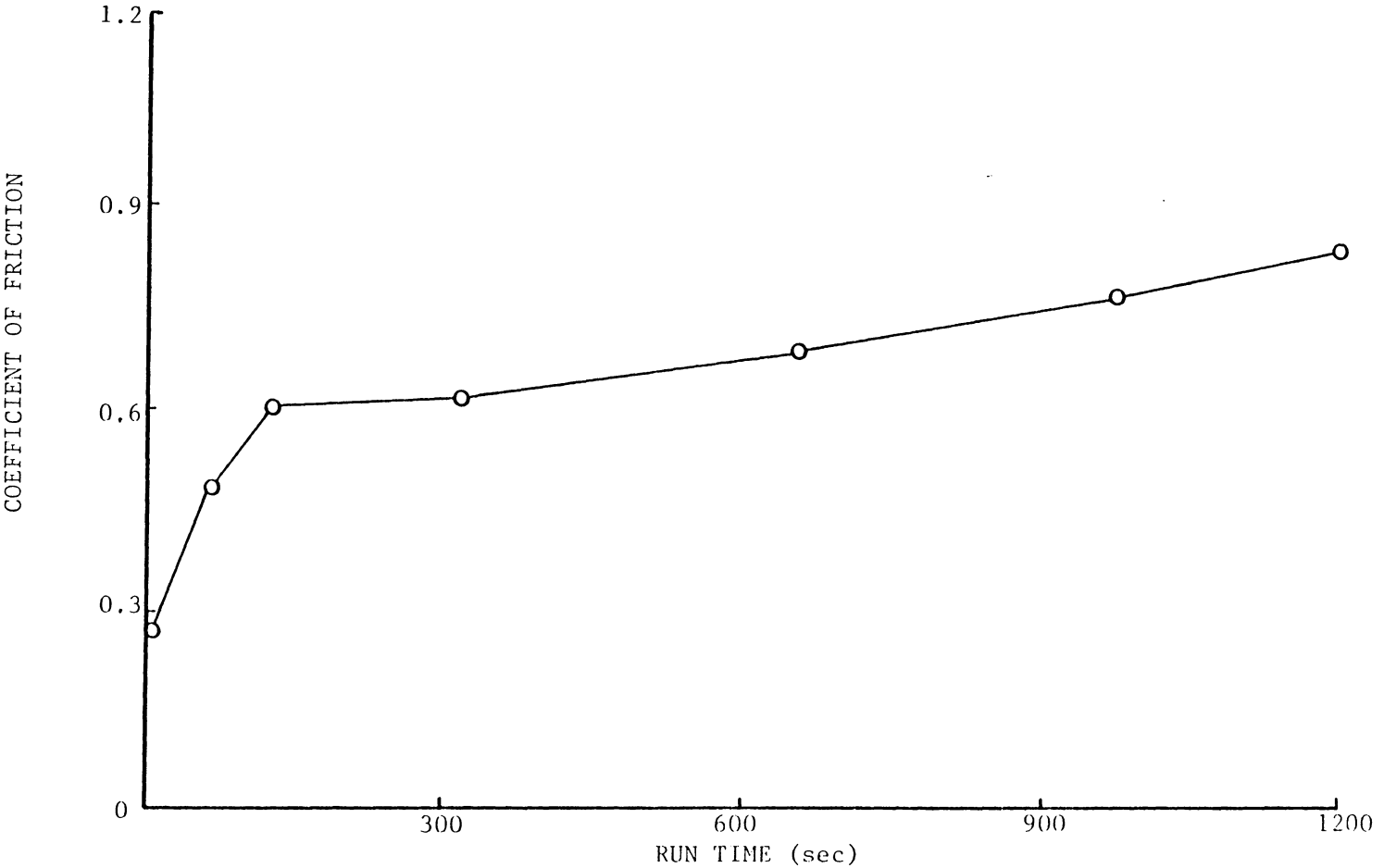

FIGURE 4-15. Frictional Behavior of PI at 22.3 N Normal Load.

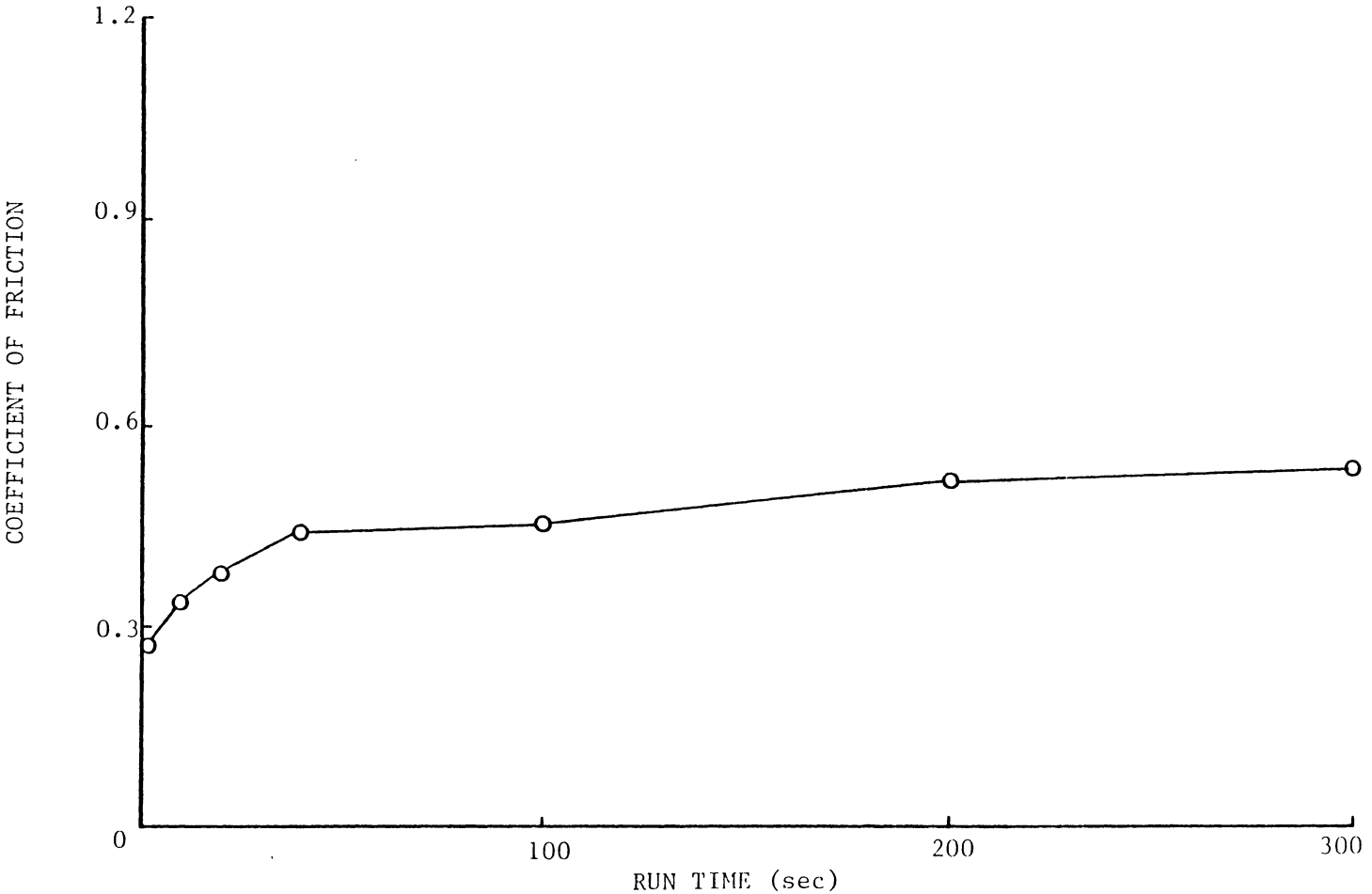

FIGURE 4-16. Frictional Behavior of PVDF at 22.3 N Normal Load.

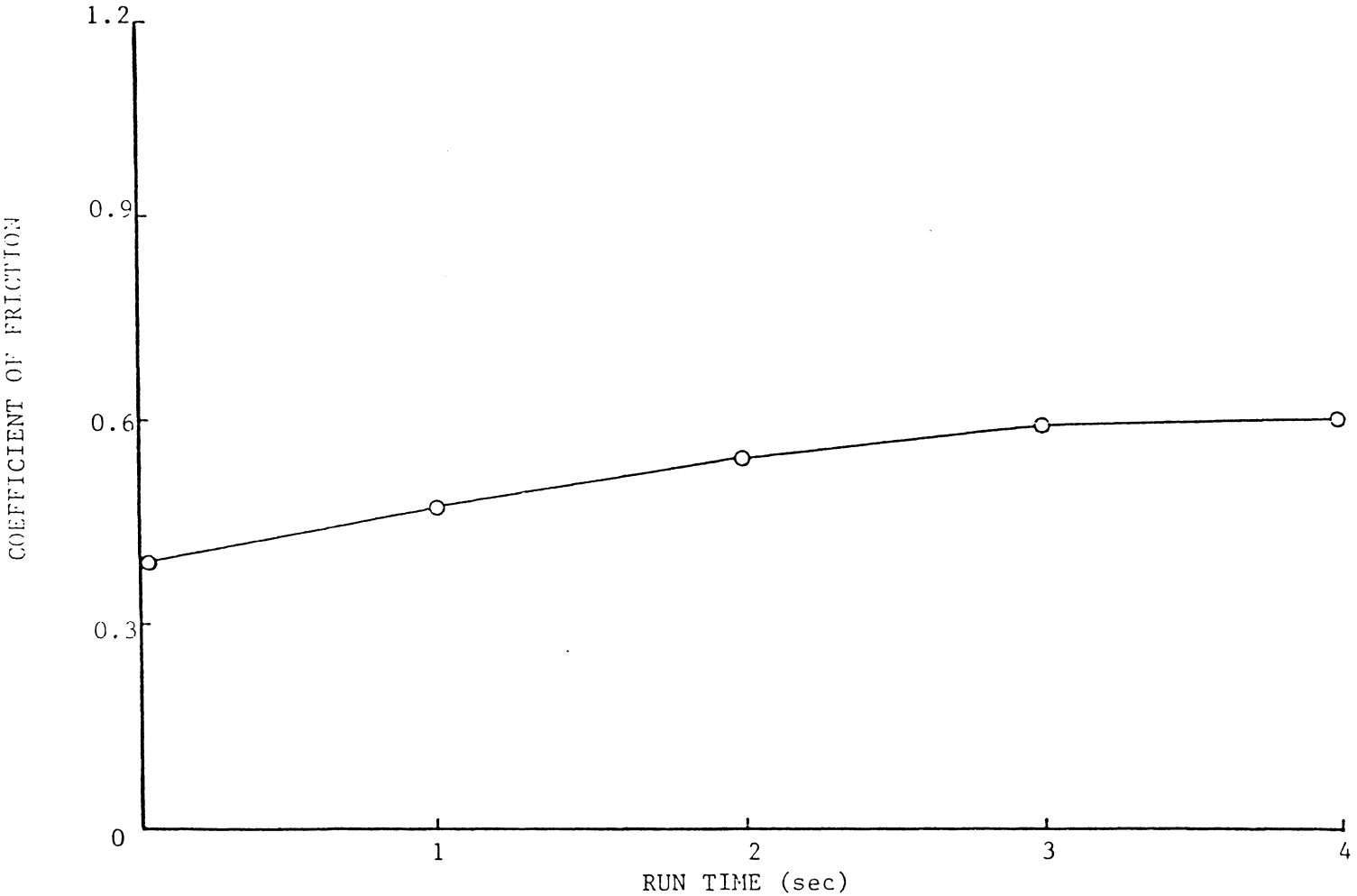

FIGURE 4-17. Frictional Behavior of PVDC at 22.3 N Normal Load.

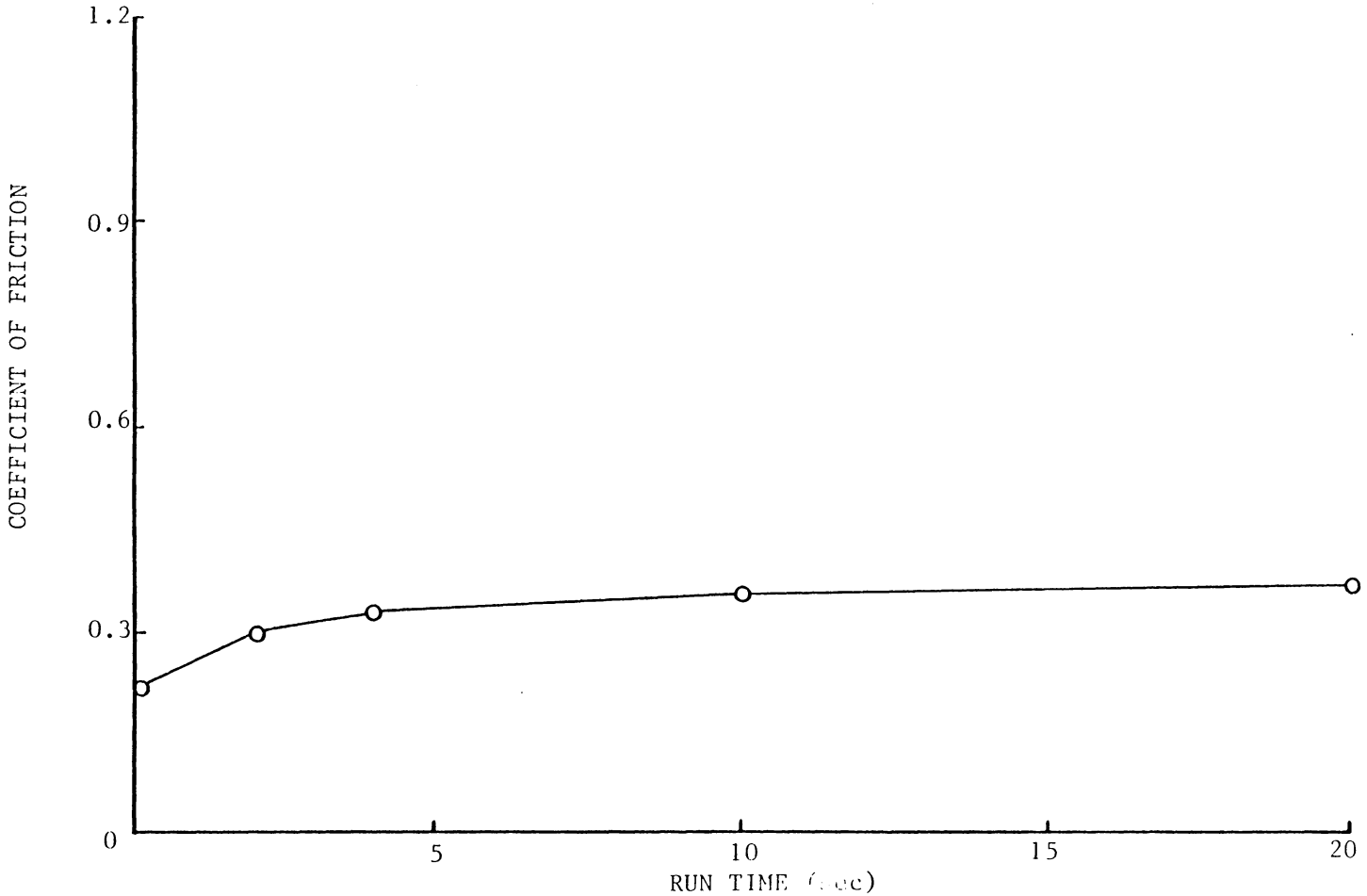

FIGURE 4-18. Frictional Behavior of LDPE at 22.3 N Normal Load.

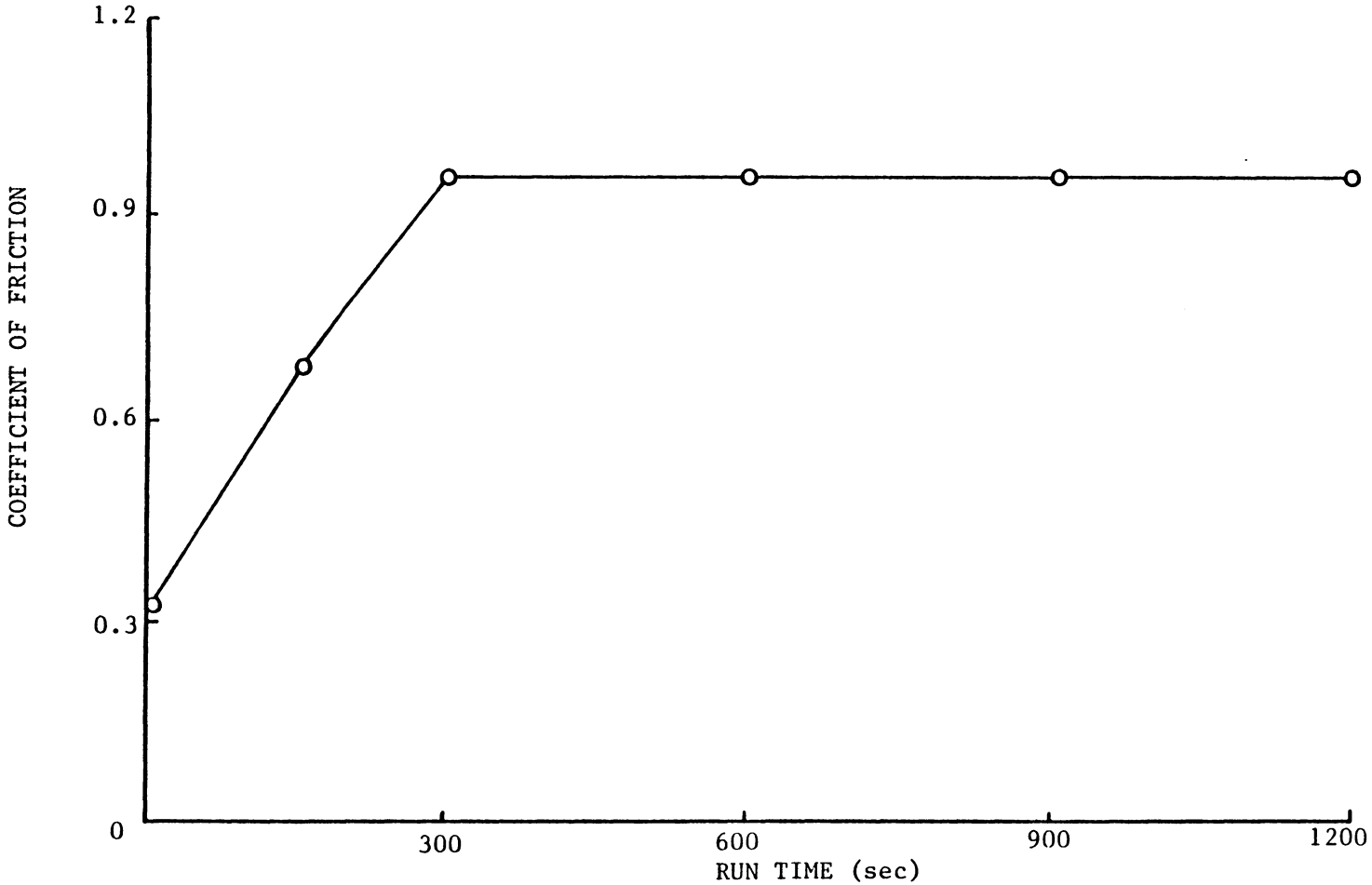

FIGURE 4-19. Frictional Behavior of PVC at 22.3 N Normal Load.

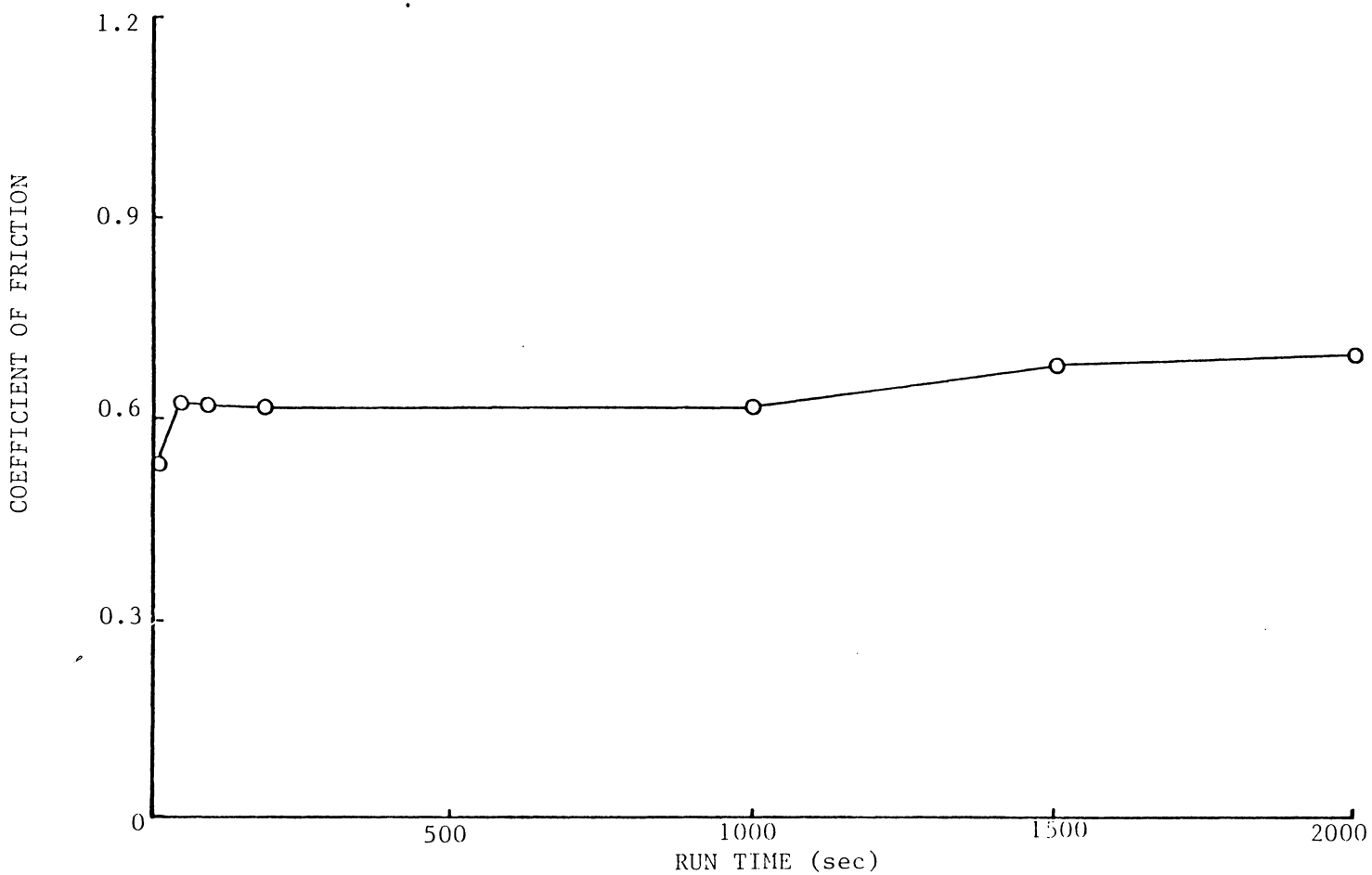

FIGURE 4-20. Frictional Behavior of PSO at 22.3 N Normal Load.

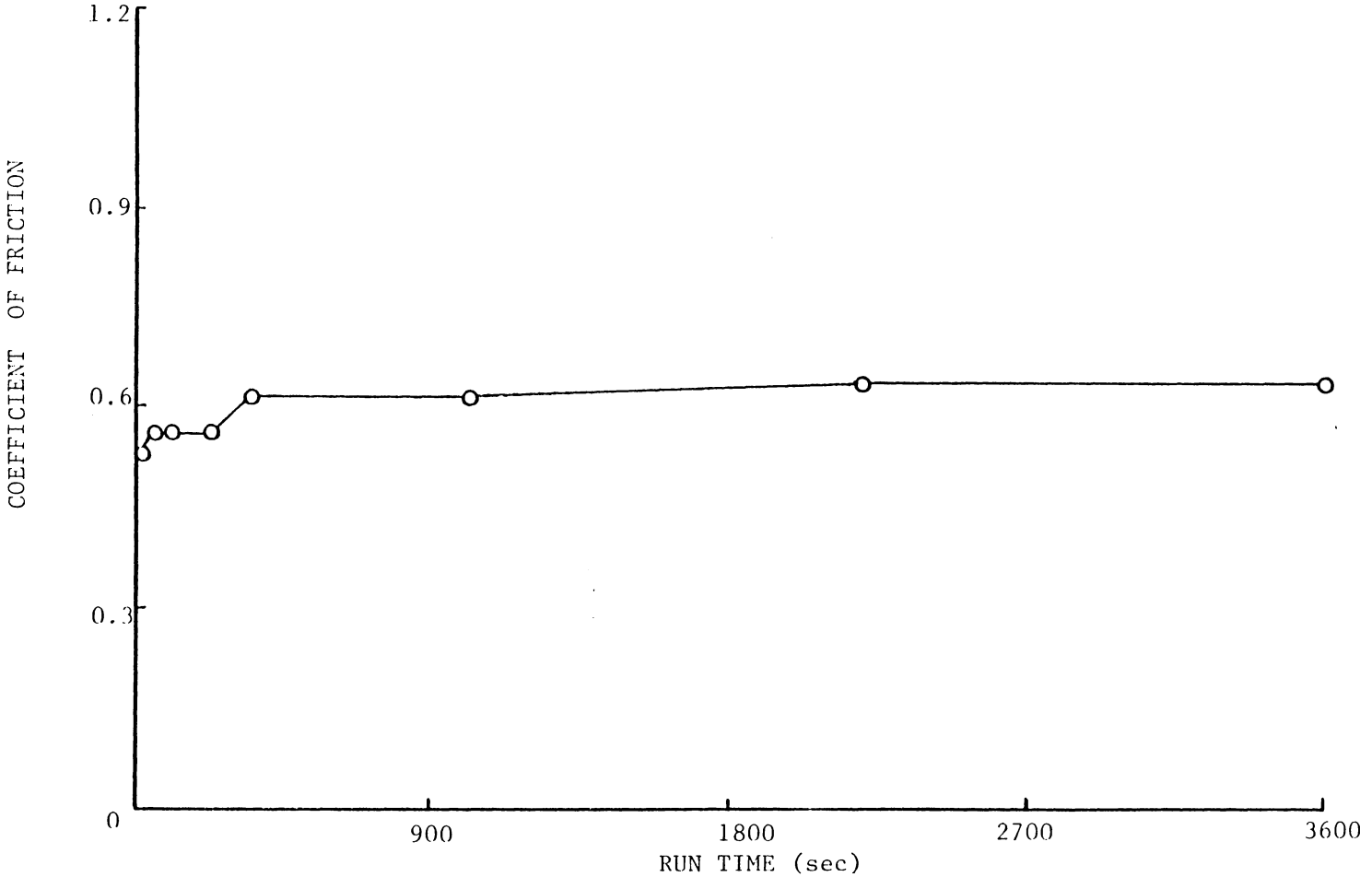

FIGURE 4-21. Frictional Behavior of PS at 22.3 N Normal Load.

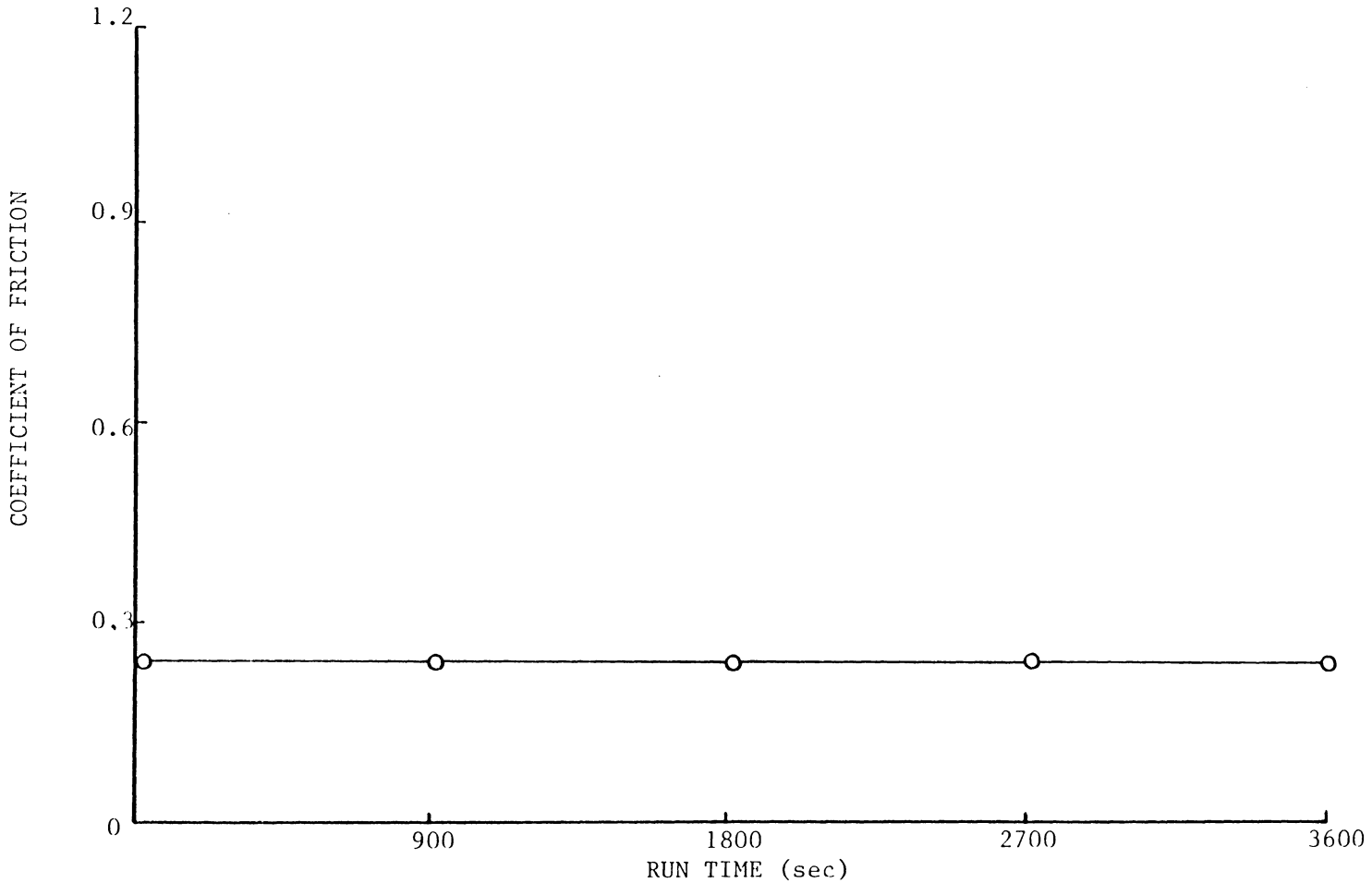

FIGURE 4-22. Frictional Behavior of HDPE at 22.3 N Normal Load.

times were selected to study the fretting behavior at a polymer-steel interface for each of the ten polymers.

4.2.1 Selection of Load

A 22.3 N normal load was selected to observe fretting behavior between the polymer films and steel. This load was chosen for two reasons: 1. the polymer films being evaluated showed a large range of life at 22.3 N; and 2. several of the films would fail during the maximum allowed test time (one hour), thus allowing investigation of the fretting process after the film ceased to prevent metallic contact.

4.2.2 Selection of Run Times

It was decided to run three fretting tests for each polymer, each test having a progressively longer run time. The life data at 22.3 N normal load was used to determine these run times.

Three major considerations entered into the selection of these times. The first consideration was that one of the tests should terminate prior to film failure. The second consideration was that one of the tests should terminate after the film has failed. The final criteria was that, whenever possible, test run times were to be equivalent for polymers with similar lives, allowing for better data comparison.

Table 4-2 shows the run times selected. Test 1 times are those chosen to show pre-failure behavior. Test 3 times show behavior after film failure (if the film had a life of less than one hour). Test 2 times were chosen to fall halfway between Test 1 and Test 3 times. As can be seen, two groups of polymers had identical run times, the first

TABLE 4-2 Fretting Behavior Test Run Times (sec)

Polymer	Test 1	Test 2	Test 3
PMMA	5	33	60
PTFE	30	240	450
PI	900	1800	2700
PVDF	100	500	900
PVDC	5	33	60
LDPE	45	173	300
PVC	900	1800	2700
PSO	900	1800	2700
PS	900	1800	2700
HDPE	900	1800	2700

group consisting of PVC, PI, HDPE, PSO and PS. The second group consisted of PMMA and PVDC.

4.2.3 Contact Status

Table 4-3 shows the state of contact of each fretting test (in Table 4-2) after it was completed. Three types of contact are noted: 1. no metallic contact; 2. intermediate contact; and 3. full contact. Characteristic contact data of all three types of behavior are shown in Figure 4-23.

4.2.4 Fretting Behavior at a Polymer-Steel Interface

After all tests in Table 4-2 were completed, the resulting ball and disk scars were observed and photographed using a Wild 420 Macroscope. Test 1 and Test 3 disk scars were observed and photographed by SEM. The use of color photomacroscopy to provide low magnification color representation of the scars was found to be valuable in identifying possible polymer decomposition and iron oxide. SEM was valued for its high resolution and use at high magnifications. Both methods together provided an excellent representation of the fretting process for each polymer-steel interface.

This section will present the photographic (both SEM and macroscopic) data obtained from the tests in Table 4-2. For all of the polymers except PMMA and PTFE, photographic data from at least two of the three test run times will be presented. Only one of the ball-disk pairs will be presented for PMMA and PTFE due to their short lives. For all of the photographs, the sliding direction is from left to right to

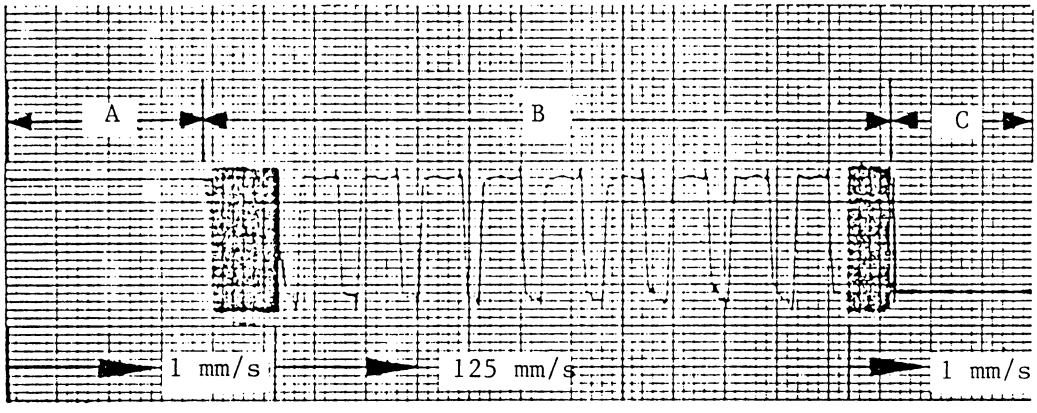

FIGURE 4-23. Characteristic Contact Data. PMMA at 44.5 N Normal Load. A: No Contact Behavior. B: Intermediate Contact Behavior. C: Full Contact Behavior.

Table 4-3 Contact Status

Polymer	Test 1	Test 2	Test 3
PMMA	N	I	I
PTFE	N	I	I
PI	N	I	I
PVDF	N	I	I
PVDC	I	I	I
LDPE	N	F	F
PVC	N	N	F
PSO	N	N	I
PS	N	N	N
HDPE	N	N	N

N = No Metallic Contact
I = Intermediate Metallic Contact
F = Full Metallic Contact

left. In a few of the optical macrographs (Figures 4-57, 4-59, 4-63, 4-67, and 4-69), a green transparent rectangle can be seen in the right end of the photograph. This rectangle has no significance and was caused by a light "leak" through the macroscope binoculars. This "leak" came from the ceiling illumination in the room where the macroscope was located, interfering with the observed image when it entered into the uncapped binoculars and hence the optical system of the macroscope.

Polymethylmethacrylate

Figures 4-24 and 4-25 are the corresponding ball and disk scars for Test 3 (60 seconds run time); the film has failed. A large groove can be seen on the ball (Figure 4-24). A rectangle of transferred material can be seen below the groove. Loose debris, possibly polymer, can be seen scattered around the scar center.

The disk scar (Figure 4-25) is elliptical in shape with polymer being removed from the contact zone at one end. Notice that the removed polymer appears to be still connected to the end of the scar. In the center of the scar, small bright regions can be seen which are areas of exposed metal, indicating that the film has broken through.

Figures 4-26 and 4-27 are scanning electron micrographs of the disk scar which show a more detailed view of the scar surface. The surface appears to be covered with "tears" which are oriented perpendicular to the sliding direction. The largest tears are at the end where polymer is being removed form the interface and are approximately 0.127 mm in length. Figure 4-27 shows the polymer that has been forced out of the contact zone.

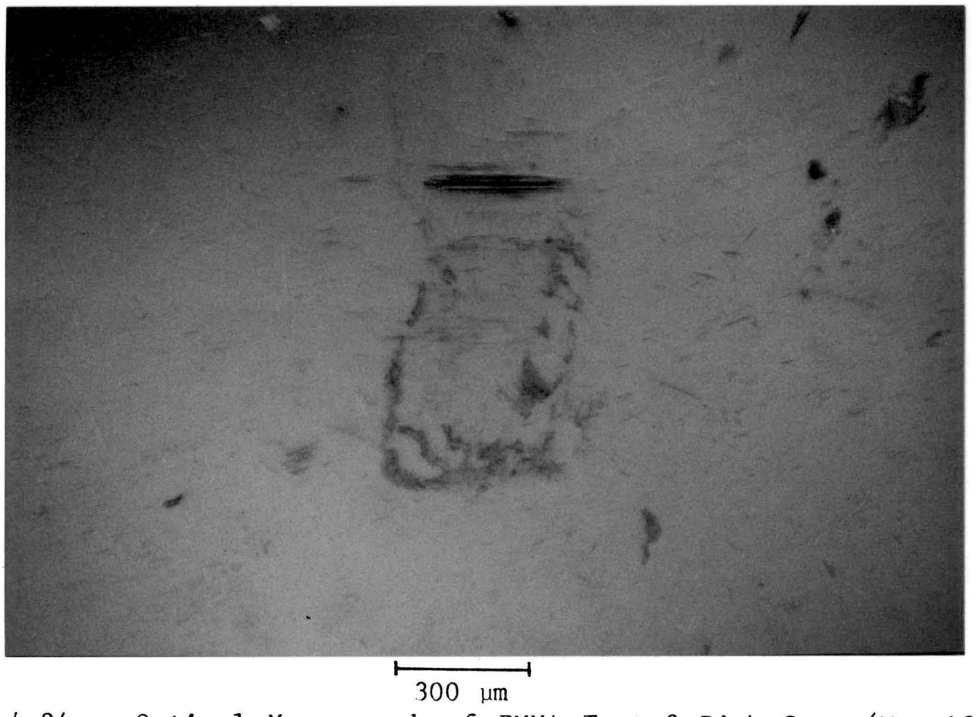

FIGURE 4-24. Optical Macrograph of PMMA Test 3 Disk Scar (Magnification: 60X).

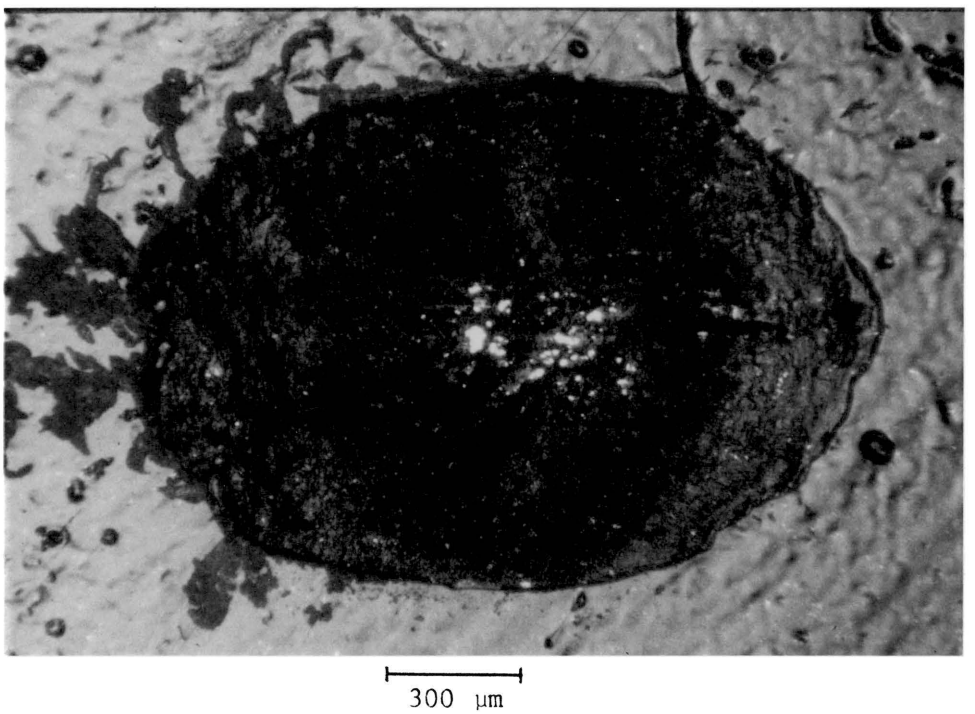

FIGURE 4-25. Optical Macrograph of PMMA Test 3 Disk Scar (Magnification: 60X).

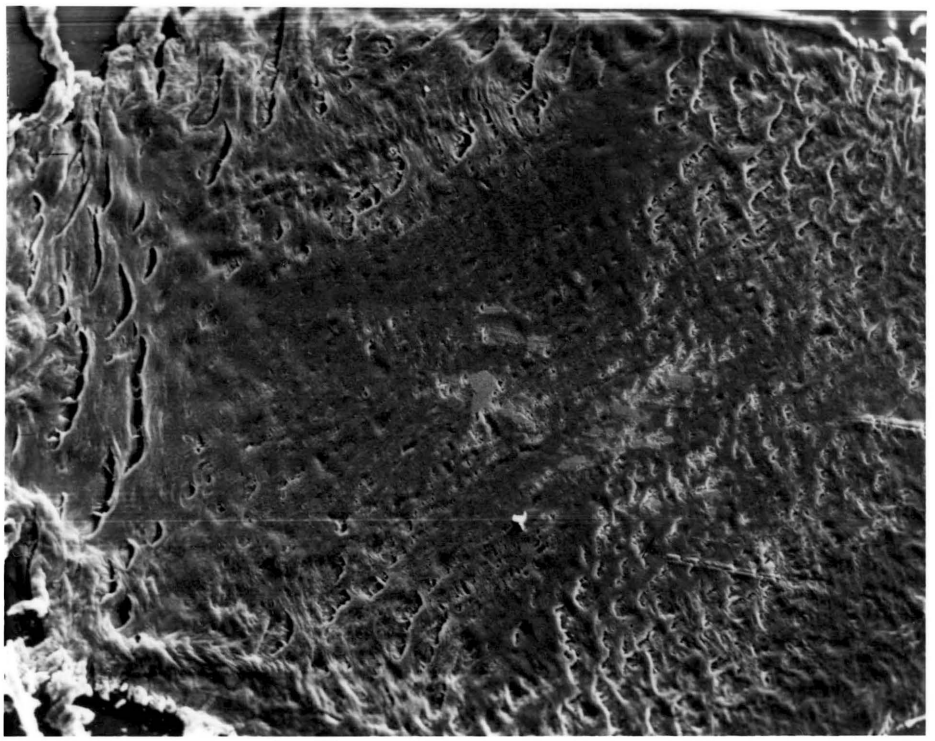

FIGURE 4-26. Scanning Electron Micrograph of PMMA Test 3 Disk Scar (Magnification: 100X).

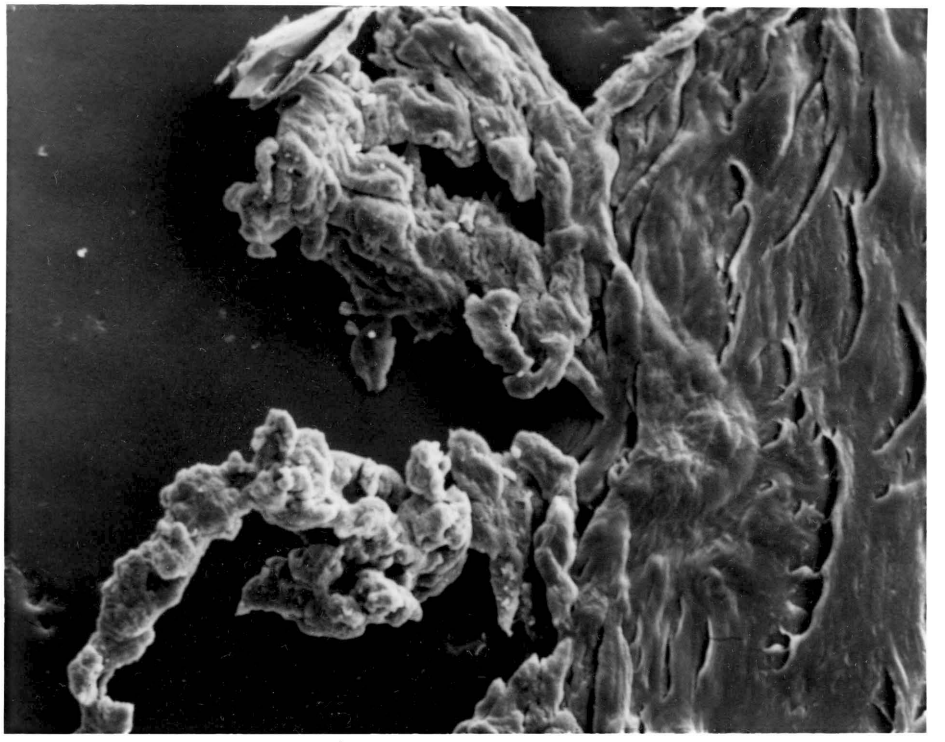

FIGURE 4-27. Scanning Electron Micrograph of PMMA Test 3 Disk Scar End (Magnification: 200X).

Polytetrafluorethylene

Ball and disk scars from Test 3 (450 seconds run time and metallic contact) for PTFE are shown in Figures 4-28 and 4-29. The ball scar, Figure 4-28, has five distinct regions. The outside region contains large amounts of highly reflective polymer debris. The next region is a diamond-shaped annulus which is free of any debris. In the center region of the scar, there appears to be two different types of thin film layers, one brown and the other a light green. The center of the scar shows metal damage due to film failure; both polished and grooved metal can be seen.

Figure 4-29 is the corresponding disk scar. The scar is elliptical in shape and has large amounts of polymer debris which appears to be connected to the scar ends. The central region shows exposed metal and the scar surface appears to be grooved in the sliding direction.

Figures 4-30 and 4-31 are scanning electron micrographs of the disk scar. The debris at each end of the scar appears to be in the form of thin sheets of polymer. Figure 4-31 is a high magnification photograph of one end of the scar which shows the thin folds of polymer debris. Small debris particles can be seen within the scar.

Polyimide

Figures 4-32 and 4-33 are ball and disk scars from Test 1 (15 minutes run time, no metallic contact). The ball (Figure 4-32) shows a large "block" of polymer transfer. The darker regions of the transferred film are thicker than the light regions.

The optical macrograph of the corresponding disk scar shows its almost rectangular shape and matches the transferred polymer on the ball

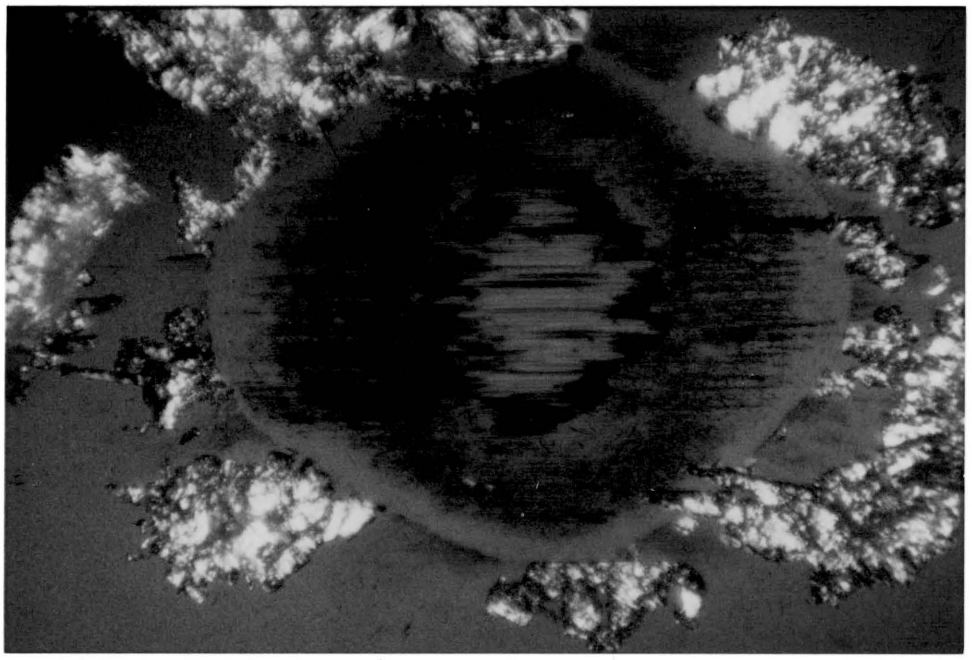

FIGURE 4-28. Optical Macrograph of PTFE Test 3 Ball Scar (Magnification: 60X).

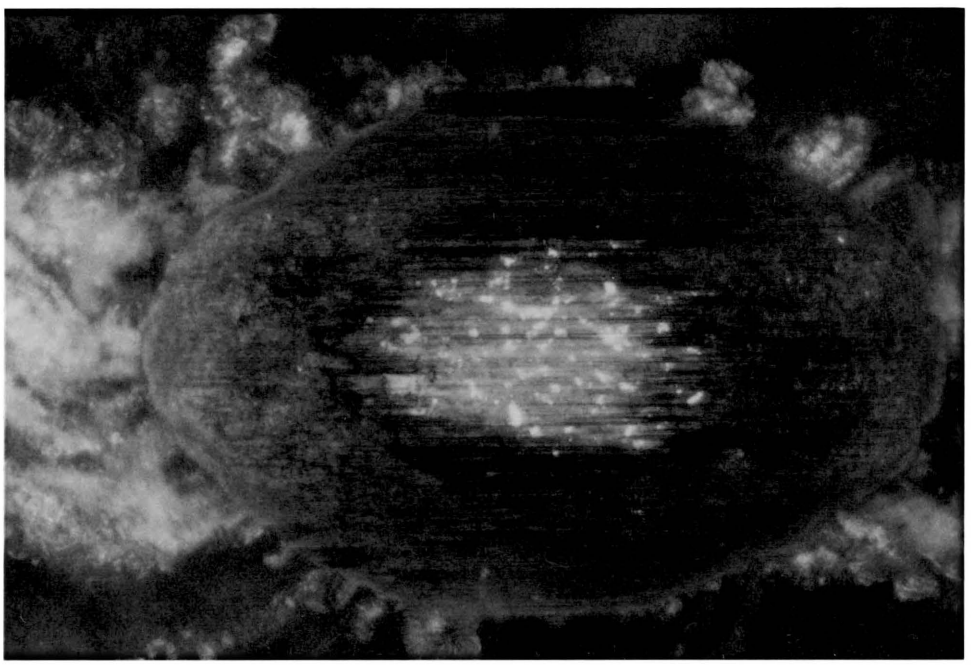

FIGURE 4-29. Optical Macrograph of PTFE Test 3 Disk Scar (Magnification: 60X).

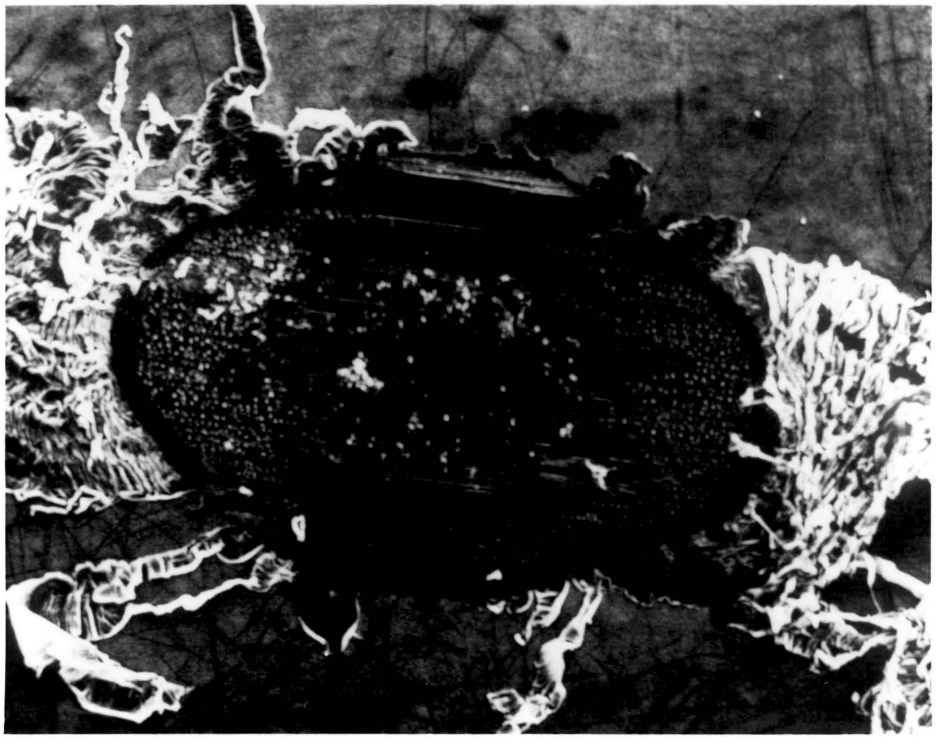

FIGURE 4-30. Scanning Electron Micrograph of PTFE Test 3 Disk Scar (Magnification: 50X).

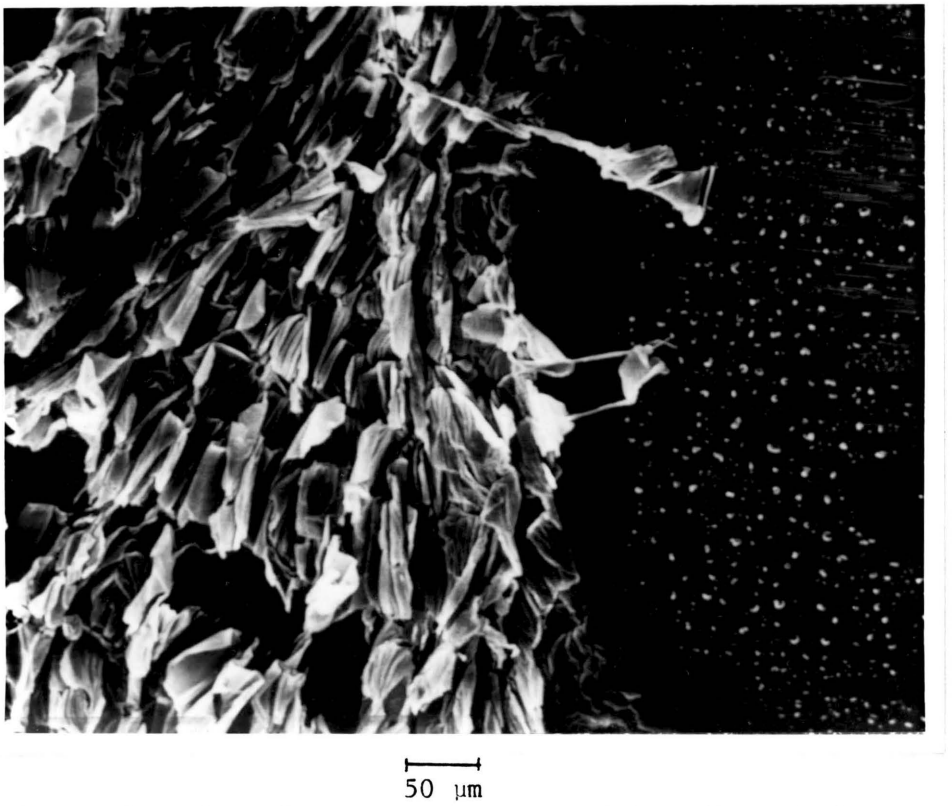

FIGURE 4-31. Scanning Electron Micrograph of PTFE Test 3 Disk Scar End (Magnification: 200X).

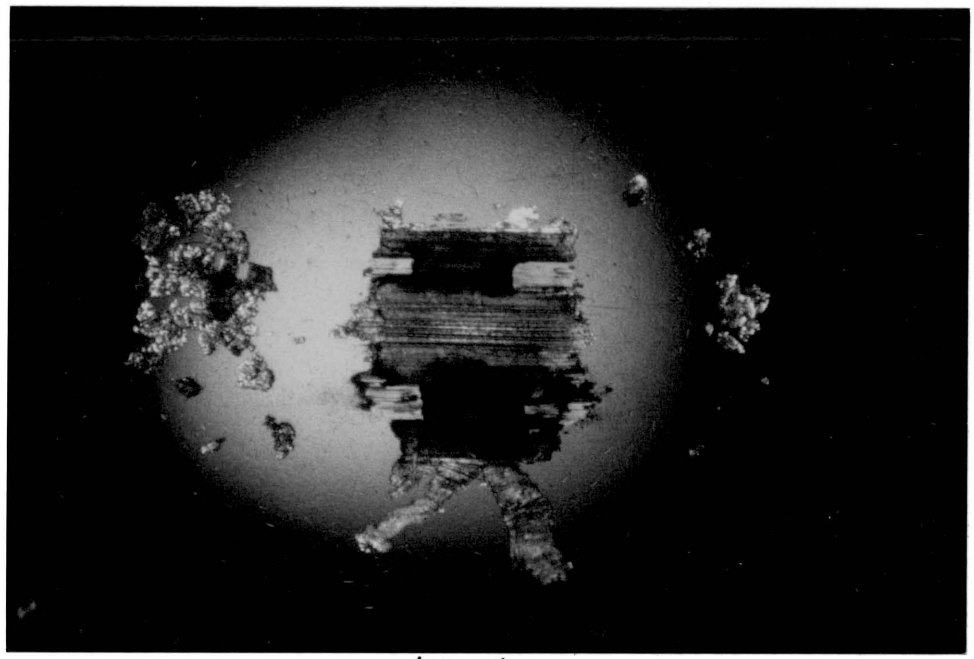

FIGURE 4-32. Optical Macrograph of PI Test 1 Ball Scar (Magnification: 37.5X).

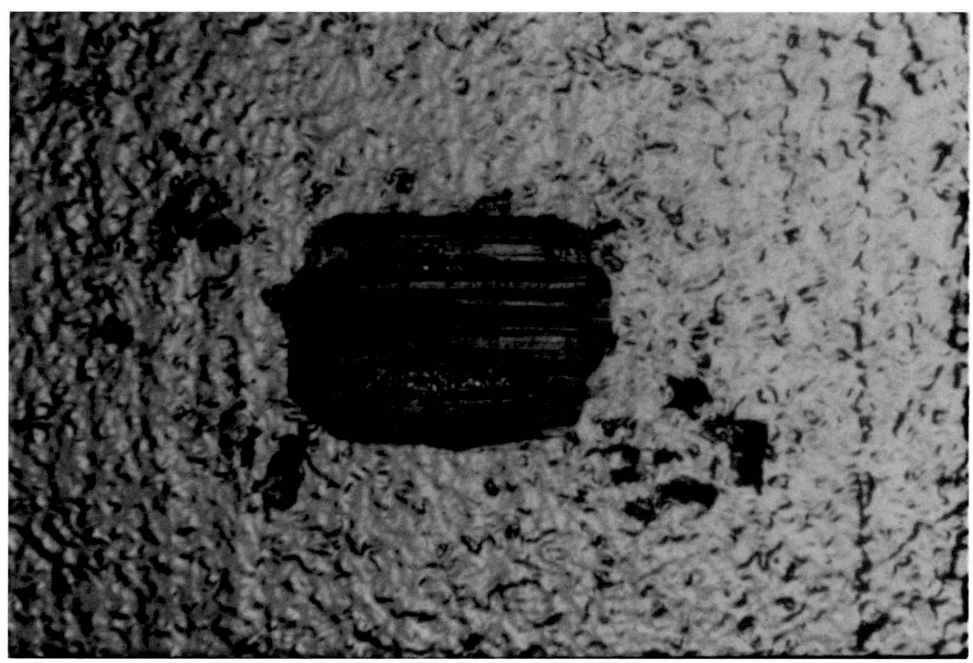

FIGURE 4-33. Optical Macrograph of PI Test 1 Disk Scar (Magnification: 37.5X).

(Figure 4-32). Polymer debris can be seen scattered around the scar. At the top and bottom of the scar, small dots of reflective material can be seen.

Figures 4-34 and 4-35 are scanning electron micrographs of the disk scar which show the uneven nature of the polymer that has been removed from the disk. These photographs also permit identification of the small areas of reflective material seen in the optical macrographs. A match of SEM photographs of an uncoated disk surface to the light regions in Figure 4-35 shows that a sufficient layer of polymer has been removed to expose the disk substrate. Large grooves can also been seen along the length of the scar in the polymer.

The ball and disk scars for Test 3 (45 minutes run time, metallic contact) are shown in Figures 4-36 and 4-37. The ball (Figure 4-36) shows extensive damage with areas of polished metal and reddish brown and black debris. Fine reddish brown material can be seen scattered around the central damaged region. Small yellow fragments of polymer debris can also be seen around the periphery of the scarred region.

Figure 4-37 shows the disk scar corresponding to Figure 4-36. The scar is more elliptical in shape than the Test 1 disk scar (Figures 4-32 and 4-33) and shows areas of exposed, polished metal. Large amounts of fine reddish brown and orange debris can be seen at both ends of the scar on the polymer surface.

Polyvinylidene fluoride

Figures 4-38 and 4-39 are PVDF ball and disk scars from Test 1 (100 seconds run time, no contact). Random-sized debris particles, possibly polymer, are at the top and bottom of the ball scar. The central region

FIGURE 4-34. Scanning Electron Micrograph of PI Test 1 Disk Scar (Magnification: 50X).

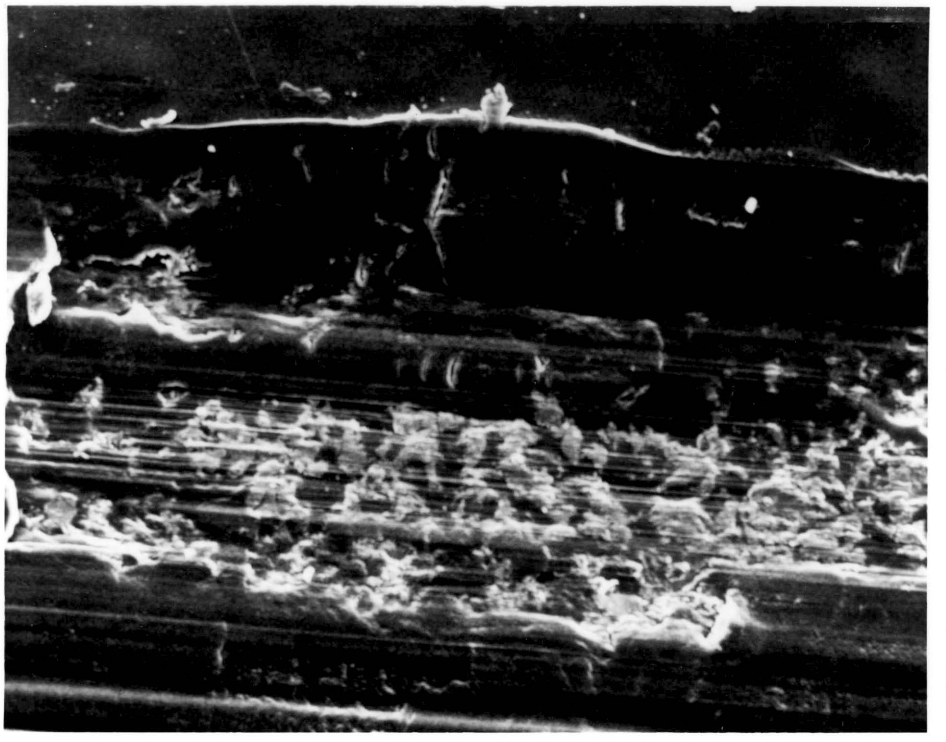

FIGURE 4-35. Scanning Electron Micrograph of PI Test 1 Disk Scar (Magnification: 200X).

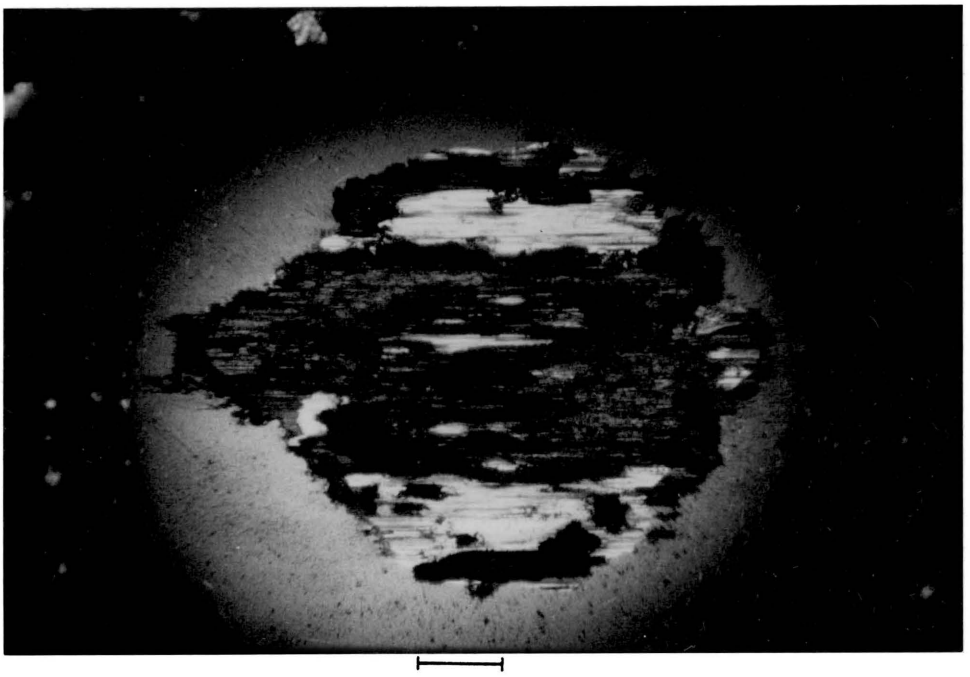

FIGURE 4-36. Optical Macrograph of PI Test 3 Ball Scar (Magnification: 37.5X).

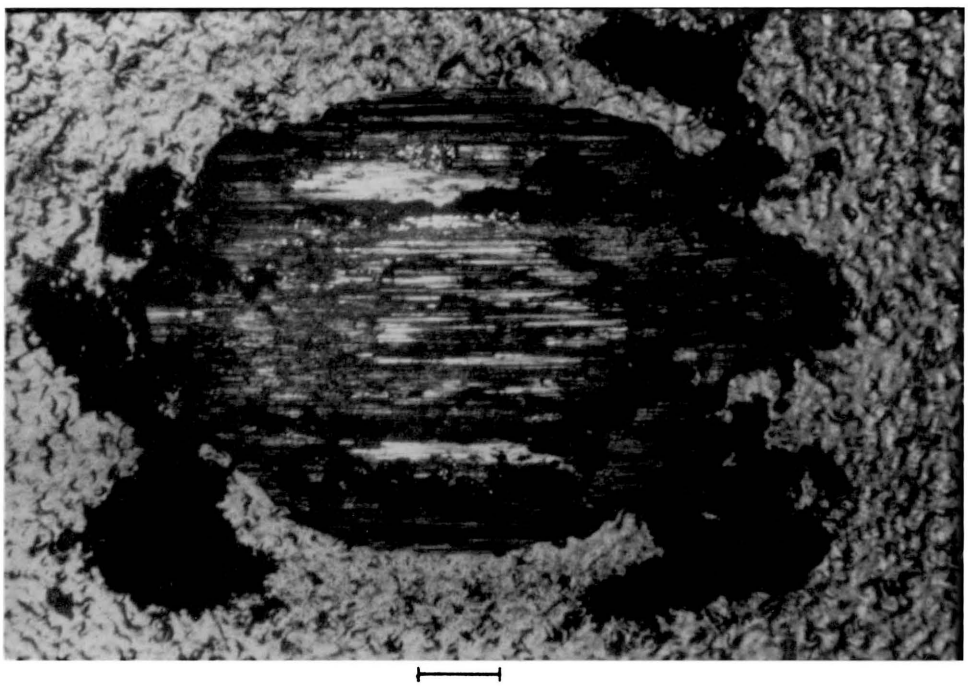

FIGURE 4-37. Optical Macrograph of PI Test 3 Disk Scar (Magnification: 37.5X).

of the scar shows lines of thin, transferred material. The ball does not appear to be damaged.

The disk scar is almost perfectly elliptical in shape. Polymer removed from the scar can be seen at both ends of the scar. The polymer debris at each end appears to be attached to the end of the scar and is intact. The central region of the scar appears to have some grooving in the sliding direction.

Figure 4-40 is a scanning electron micrograph of the top edge of the Test 1 disk scar. The scar surface is definitely grooved and also has numerous small cavities, more concentrated at the center. Small fibers of polymer can be seen at the scar edge. Scattered debris can be seen on the undamaged surface at the top of the photograph.

Figure 4-41 shows the polymer debris at the end of the scar. The debris has a layered appearance in contrast to the scar surface (to the left) which is relatively smooth.

Test 3 (15 minute run time, metallic contact) ball and disk scars are shown in Figures 4-42 and 4-43. The ball scar has a very distinct pattern. At the top and bottom of the scar, small fibers of polymer can be seen. The central region of the scar has an elongated, almost rectangular area containing a circular damaged region at the center. Brownish red debris can be seen within the scarred area. Semicircular regions of a thin layer of brown material are located at the top and bottom of the scar.

The disk scar shows that the end debris is far less intact than the scar of Test 1. A large region of exposed metal can be seen at the scar center. Two bands of brown material are also present on the exposed

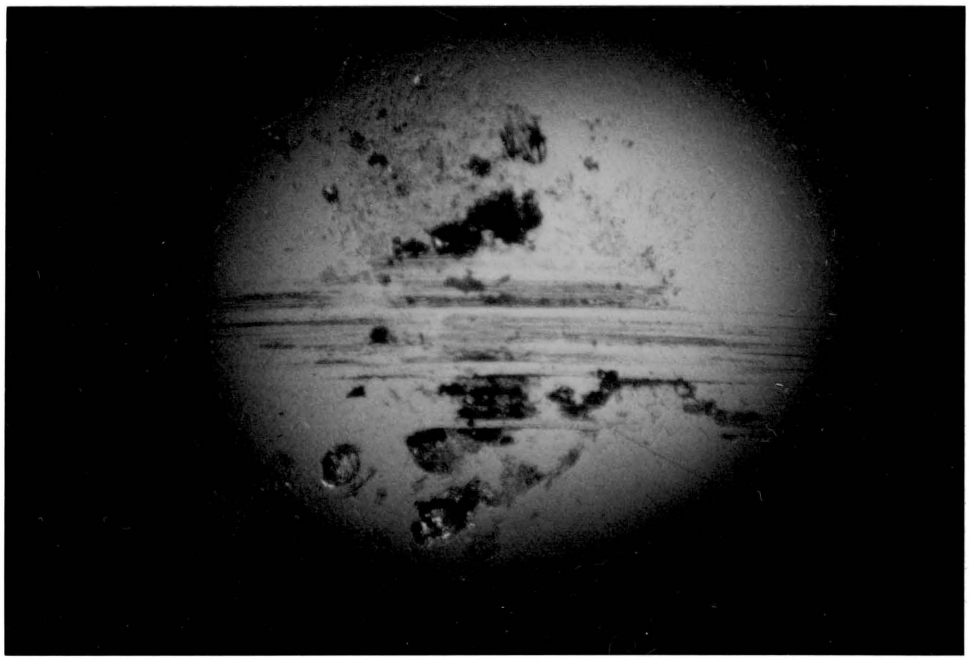

FIGURE 4-38. Optical Macrograph of PVDF Test 1 Ball Scar (Magnification: 37.5X).

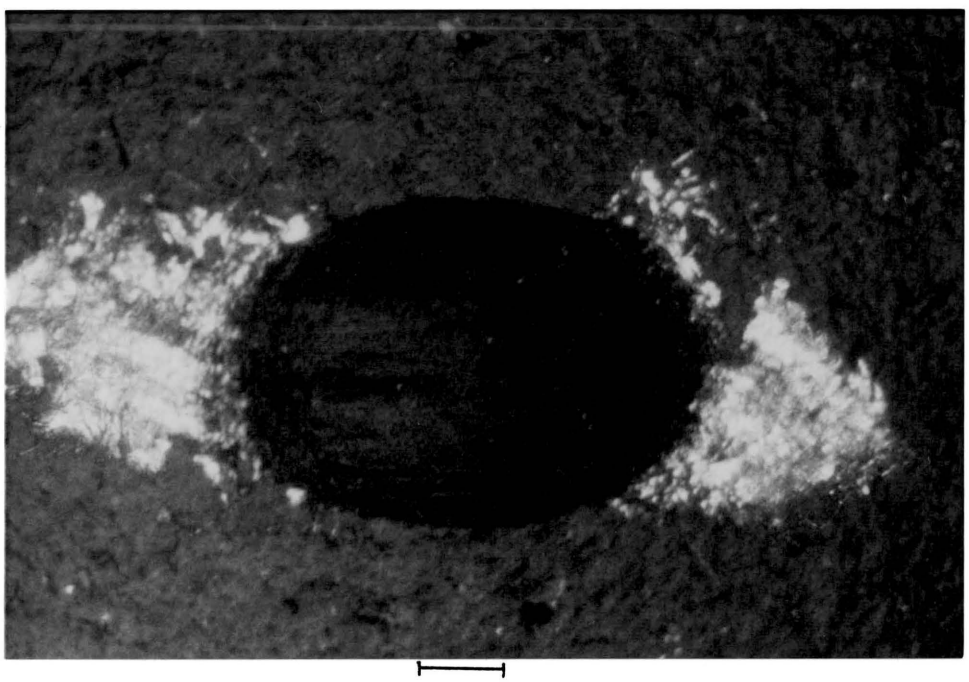

FIGURE 4-39. Optical Macrograph of PVDF Test 1 Disk Scar (Magnification: 37.5X).

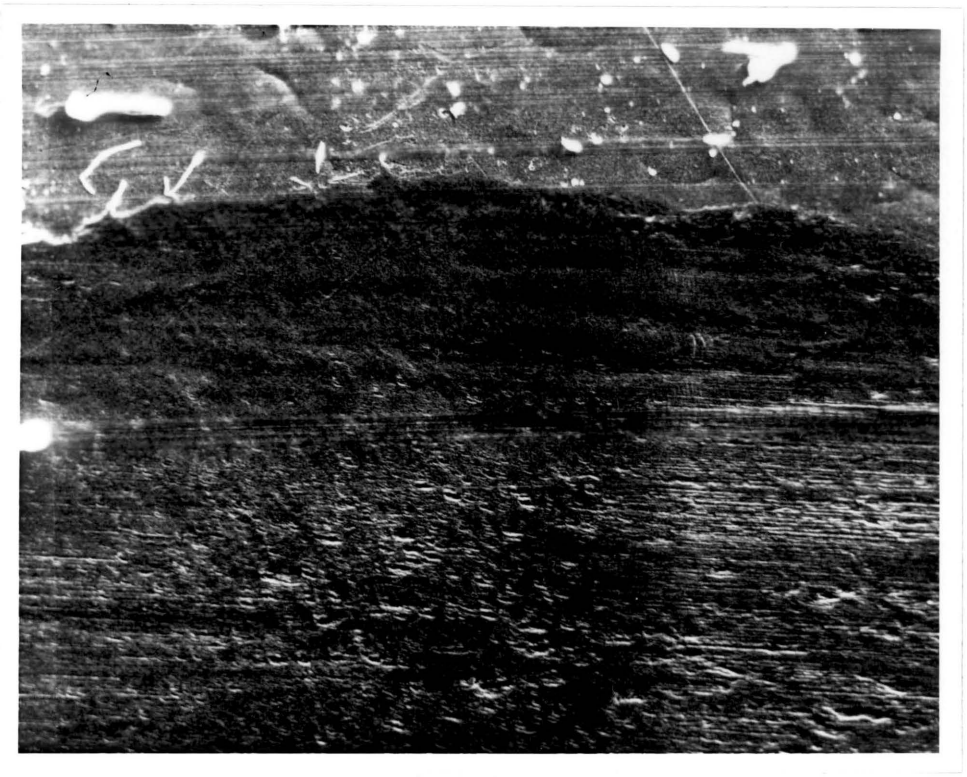

FIGURE 4-40. Scanning Electron Micrograph of PVDF Test 1 Disk Scar (Magnification: 200X).

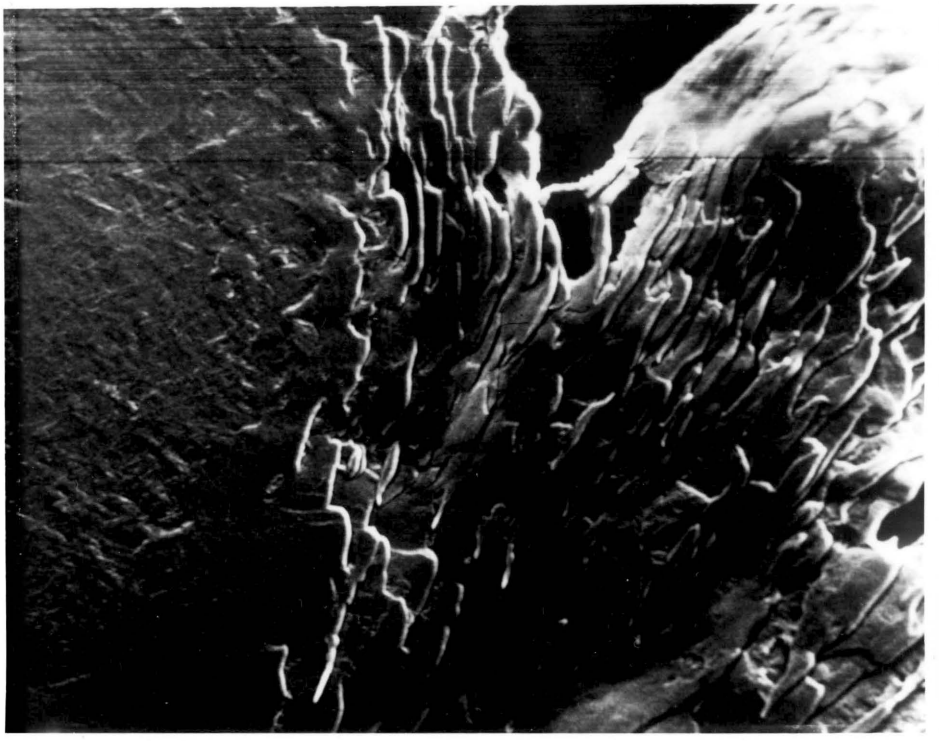

FIGURE 4-41. Scanning Electron Micrograph of PVDF Test 1 Polymer Debris (Magnification: 200X).

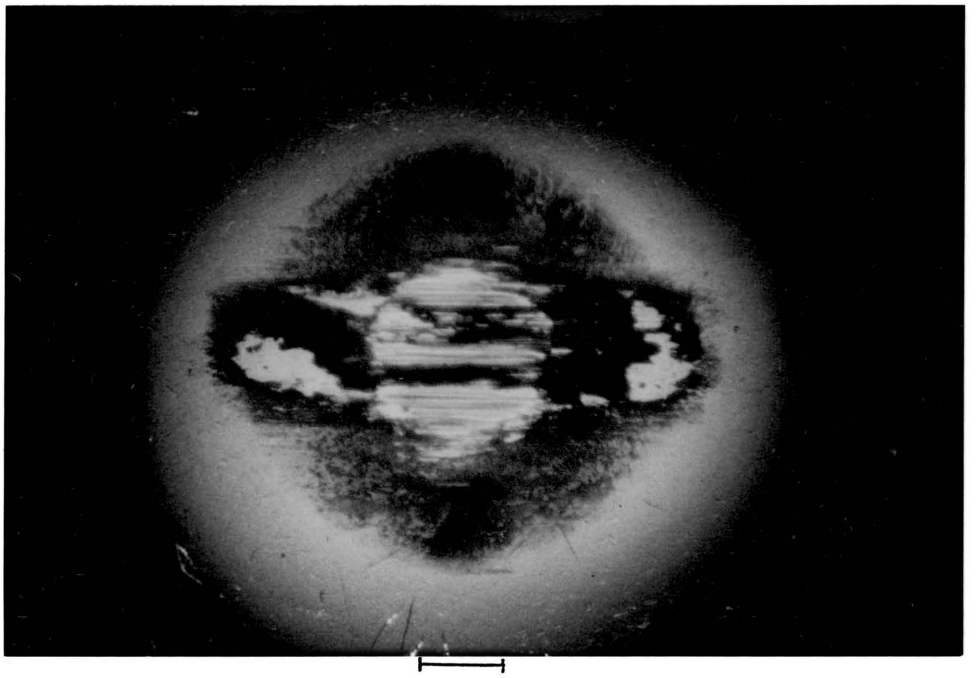

FIGURE 4-42. Optical Macrograph of PVDF Test 3 Ball Scar (Magnification: 37.5X).

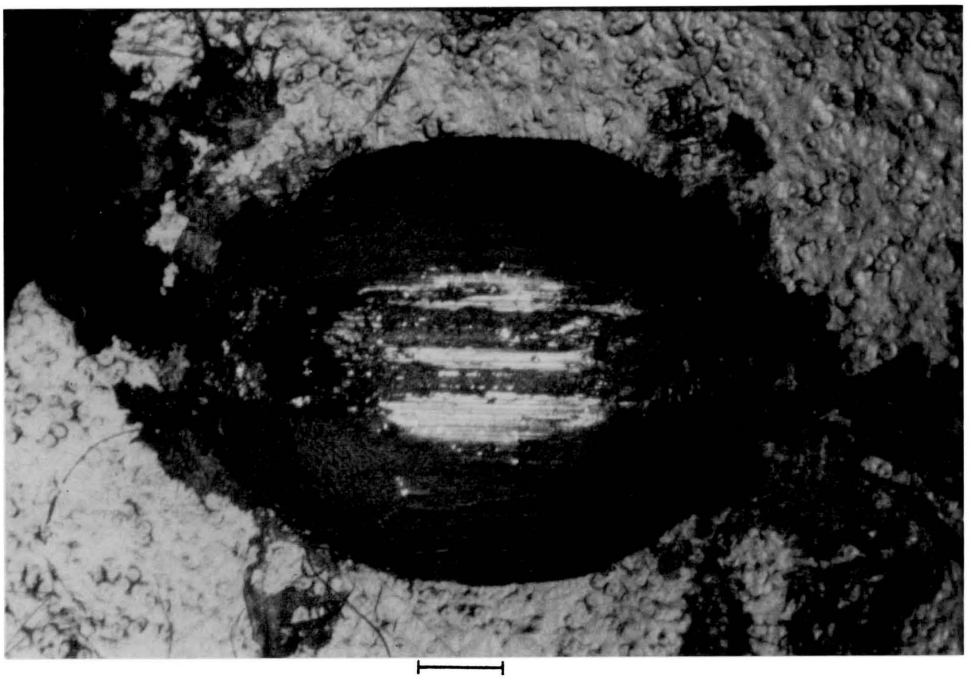

FIGURE 4-43. Optical Macrograph of PVDF Test 3 Disk Scar (Magnification: 37.5X).

metal. Also note that the scarred area is larger than the Test 1 scar, indicating more penetration.

Polyvinylidene chloride

Test 1 ball and disk scars (5.0 seconds run time, metallic contact) are presented in Figures 4-44 and 4-45. The ball scar is covered with small brown deposits and has a shape similar to the disk scar (note that the ball scar is presented at a higher magnification). A small groove can be seen in the ball just above the center of the scar. Scratches can be seen at the left end of the scar.

The disk scar is fairly elliptical in shape and polymer that has been removed from the interface can be seen at each end of the scar. At the right of the scar a "roll" of polymer debris can be seen. Also note the peculiar structure of the polymer surface. Figure 4-46 is a SEM photograph of the disk scar which shows the detail of the scar surface. The scar interior has a rough texture, being slightly smoother at the center region. The indented region of the scar appears to be slightly larger than the roughened region. Stretch marks can be seen at the ends of the scar on the periphery. Figure 4-47 is a higher magnification photograph of one of the scar ends.

Figure 4-48 is an optical macrograph of the ball scar for Test 3 (60 seconds run time, metallic contact). The brown deposits appear to be larger and more concentrated at the scar ends. An almost rectangular region, containing fewer brown deposits, can be seen in the center of the scar. A few grooves can be seen on the steel in the center of the scar.

The corresponding Test 3 disk scar shown in Figure 4-49 is more

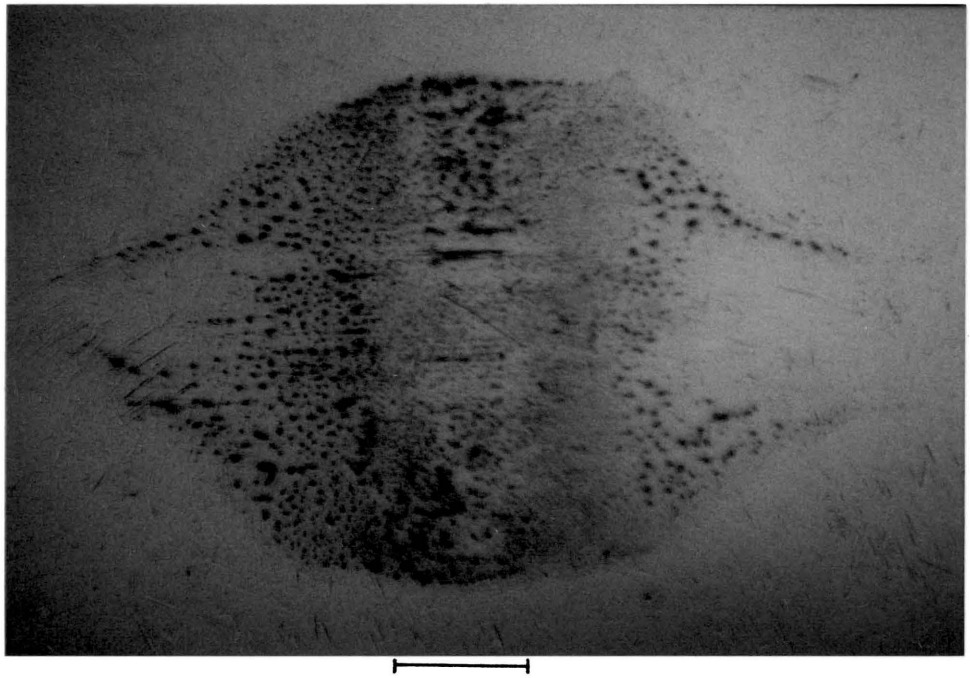

FIGURE 4-44. Optical Macrograph of PVDC Test 1 Ball Scar (Magnification: 60X).

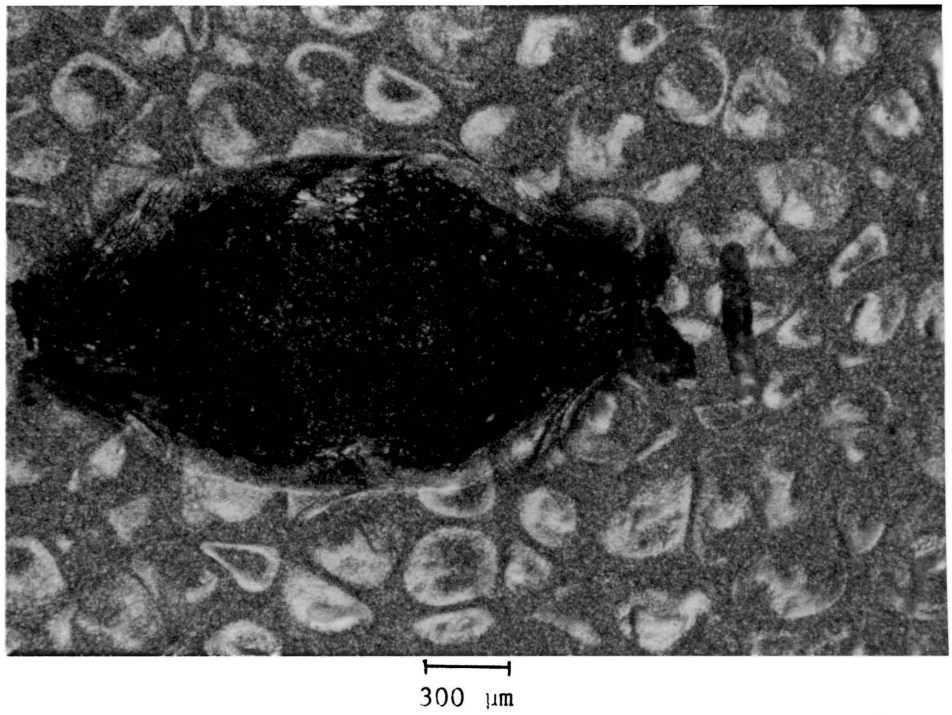

FIGURE 4-45. Optical Macrograph of PVDC Test 1 Disk Scar (Magnification: 37.5X).

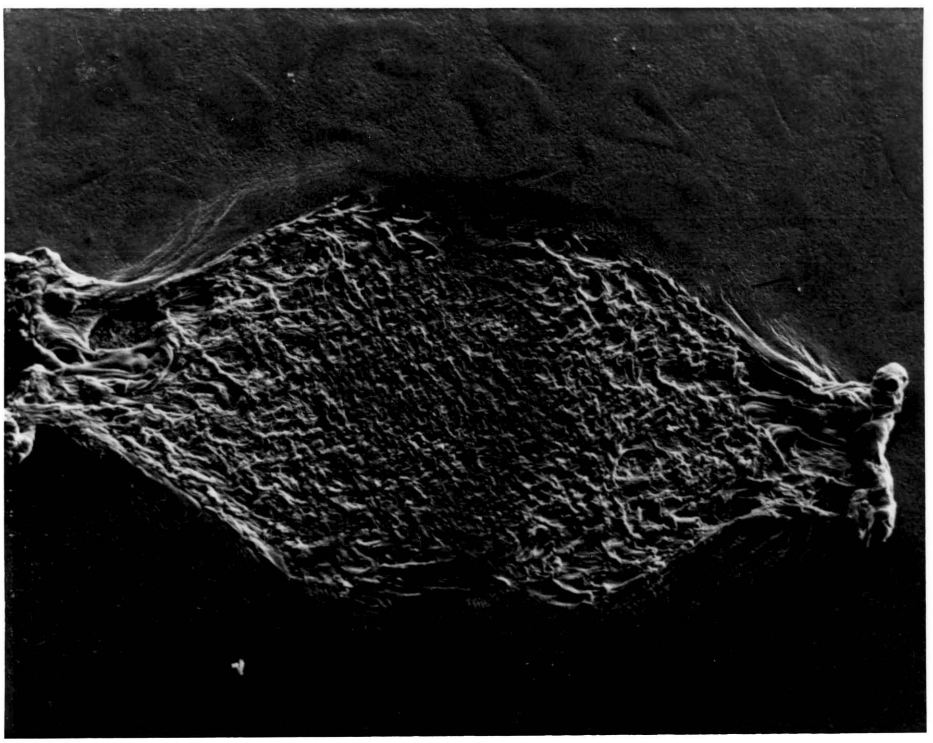

FIGURE 4-46. Scanning Electron Micrograph of PVDC Test 1 Disk Scar (Magnification: 50X).

50 μm

FIGURE 4-47. Scanning Electron Micrograph of PVDC Test 1 Disk Scar (Magnification: 200X).

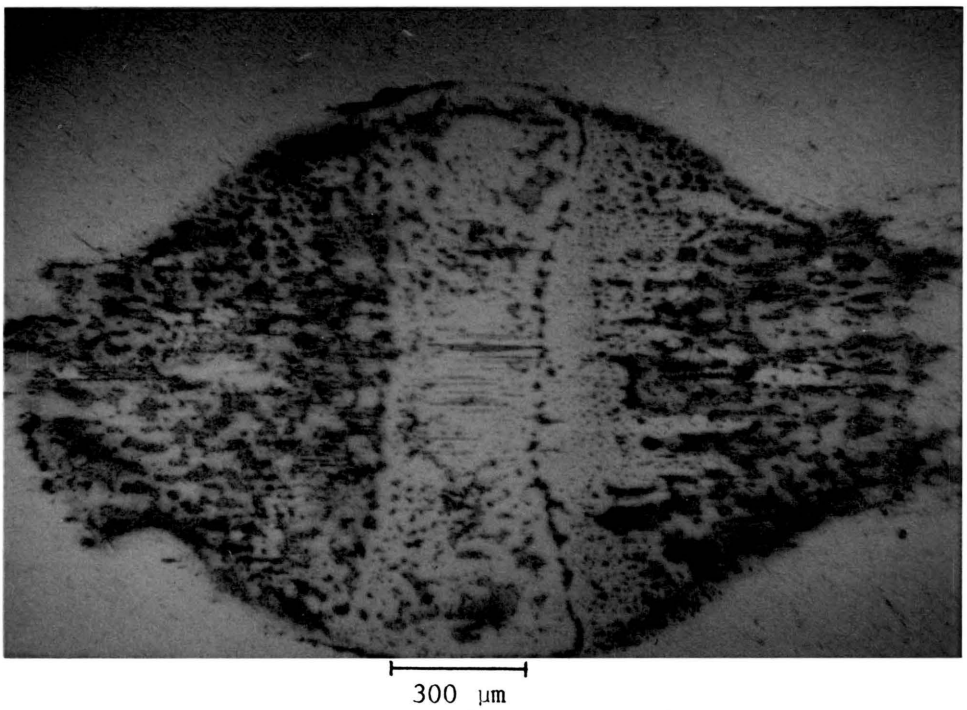

FIGURE 4-48. Optical Macrograph of PVDC Test 3 Ball Scar (Magnification: 60X).

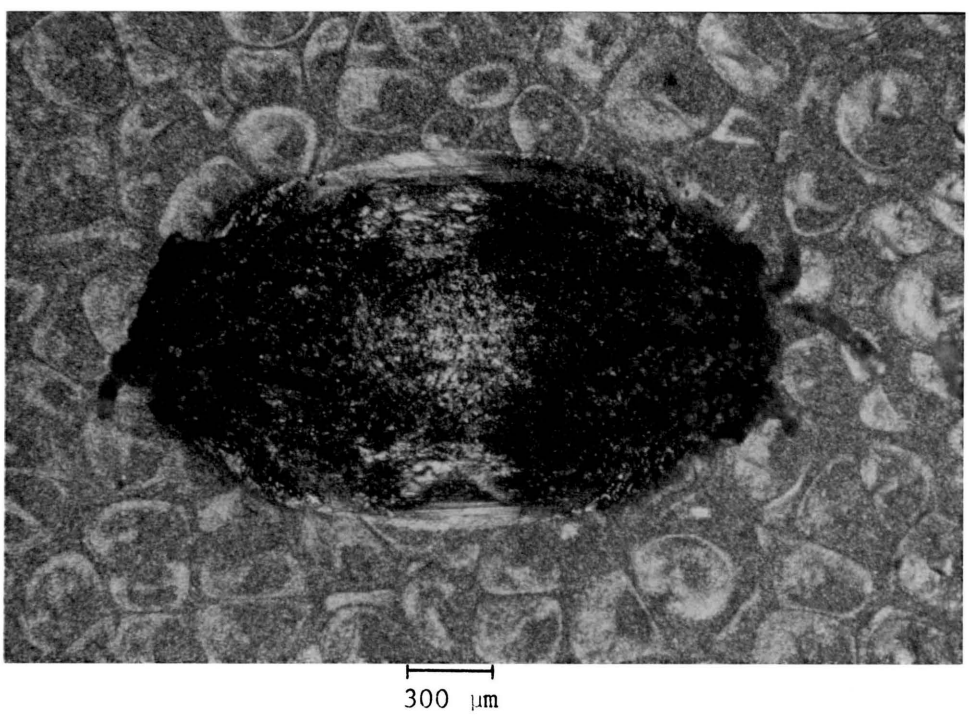

FIGURE 4-49. Optical Macrograph of PVDC Test 3 Disk Scar (Magnification: 37.5X).

elliptical in shape than the Test 1 scar, indicating more penetration. A light region, similar to the rectangular region on the ball can be seen at the center of the scar. This region is exposed metal substrate. Rolls of polymer debris can be seen at the scar ends.

Low-density polyethylene

The ball and disk scars for LDPE Test 1 (45 seconds run time, no metallic contact) are presented in Figures 4-50 and 4-51. The ball scar, because of its larger size, is shown at a lower magnification. Large piles of polymer fibers can be seen at the scar ends. Small fibers can be seen at the top and bottom of the scar. Also note that the ball appears to be undamaged.

The disk scar is almost perfectly elliptical in shape and polymer fibers can be seen at each end. The scar interior is much rougher than the undamaged surface. At the left end of the scar, small areas of bright colors (blue and yellow) can be seen, possibly due to refraction of the light used to illuminate the scar. Figure 4-52 is a scanning electron micrograph of one end of the disk scar which shows the formation of the polymer fibers.

Test 3 ball and disk scars are shown in Figures 4-53 and 4-54 (300 seconds run time and metallic contact). The ball shows evidence of grooving. Reddish-brown material can be seen within and around the scarred region. The polymer debris at the end of the scar appears to be a combination of the fibers seen in the Test 1 scar and the reddish brown material.

Figure 4-54, the Test 3 disk scar, is elliptical in shape with lobes at each end. A large area of exposed metal substrate can be seen

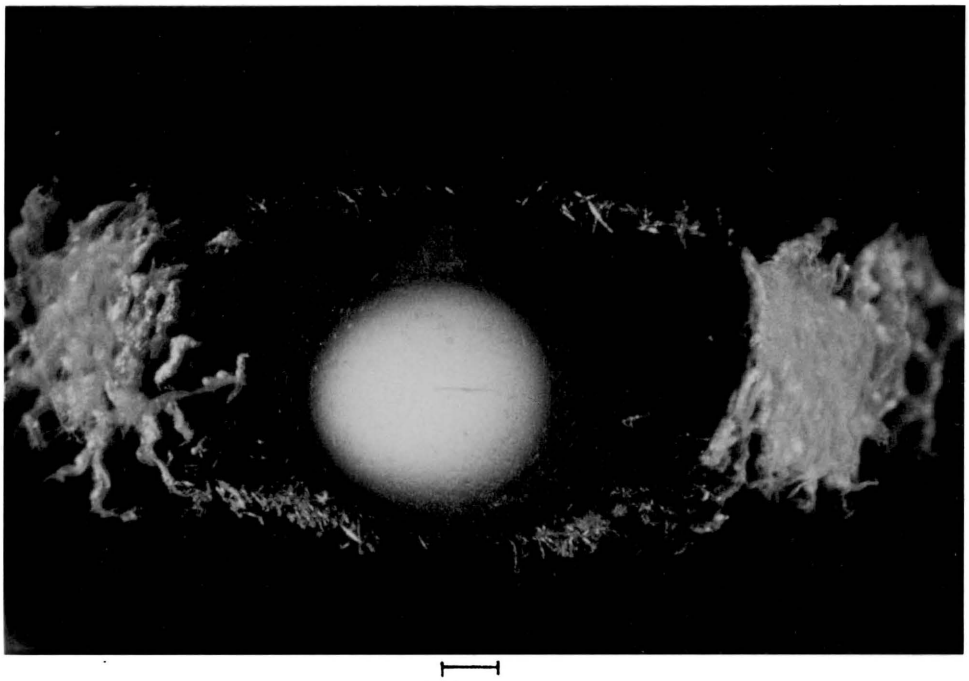

300 μm

FIGURE 4-50. Optical Macrograph of LDPE Test 1 Ball Scar (Magnification: 24X).

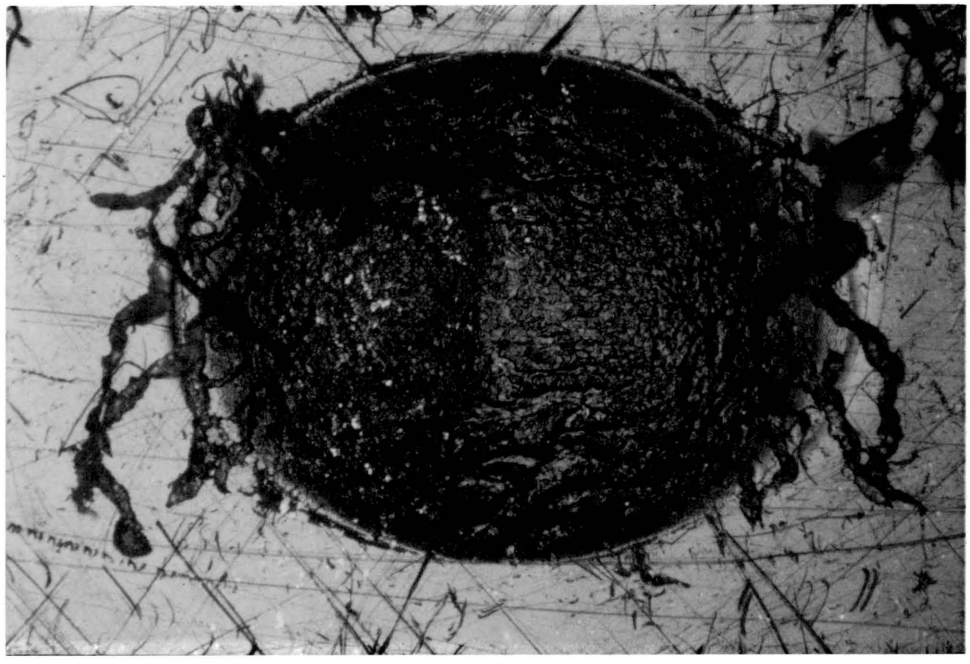

300 μm

FIGURE 4-51. Optical Macrograph of LDPE Test 1 Disk Scar (Magnification: 37.5X).

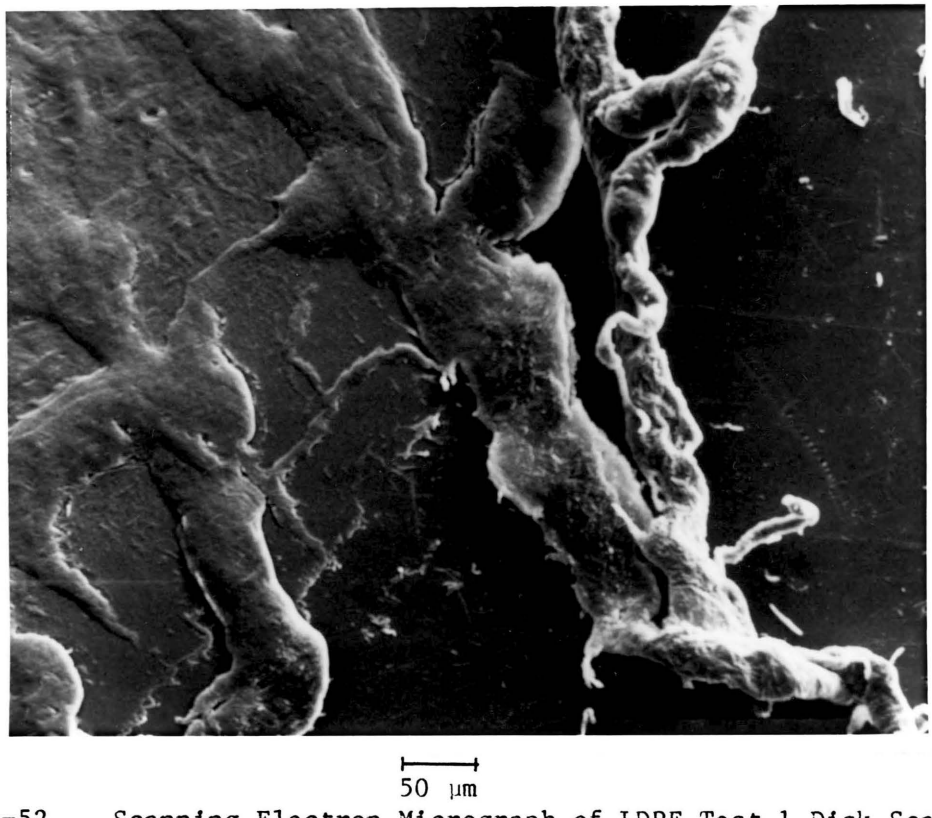

FIGURE 4-52. Scanning Electron Micrograph of LDPE Test 1 Disk Scar End (Magnification: 200X).

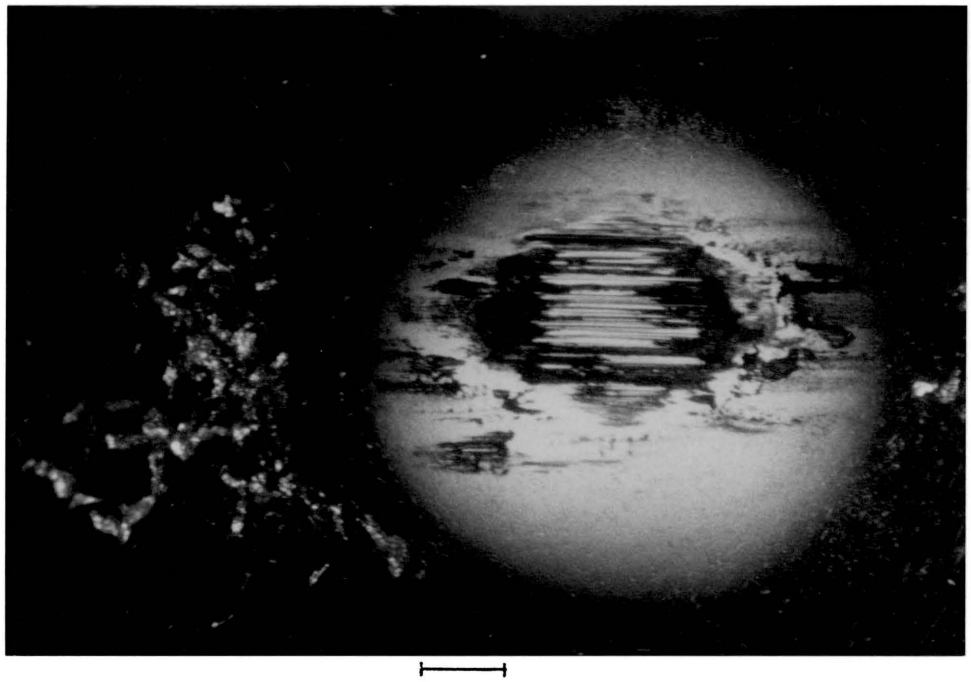

300 μm

FIGURE 4-53. Optical Macrograph of LDPE Test 3 Ball Scar (Magnification: 37.5X).

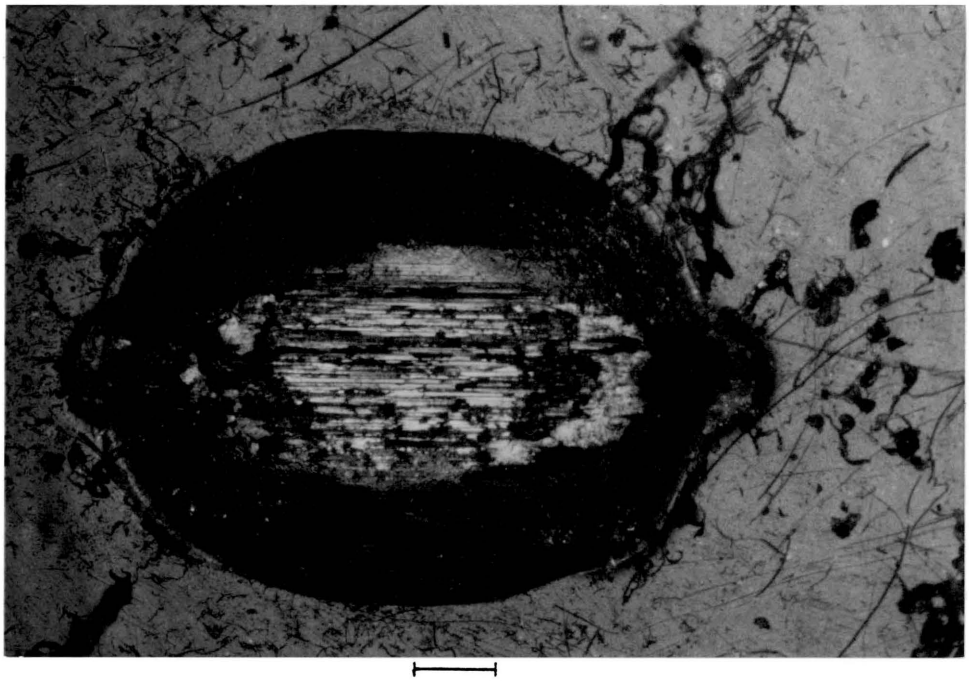

300 μm

FIGURE 4-54. Optical Macrograph of LDPE Test 3 Disk Scar (Magnification: 37.5X).

at the scar center. The fibers scattered around the scar appear to be smaller and darker in color than the Test 1 fibers. Notice also that the polymer surface within the scar appears to be grooved in the sliding direction and has a smoother texture than the Test 1 disk scar.

Polyvinyl chloride

Ball and disk scars from all three tests are shown for PVC in Figures 4-55 thru 4-62. The Test 1 ball scar (Figure 4-55) is after fifteen minutes run time and no metallic contact. The ball appears to be grooved in the sliding direction over the entire damaged region. Within the almost diamond-shaped scar, large areas of a black transferred material can be seen.

Figure 4-56 is the corresponding disk scar at a lower magnification. Notice the light region surrounding the scar. The contact region is much darker than the polymer surface and a large crack can be seen just right of center. Reddish brown debris can be seen in the right end of the scar and scattered around the scar on the polymer surface.

The Test 2 ball scar (30 minutes run time, no metallic contact) is shown in Figure 4-57. The scar is diamond-shaped and large areas of grooved, polished metal can be seen in the center of the scar. Large amounts of fine, particulate reddish brown debris can be seen all over the damaged region. Black transferred material, similar to that seen in Test 1, is concentrated at the ends of the scar.

Figure 4-58 is the Test 2 disk scar at a lower magnification. The scar is irregular in shape and much darker than the surrounding undamaged polymer surface. Large amounts of reddish brown and orange debris, similar to that seen on the ball, can be seen within the scar and scat-

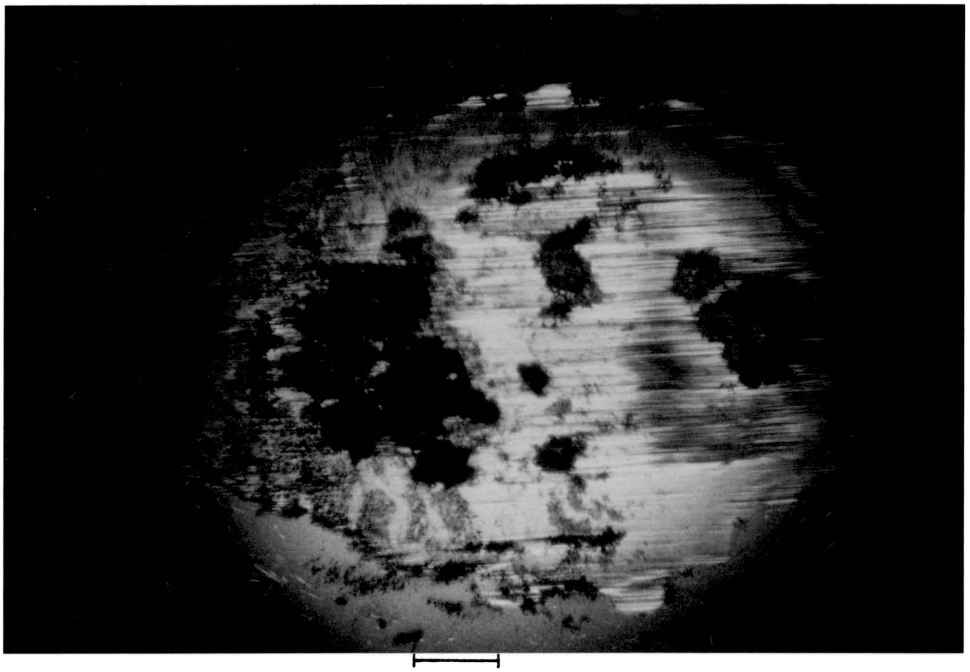

FIGURE 4-55. Optical Macrograph of PVC Test 1 Ball Scar (Magnification: 37.5X).

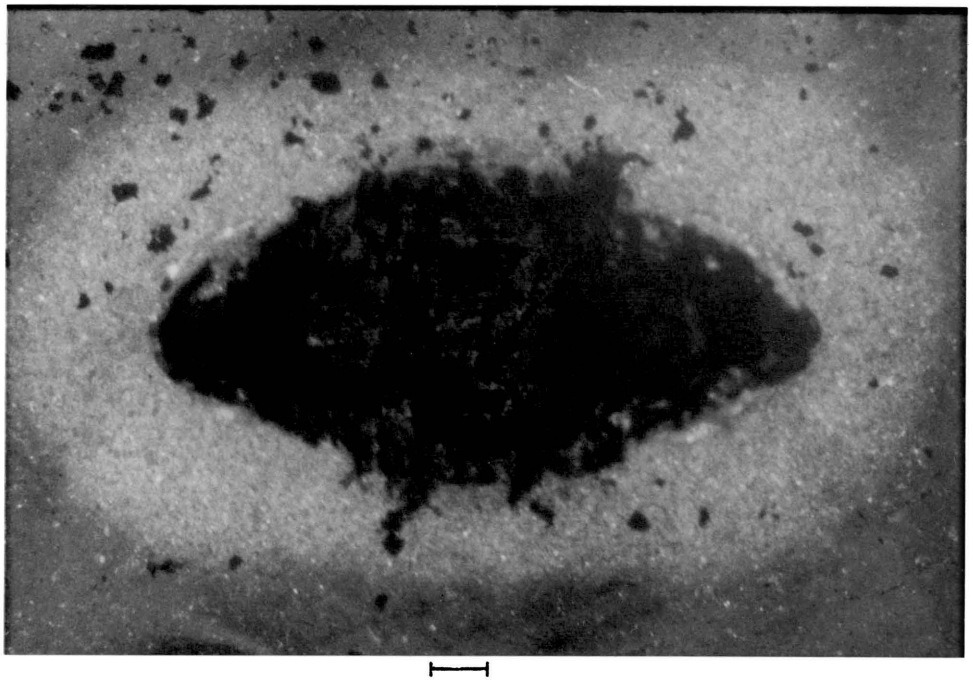

FIGURE 4-56. Optical Macrograph of PVC Test 1 Disk Scar (Magnification: 24X).

FIGURE 4-57. Optical Macrograph of PVC Test 2 Ball Scar (Magnification: 37.5X).

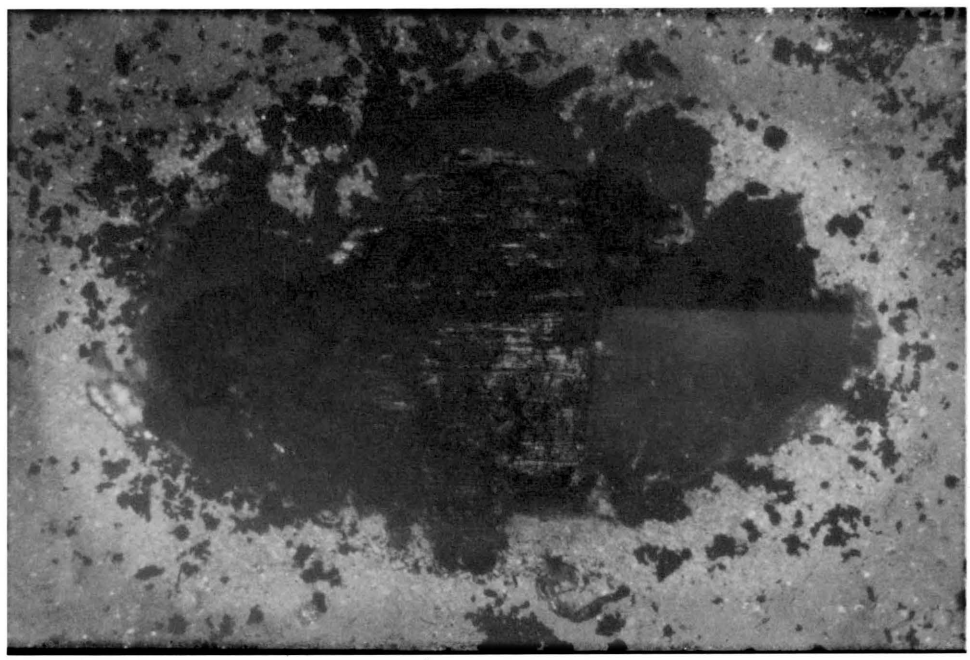

FIGURE 4-58. Optical Macrograph of PVC Test 2 Disk Scar (Magnification: 24X).

tered around its periphery.

Test 3 (45 minutes run time, metallic contact) ball and disk scars are shown in Figures 4-59 and 4-60. The ball scar is fairly elliptical in shape and shows the large amounts of reddish brown debris seen in the previous two test scars. Areas of polished metal can be seen of the scar. A blackish-gray colored material can be seen over most of the scar surface and is concentrated more on the left end.

The disk scar (Figure 4-60) is similar to the Test 2 scar but is more elliptical in shape. Again, large amounts of fine red debris can be seen within and around the scar.

Figures 4-61 and 4-62 are scanning electron micrographs which show characteristic details of the Test 1 and Test 3 disk scars, respectively. The Test 1 scar surface, Figure 4-61 shows cracked and broken up polymer debris. The cracks are oriented perpendicular to the sliding direction. In contrast, the Test 3 scar (Figure 4-62) shows an irregular but smooth polymer surface. Cracking is much less severe. The white particles which are adhering to the polymer surface are the reddish brown debris identified in the optical macrographs.

Polysulfone

Test 1 ball and disk scars (15 minutes run time, no metallic contact) are presented in Figures 4-63 and 4-64. The ball scar is shown at a higher magnification than the disk scar. The ball scar has an unusual shape and shows evidence of grooving in the sliding direction. Fine particulate brown debris can be seen within the scarred region. Highly reflective polymer debris can be seen scattered around the periphery of the scar.

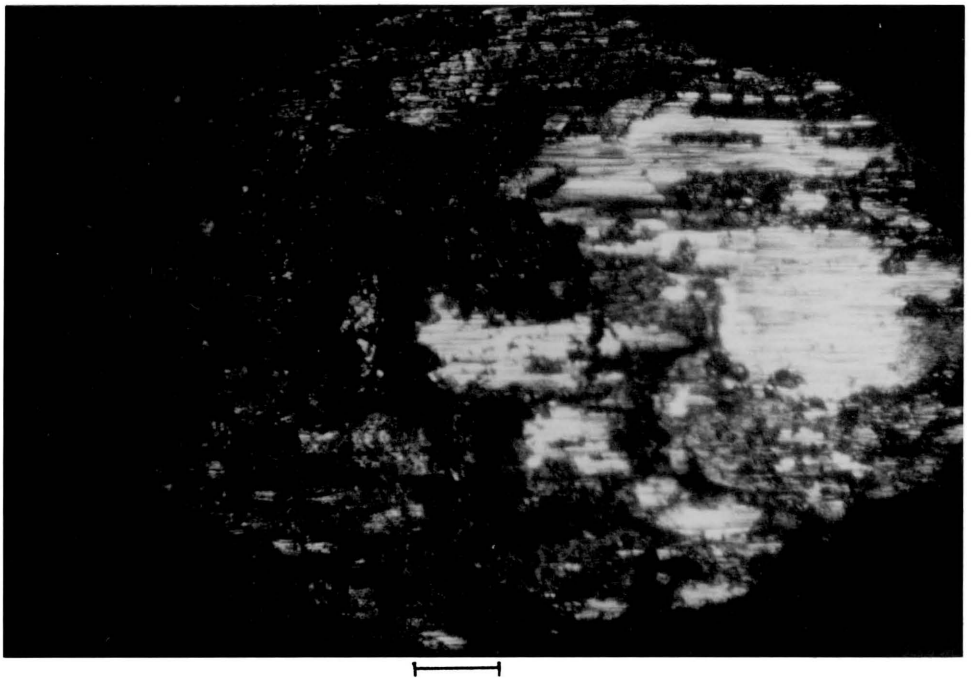

FIGURE 4-59. Optical Macrograph of PVC Test 3 Ball Scar (Magnification: 37.5X).

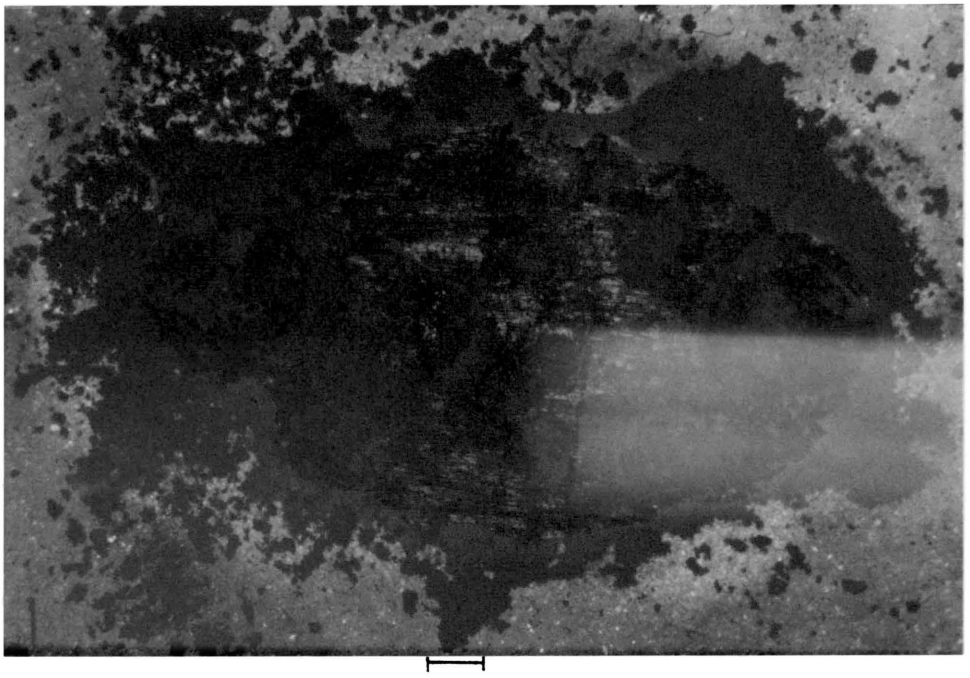

FIGURE 4-60. Optical Macrograph of PVC Test 3 Disk Scar (Magnification: 24X).

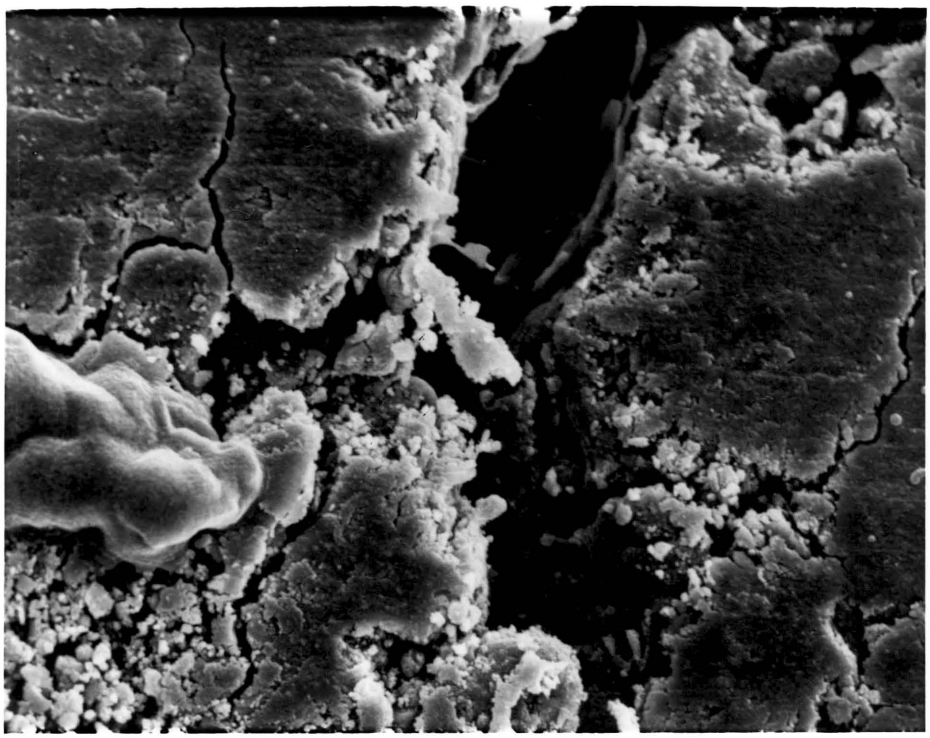

10 μm

FIGURE 4-61. Scanning Electron Micrograph of PVC Test 1 Disk Scar Center (Magnification: 1000X).

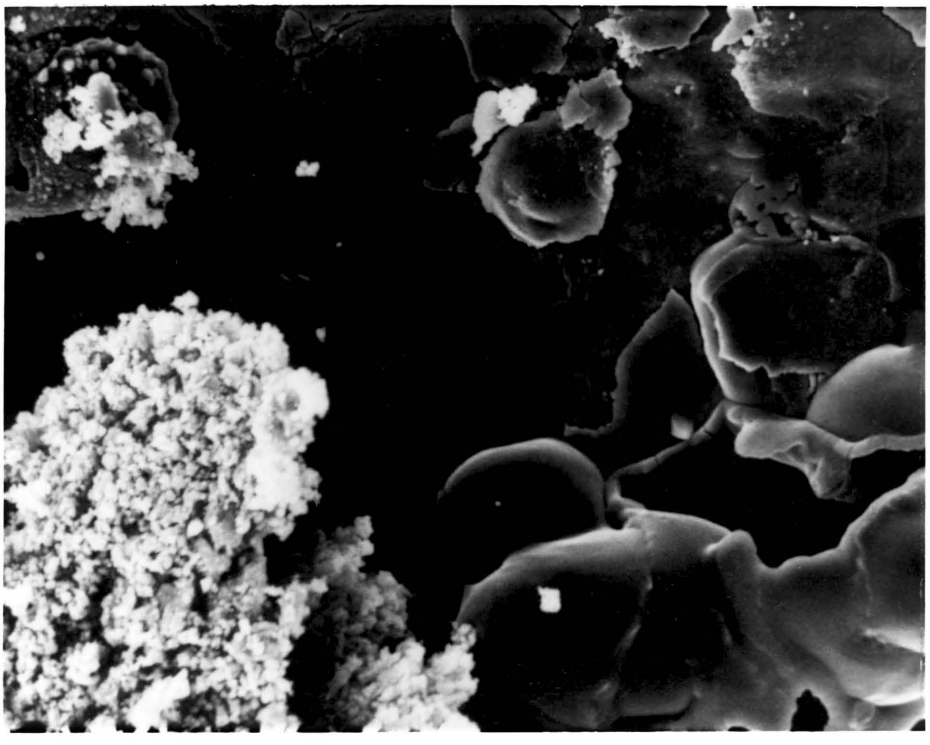

FIGURE 4-62. Scanning Electron Micrograph of PVC Test 3 Disk Scar Center (Magnification: 1000X).

The disk scar is shown in Figure 4-64. Note the light hour-glass shaped region around the contact area. The contact region shows a peculiar brown ridge structure. The ridges are oriented perpendicular to the sliding direction. Referring back to the ball scar (Figure 4-63), the pattern of the scarred region on the disk can be recognized.

Scanning electron micrographs of the disk scar show the detail of the ridge structure (Figures 4-65 and 4-66). The ridges are separated by cracks in the polymer which run perpendicular to the sliding direction. Figure 4-66 is a high magnification micrograph of one of the ridges. Large cracks can be seen on either side of the ridge. Smaller cracks can be seen developing within the ridge. The ridge surface is fairly smooth with the exception of four grooves which are directed along the sliding path.

The Test 2 ball and disk scars are presented in Figures 4-67 and 4-68. No metallic contact has occurred after 30 minutes of run time. The shape is similar to the Test 1 scar with the exception that a large damaged region can be seen at the bottom of the ball scar. The rest of the scar surface appears to be polished and small grooves can be seen along the sliding direction. There does not appear to be as much fine brown debris scattered over the scar surface as was seen with the Test 1 scar.

The disk scar (Figure 4-68) shows that more of the ridge structures have developed. Also note the large amount of fine reddish brown debris at the bottom of the scar. This corresponds to the damaged region on the ball scar. As in the Test 1 scar, the light hour glass region surrounding the scar is still present. Polymer that has been forced out

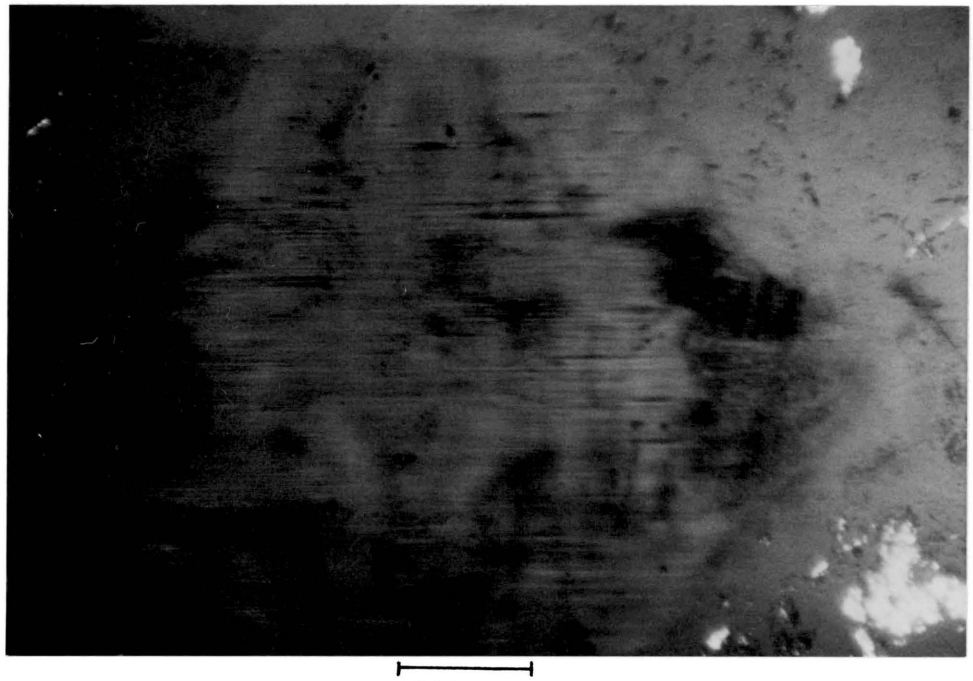

FIGURE 4-63. Optical Macrograph of PSO Test 1 Ball Scar (Magnification: 60X).

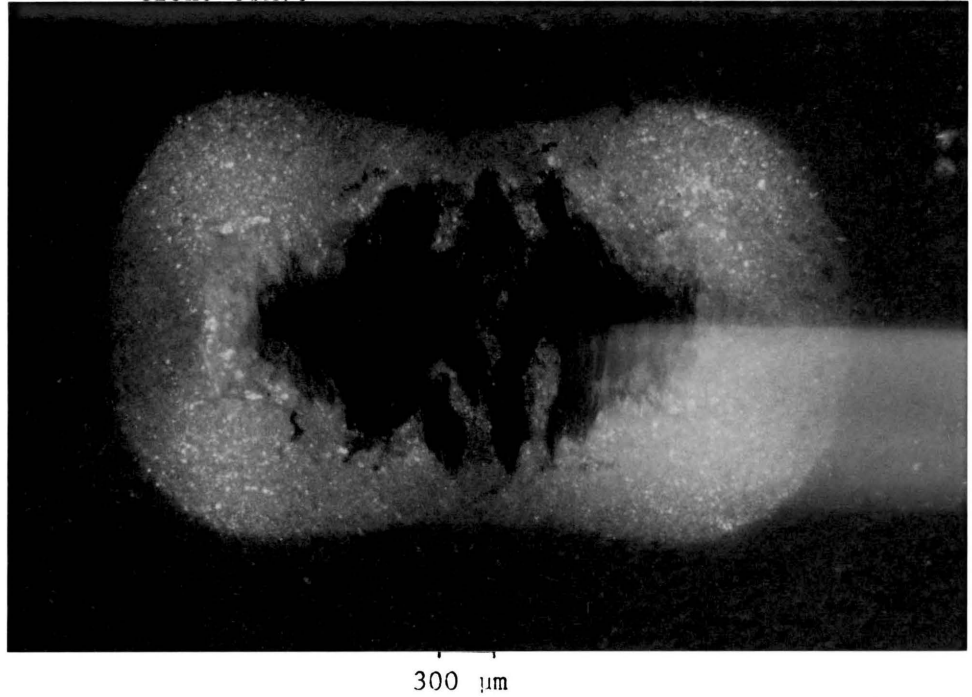

FIGURE 4-64. Optical Macrograph of PSO Test 1 Disk Scar (Magnification: 24X).

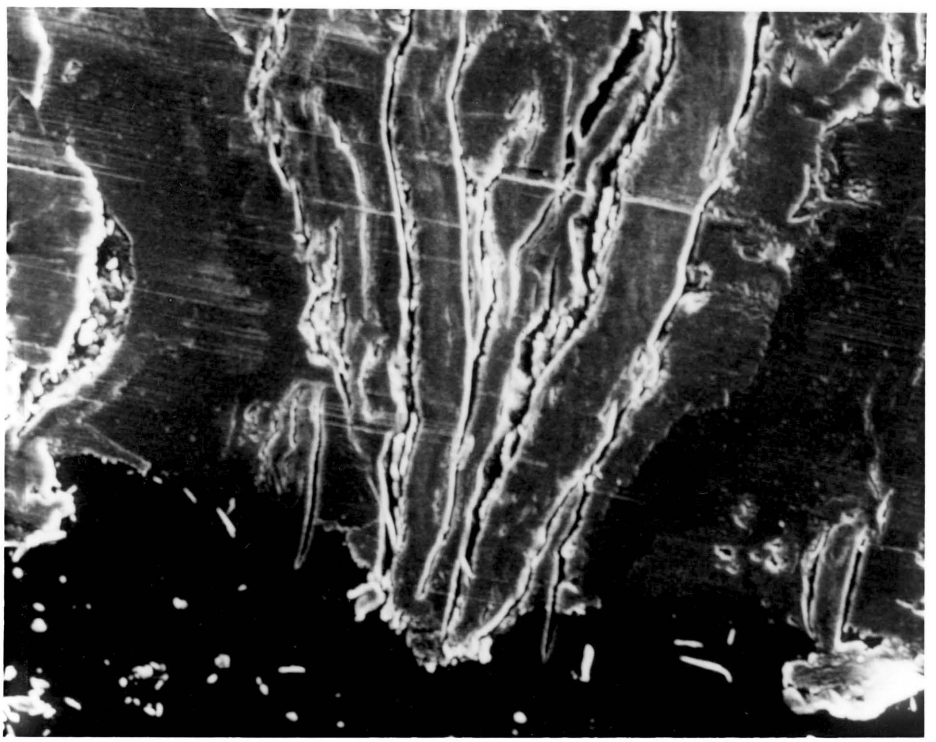

FIGURE 4-65. Scanning Macrograph of PSO Test 1 Disk Scar (Magnification: 200X).

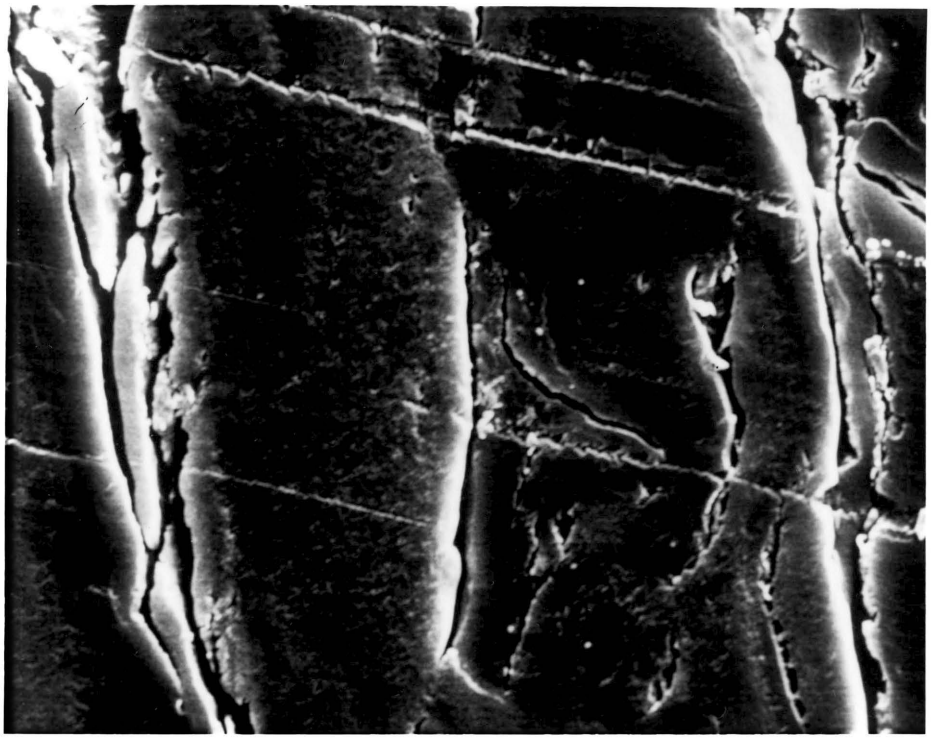

FIGURE 4-66. Scanning Electron Micrograph of PSO Test 1 Disk Scar Showing One of the Ridge Structures (Magnification: 1000X).

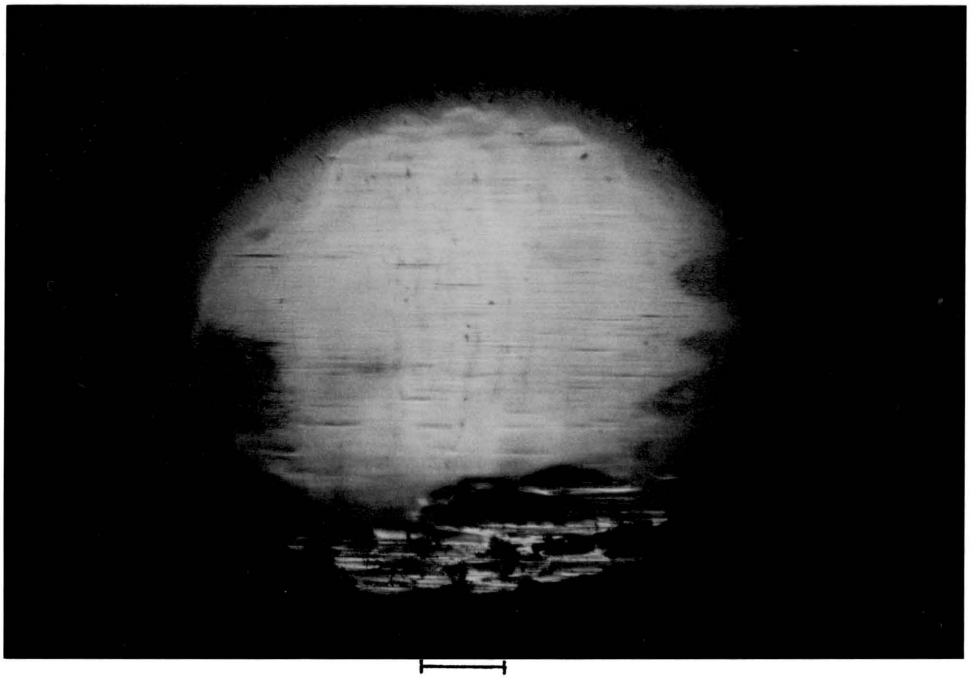

FIGURE 4-67. Optical Macrograph of PSO Test 2 Ball Scar (Magnification: 37.5X).

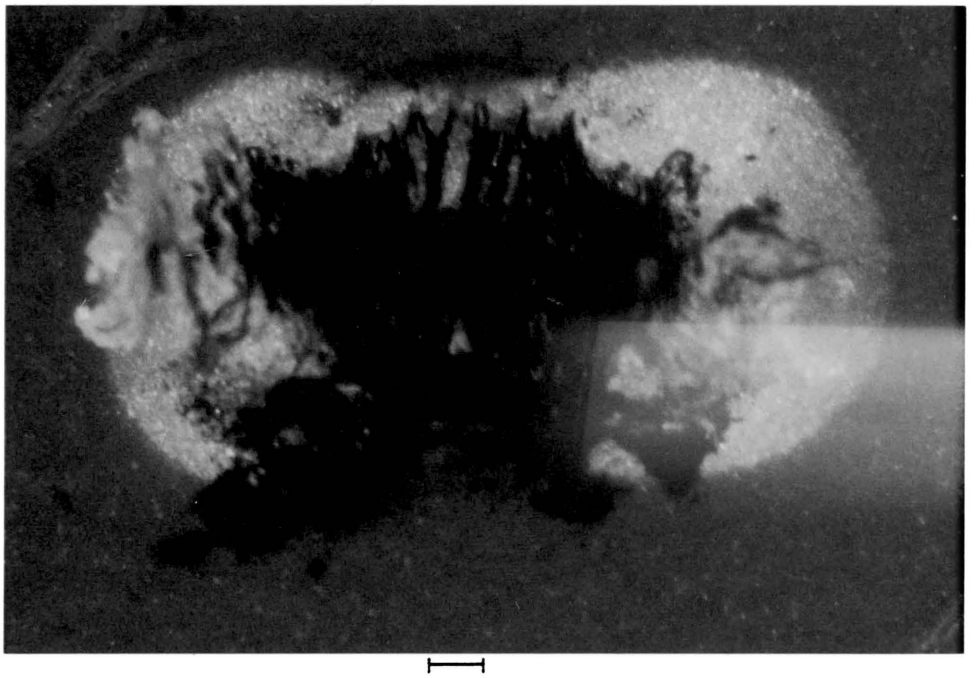

FIGURE 4-68. Optical Macrograph of PSO Test 2 Disk Scar (Magnification: 24X).

of the contact zone can be seen at the ends of the scar.

The Test 3 scars (shown in Figures 4-69 and 4-70) are after 45 minutes run time; metallic contact has occurred. The ball scar is very similar to the Test 2 scar with the exception that the surface appears to be deformed, especially at the top and bottom of the scar. Again there is a large damaged region at the bottom of the ball scar. The disk scar is very similar to the Test 2 scar and fine red debris can be seen corresponding to the damaged region on the ball. Red debris can also be seen at the top of the scar. More polymer appears to be piled up at the scar ends. Figure 4-71 is a scanning electron micrograph of the disk scar center which is at the same magnification as Figure 4-66, the Test 1 scar center. As can be seen, the large ridges in the Test 1 scar have been broken up into smaller ridges which support the load. Large amounts of broken up polymer debris can be seen between the load supporting ridges.

Polystyrene

Optical macrographs of the polystyrene Test 1 ball and disk scars are shown in Figures 4-72 and 4-73 (15 minutes run time, no metallic contact). Some very small scratches can be seen on the ball surface, but the ball appears to be relatively undamaged. Particles of polymer debris can be seen piled up around the contact area. Notice that the larger particles appear to be at the outside of the pile, the smaller particles at the inside of the pile. It is possible that the lack of polymer debris at the left end of the scar could be due to handling during observation.

The disk scar, shown in Figure 4-73, is more rectangular in shape

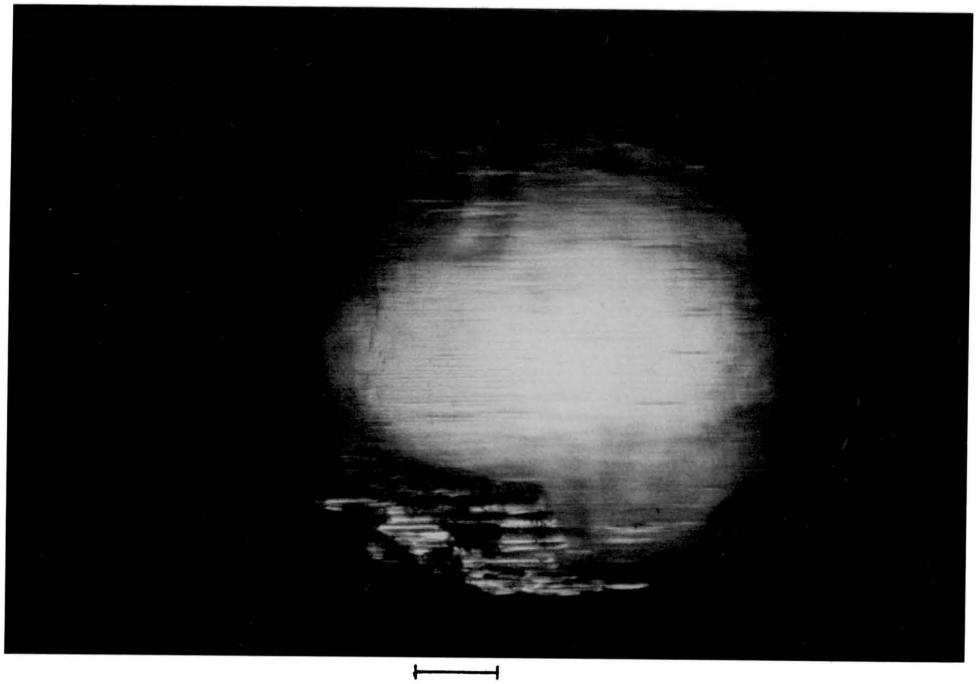

FIGURE 4-69. Optical Macrograph of PSO Test 3 Ball Scar (Magnification: 37.5X).

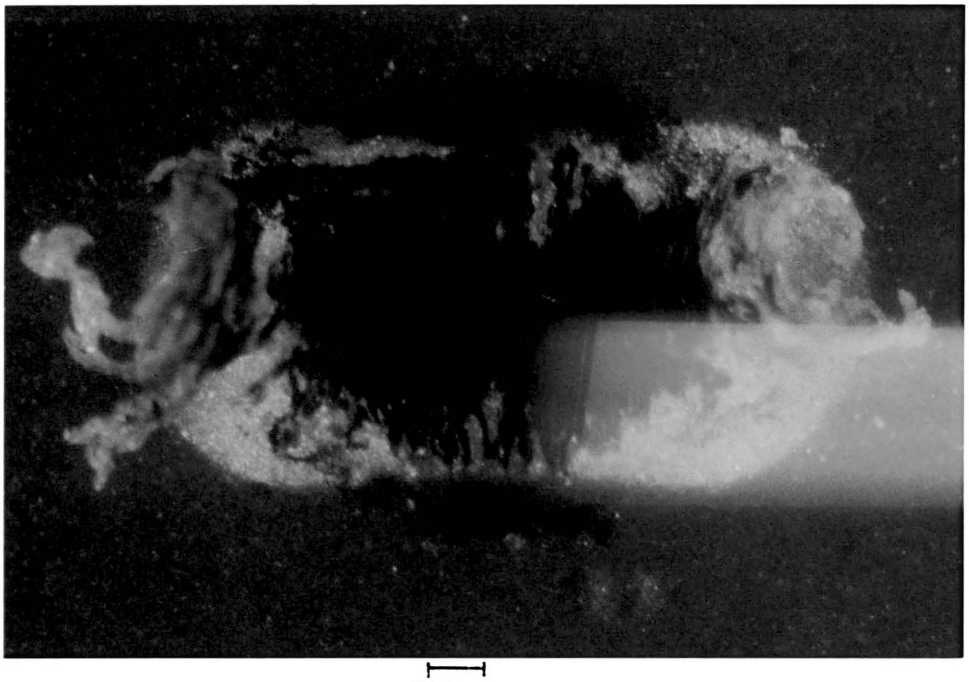

FIGURE 4-70. Optical Macrograph of PSO Test 3 Disk Scar (Magnification: 24X).

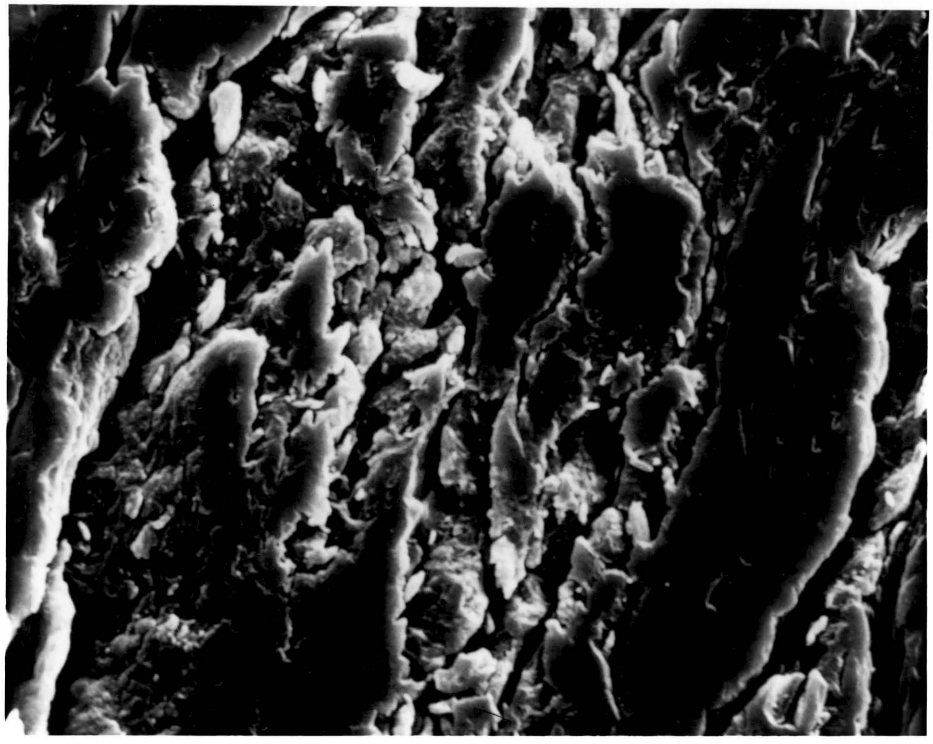

FIGURE 4-71. Scanning Electron Micrograph of PSO Test 3 Disk Scar Center (Magnification: 1000X).

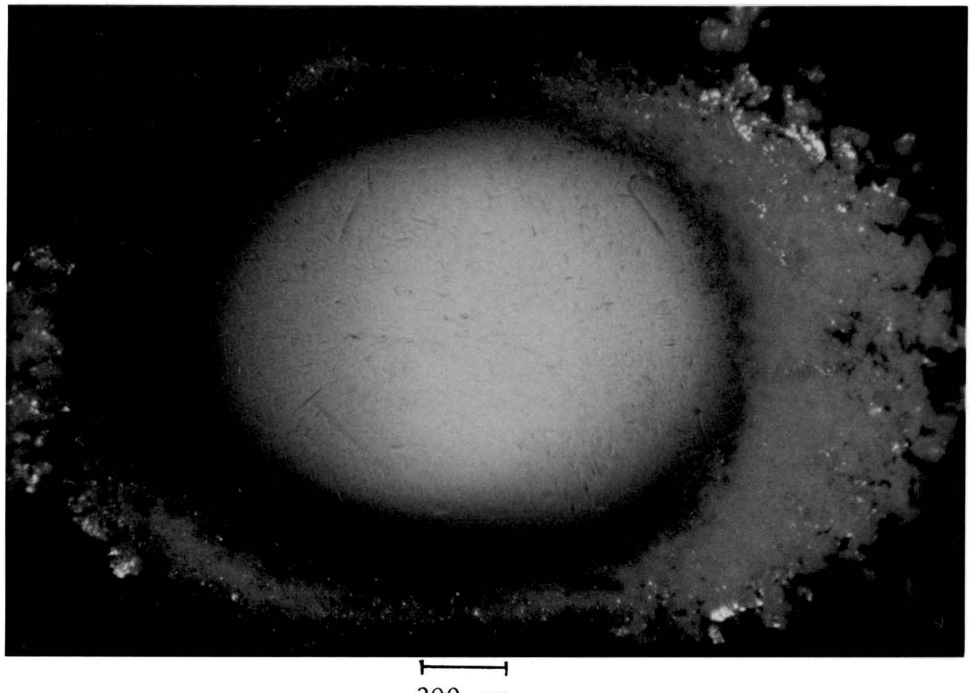

FIGURE 4-72. Optical Macrograph of PS Test 1 Ball Scar (Magnification: 37.5X).

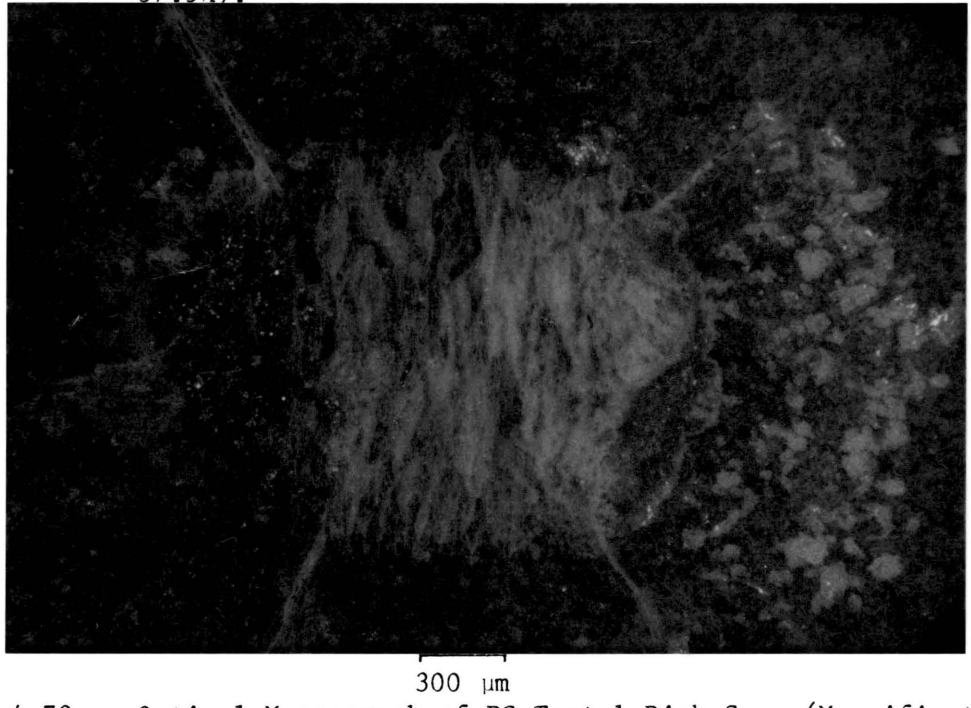

FIGURE 4-73. Optical Macrograph of PS Test 1 Disk Scar (Magnification: 37.5X).

than elliptical. A large position of the scar interior is white in color, contrasting with the undamaged gray surface. This area seems to be composed of ridges which are oriented perpendicular to the sliding direction. Four cracks can be seen at the edges of the scar. Figure 4-74 is a SEM photograph of the disk scar which provides a more detailed view. The damaged region appears to be very rough and there is little evidence of penetration by the ball. A large crack can be seen at the right end of the scar. Large debris particles can also be seen at the right end of the scar. Figure 4-75 is a high magnification micrograph of the central region of the disk scar. As can be seen, the surface is indeed very rough and has a layered appearance.

Test 3 ball and disk scars are presented in Figures 4-76 and 4-77 (45 minute run time, no metallic contact). The ball appears to be undamaged. The scar is similar to the Test 1 scar with the exception that there is more polymer debris and it is more evenly distributed around the contact zone. Notice that most of the debris is piled at the scar ends. Large debris particles are only found at the ends on the outside of the debris pile.

The disk scar shows less of the white regions seen in Test 1. Reflective particles can be seen within the scar. Figure 4-78, a corresponding SEM photograph, illustrates the scar structure. The scar is almost perfectly elliptical in shape and the central region appears to be smoother than the Test 1 scar. Note that the debris is more heavily concentrated at the ends and is displaced from the damaged region by a small amount. Figure 4-79 is a higher magnification shot of the scar center showing that the surface is much smoother than the Test 1 scar.

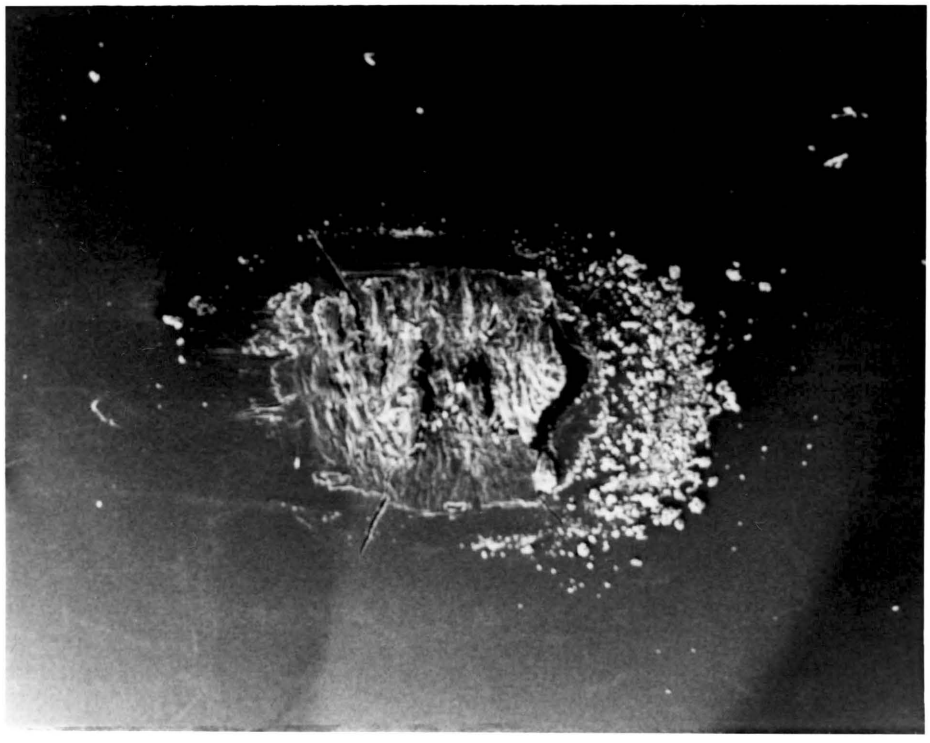

300 μm

FIGURE 4-74. Scanning Electron Micrograph of PS Test 1 Disk Scar (Magnification: 20X).

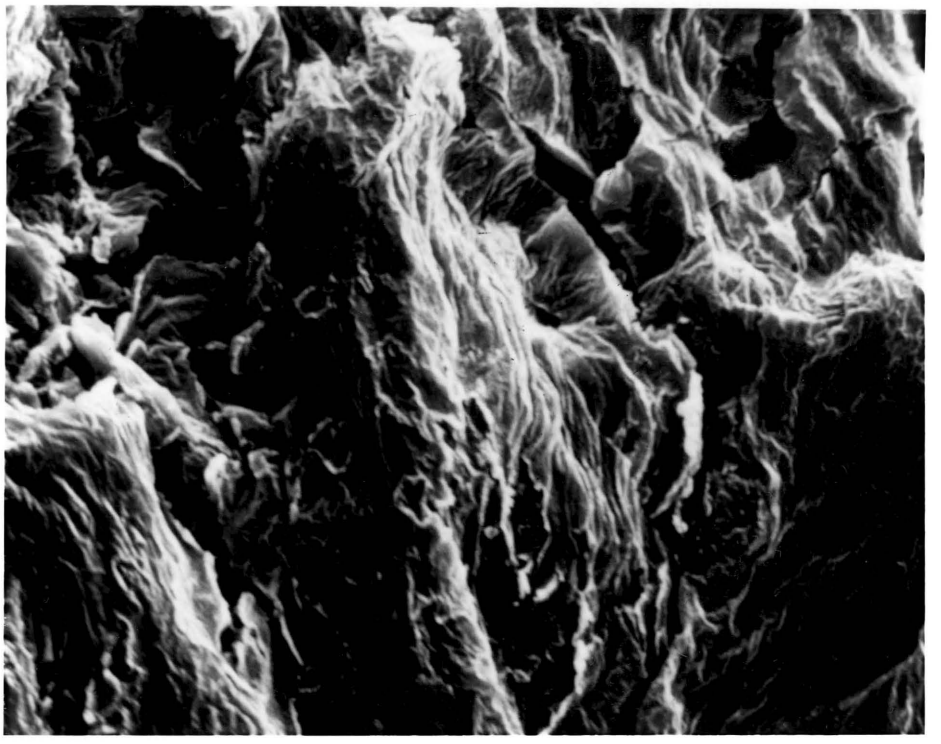

FIGURE 4-75. Scanning Electron Micrograph of PS Test 1 Disk Scar Center (Magnification: 1000X).

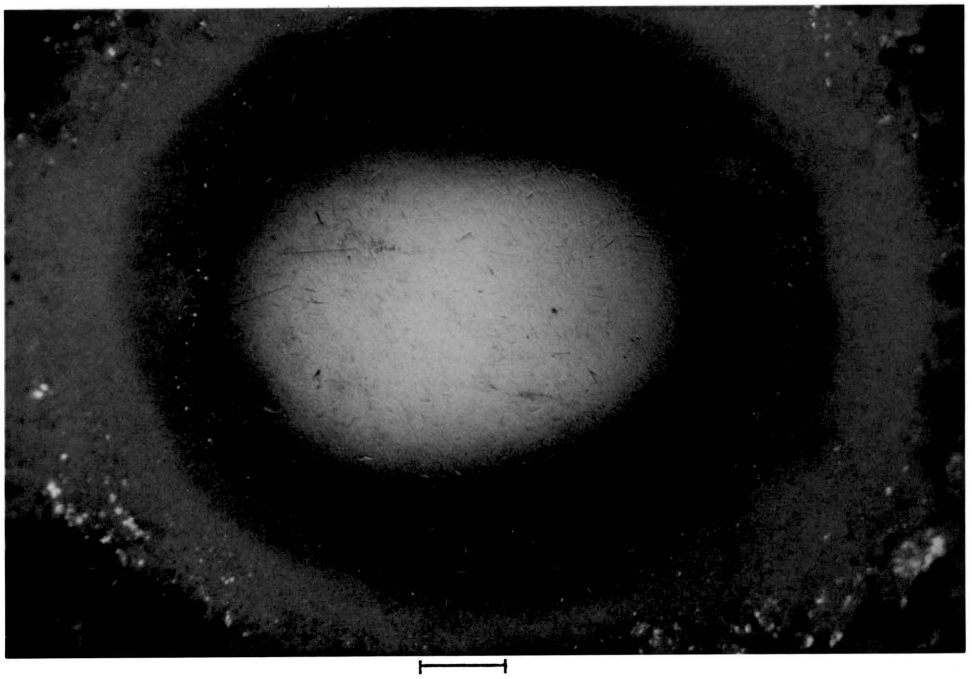

FIGURE 4-76. Optical Macrograph of PS Test 3 Ball Scar (Magnification: 37.5X).

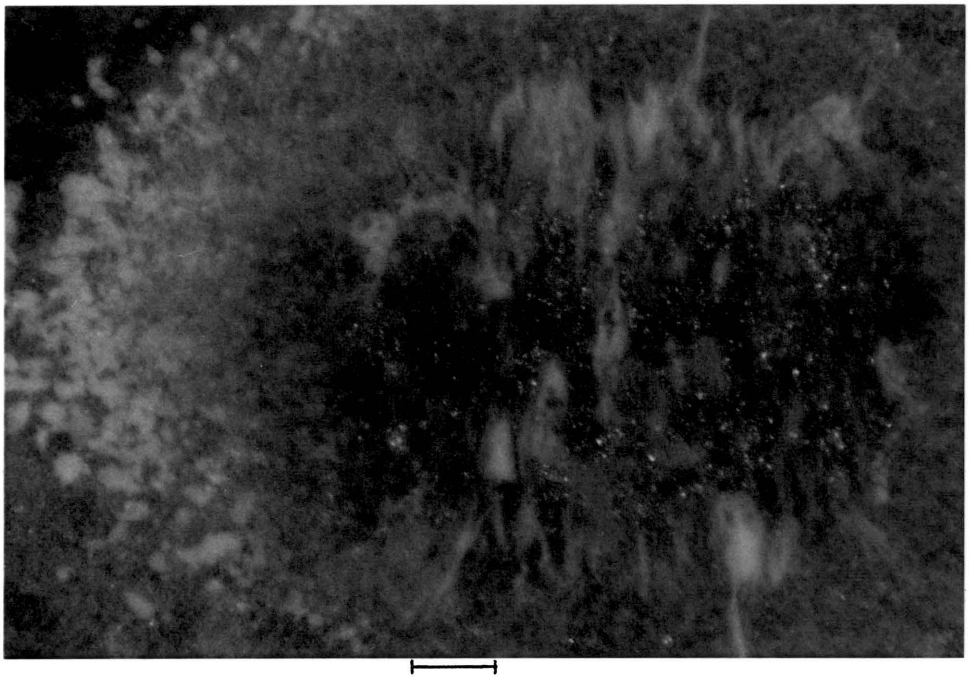

FIGURE 4-77. Optical Macrograph of PS Test 3 Disk Scar (Magnification: 37.5X).

FIGURE 4-78. Scanning Electron Micrograph of PS Test 3 Disk Scar (Magnification: 20X).

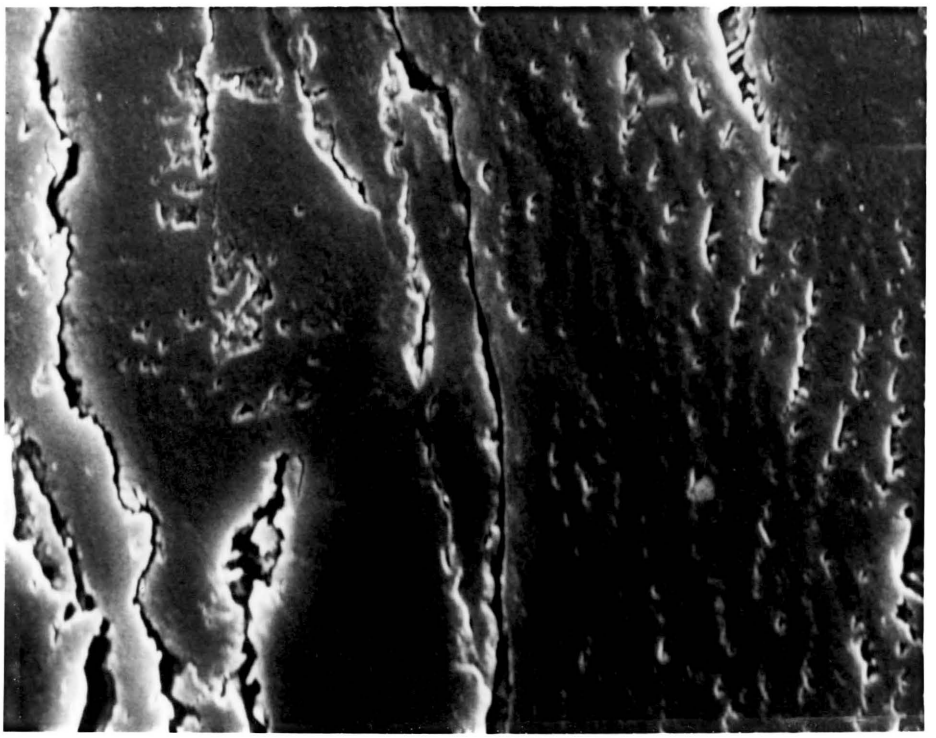

FIGURE 4-79. Scanning Electron Micrograph of PS Test 3 Disk Scar Center (Magnification: 1000X).

Cracks can be seen in the polymer running perpendicular to the sliding direction.

High-density polyethylene

Shown in Figures 4-80 and 4-81 are the corresponding ball and disk scars for HDPE Test 1 (15 minutes run time, no metallic contact). The ball scar is circular in shape and is covered with "streaks" of brown material. The streaks in the center of the scar are larger and less concentrated than those on the outer edges. It is not clear whether the ball is damaged; however, a small groove can be seen at the top center of the scar.

The disk scar (presented in Figure 4-81) is almost perfectly circular in shape. The scar shows two distinct regions--an outer annulus which appears to be fairly smooth and a more reflective inner area which has a contorted uneven texture. Note that the central region appears to be more elliptical in shape than the outside boundary of the outside region. Grooves can also be seen within the scar running parallel to the sliding direction.

Figures 4-82 and 4-83 are SEM photographs of the Test 1 disk scar. Figure 4-82, a low magnification overview, shows the grooves seen in Figure 4-81. Close examination shows some waves in the central region of the scar. Also note the difference between the inner and outer surfaces of the scar. The center surface appears to be solid while the outer annulus and the undamaged surface are covered with holes and crevices. Figure 4-83 is a SEM photograph of the end of the scar which shows the transition from the inner surface to the outer annulus. Note that the outer annulus (to the right) appears to be worn.

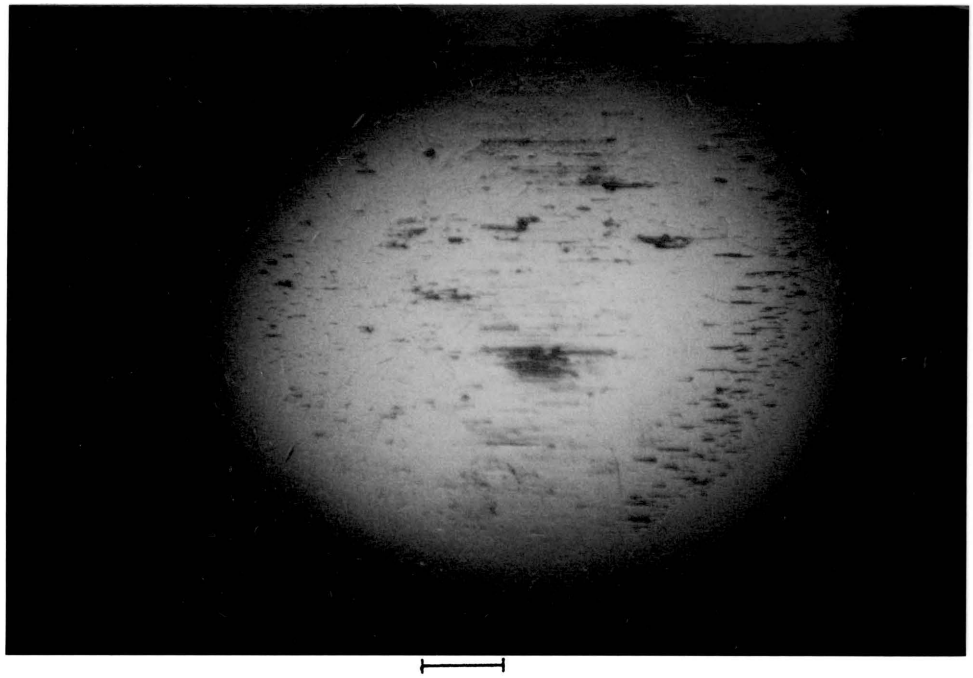

FIGURE 4-80. Optical Macrograph of HDPE Test 1 Ball Scar (Magnification: 37.5X).

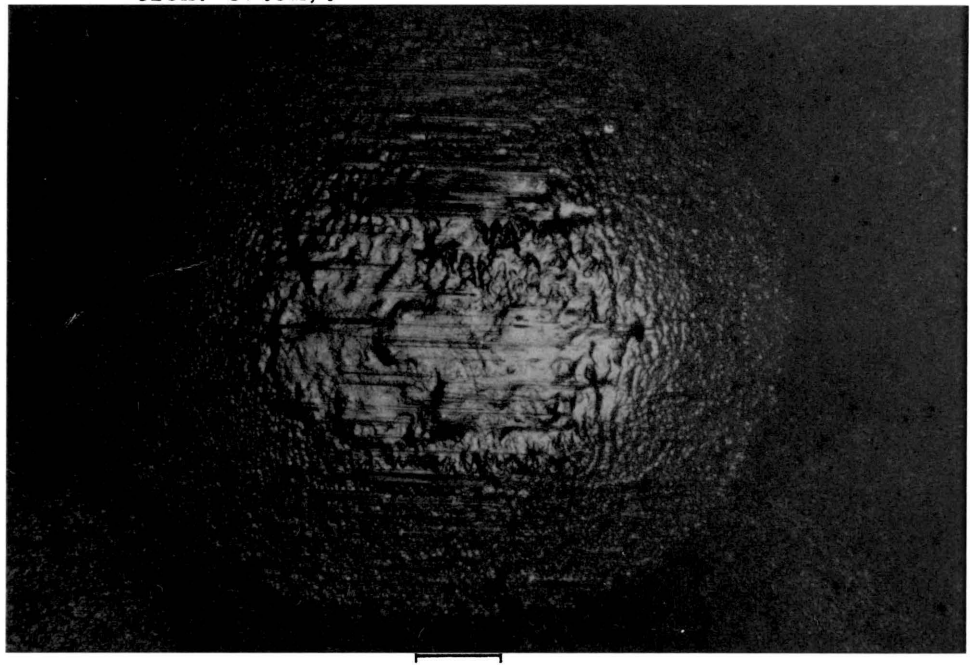

FIGURE 4-81. Optical Macrograph of HDPE Test 1 Disk Scar (Magnification: 37.5X).

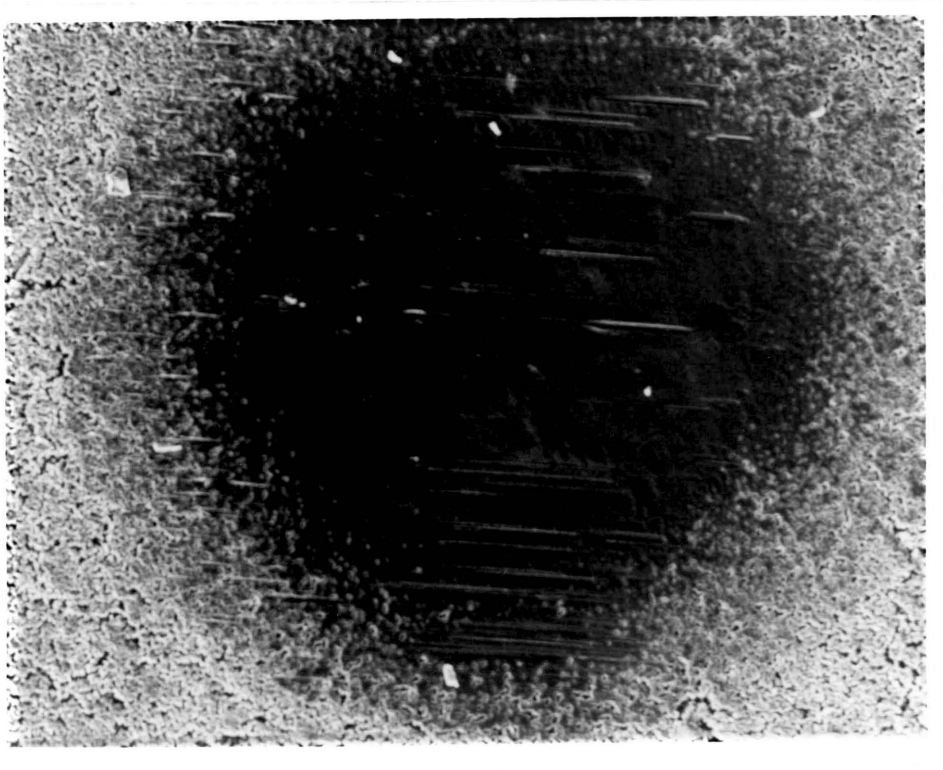

FIGURE 4-82. Scanning Electron Micrograph of HDPE Test 1 Disk Scar (Magnification: 50X).

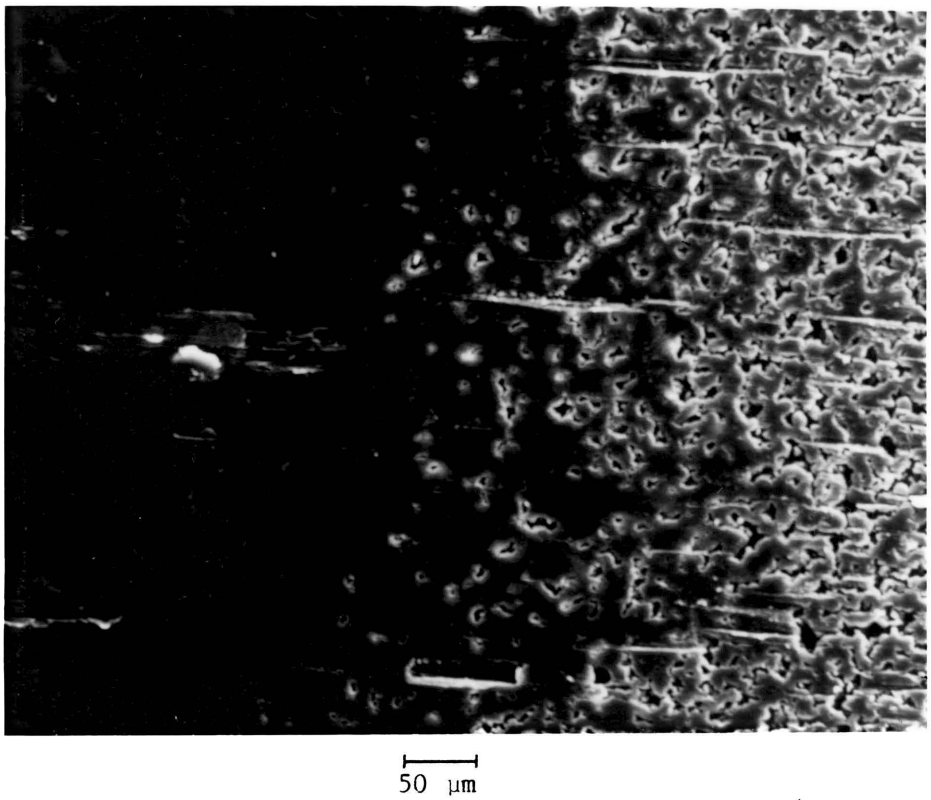

FIGURE 4-83. Scanning Electron Micrograph of HDPE Test 1 Disk Scar Edge (Magnification: 200X).

Test 3 HDPE (45 minutes run time, no metallic contact) ball and disk scars are presented in Figures 4-84 and 4-85. The ball scar is very similar to the Test 1 scar with the exception that there is more of the brown material. A definite groove can be seen at the top of the scar. Smaller grooves can be seen at the bottom of the scar.

The disk scar shows a larger central region than the Test 1 scar with more extensive grooving. The center surface also appears to be more deformed than the Test 1 scar.

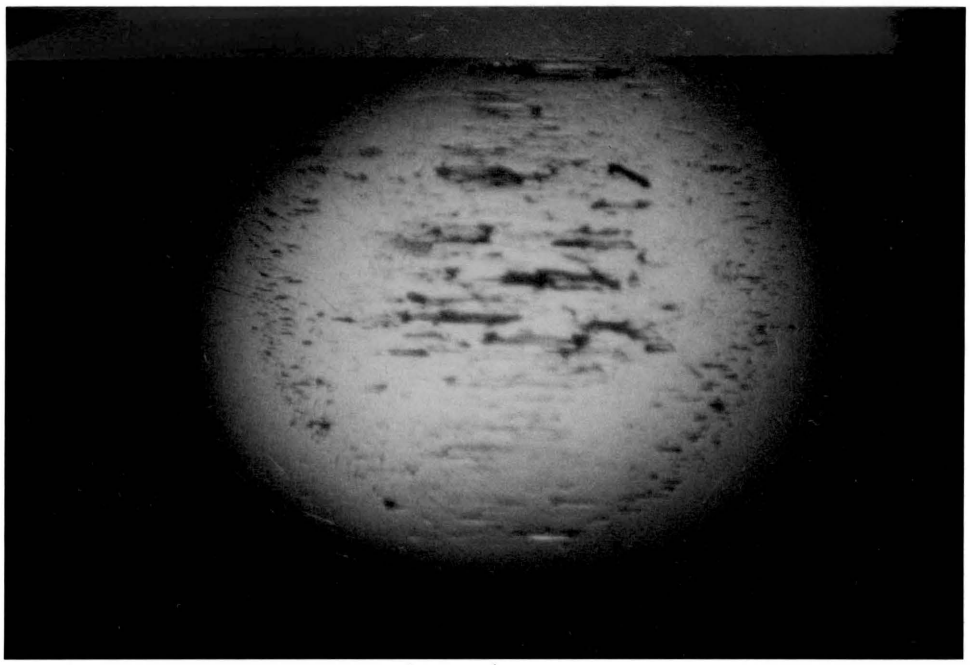

FIGURE 4-84. Optical Macrograph of HDPE Test 3 Ball Scar (Magnification: 37.5X).

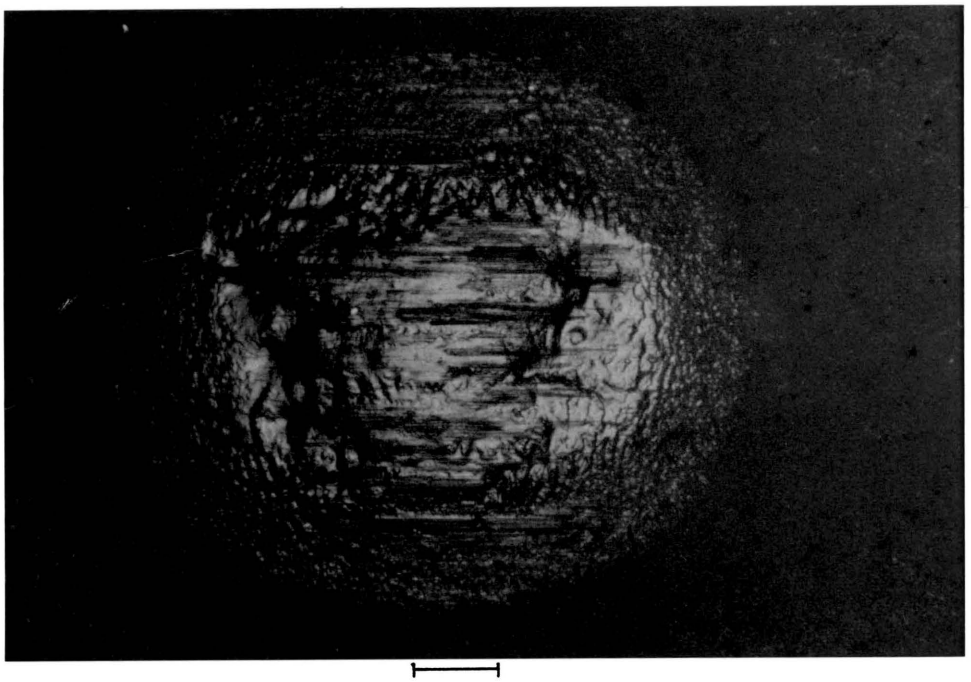

FIGURE 4-85. Optical Macrograph of HDPE Test 3 Disk Scar (Magnification: 37.5X).

5.0 DISCUSSION

In this research the use of the polymer coatings was studied as a method to prevent metallic contact and fretting corrosion in steel-on-steel systems. The behavior of these films was studied in various ways. An electrical resistance technique (45) was used to determine film breakthrough, and hence, a measure of the effective life of each film. Frictional forces between the steel ball and coated disk were also monitored on a continuous basis. Microscopic data, both optical and electronic, provided a pictorial description of the process as a function of time.

The discussion that follows is divided into three sections. In the first section, the general behavior of the contact system used in this work will be discussed. The second section will present the general findings of this investigation with respect to the life of polymer films, their frictional behavior and their ability to prevent fretting corrosion. In a final section, general and specific observations based on the photomacrographs and SEM photographs obtained in phase two of the experimental work will be given.

5.1 General Behavior of the Contact System

In order to understand the types of behavior which were observed in this investigation, detailed examination of the contact system is necessary. For clarity, the entire fretting process can be divided into two stages. The first is static normal loading of the steel sphere against the polymer-coated steel flat. In the second stage, vibration is intro-

duced to the system, resulting in relative tangential motion between the sphere and steel substrate.

5.1.1 Static Normal Loading

In the first stage, static normal loading, the contact geometry can fall into one of the three categories which are illustrated in Figure 5-1. The first, Figure 5-1(a), is only valid if the thickness of the film is less than the surface roughness of the disk upon which it is coated. In this case, stresses at the interface are accurately predicted by classical Hertzian theory for a steel sphere on a steel half-space. The second case, Figure 5-1(b), considers the effect of a layered half-space which has been studied by Matthewson (33), considering only elastic deformation. In the third case, shown in Figure 5-1(c), the thickness of the film is sufficient to eliminate the effect of the rigid substrate on the stresses within the layer and Hertzian theory again applies, considering the steel sphere to act on a semi-infinite half-space of the polymer film material.

The first case is not applicable to this work because all of the film thicknesses were larger (by at least a factor of four) than the surface roughness of the disk. Since the system will obviously be described by either the second or third case, a method must be devised to distinguish between them. Matthewson (33) states that for values of $a/h < 1$ (where a is the Hertzian contact radius and h is the film thickness), stresses at the interface will be accurately predicted by considering the third case and Hertzian theory. For values of $a/h > 1$, stresses within the layer and at the interface can be predicted by the theory developed (however not completely published) by Matthewson.

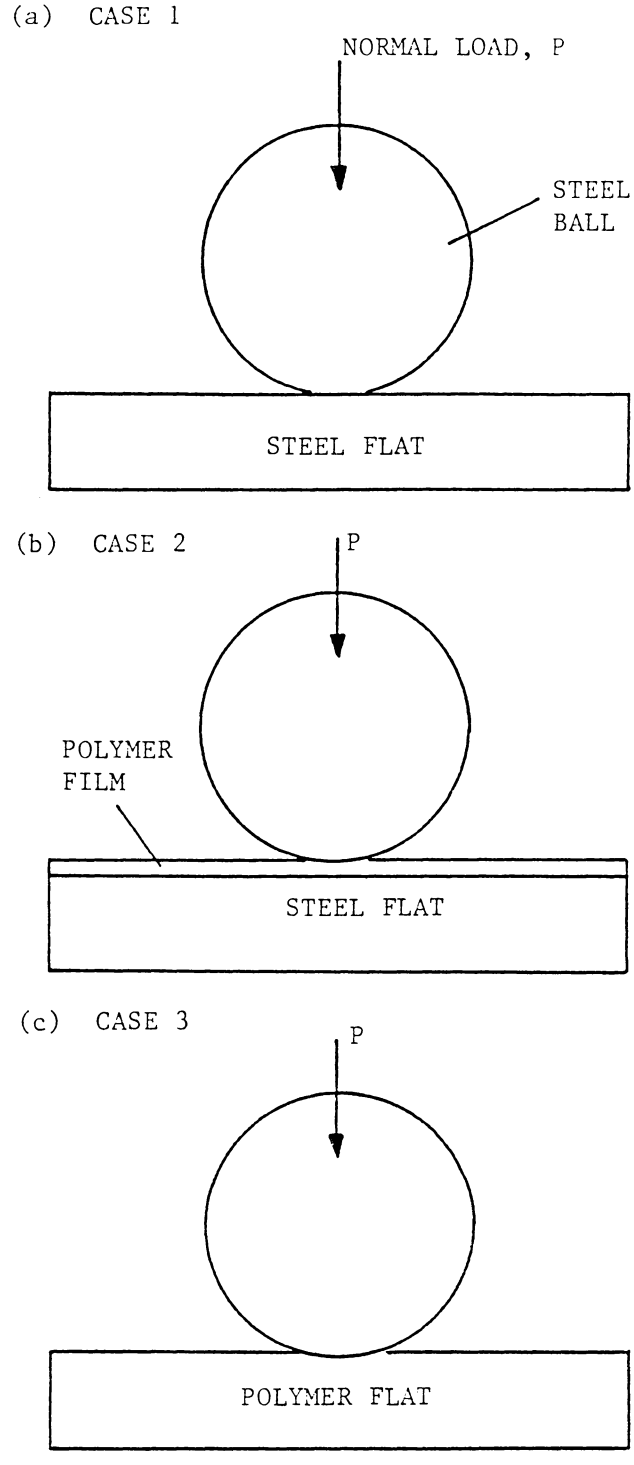

FIGURE 5-1. Possible Contact Geometries: (a) Steel Sphere-on-Steel Flat; (b) Steel Sphere-on-Polymer-Coated Flat; and (c) Steel Sphere-on-Polymer Flat.

To ascertain what factors distinguish between these two cases we must examine the expression for a, the Hertzian contact radius:

$$a = 0.721 \left[P \left(\frac{1 - \nu_1^2}{E_1} + \frac{1 - \nu_2^2}{E_2} \right) D \right]^{1/3}$$

Where: a = contact area radius

P = applied normal load

ν_1 = Poisson's ratio of the sphere

E_1 = Young's modulus of the sphere

ν_2 = Poisson's ratio of the half-space

E_2 = Young's modulus of the half-space

D = Diameter of the sphere

Given a film thickness (h), an increase in load (P) or sphere diameter (D) can cause a transition from case 3 (sphere-on-polymer flat) to case 2 (sphere-on-polymer-coated steel flat). A decrease in the modulus or an increase in Poisson's ratio of either material can also cause the same change.

Table 5-1 presents the values for a/h for all of the films tested. As can be seen all of the values are greater than 1.0, indicating that the substrate-film interaction is important. If we now only consider the system defined by case 2, the behavior of the polymer coating will be determined by its response to the state of stress within the layer. Four types of behavior are possible:

1. Elastic
2. Viscoelastic
3. Plastic-Elastic

TABLE 5-1 Values of a/h for Polymer Films Tested[a]

(22.3 N Normal Load)

Polymer Type	a/h
PMMA	49.8
PTFE	63.0
PI	33.1
PVDF	15.5
PVDC	15.5
LDPE	16.6
PVC	5.5
PSO	5.8
PS	4.1
HDPE	4.1

(a) a is the calculated Hertzian contact radius for a steel sphere on a polymer flat.

h is the average film thickness of the polymer film.

4. Plastic

Elastic Behavior

If we assume the film behaves in a linearly elastic fashion, several factors have an effect on the stresses within the layer:

(a) Film Thickness.

(b) Load.

(c) Young's Modulus of the Film.

(d) Poisson's Ratio of the Film.

(e) Adhesive and Frictional Forces at the Sphere-Film Interface.

Note that the contact geometry is not considered as a variable since only a sphere-on-flat system was used in this research. Both the steel sphere and the substrate are assumed to be perfectly rigid, since the modulus of the polymer films is less than that of steel, often by more than a factor of 100. The effects of these factors (a-e) will now be discussed with respect to the case 2 contact geometry.

Film Thickness: An increase in film thickness will cause a corresponding decrease in stresses within the film. Although a complete solution for the case 2 geometry with respect to stresses and strains within the layer was not found, this trend can be shown by considering the two "boundary cases:" steel-on-steel (case 1) and steel-on-polymer (case 3). Table 5-2 shows the maximum Hertzian contact pressure for both cases and the polymers tested. The actual mean contact pressure for case 2 will be between these two contact pressures, the first (steel-on-steel) assuming zero film thickness and the second (steel-on-polymer) assuming infinite film thickness. Also note that the pressure

TABLE 5-2 Maximum Hertzian Contact Pressure for Steel-on-Steel (Case 1) and Steel-on-Polymer (Case 3) Contact Geometries (22.3 N Normal Load)

Polymer Type	Case 1 (MPa)	Case 3 (MPa)
PMMA	958.5	85.1
PTFE	958.5	26.2
PI	958.5	71.9
PVDF	958.5	68.7
PVDC	958.5	26.1
LDPE	958.5	17.8
PVC	958.5	97.3
PSO	958.5	81.9
PS	958.5	87.2
HDPE	958.5	50.2

developed in case 1 with 22.3 N normal load is higher than the yield strength of 1045 steel (about 620 MPa).

Load: An increase in normal load will obviously cause an increase in the contact pressure and penetration of the steel ball into the film.

Young's Modulus: An increase in Young's modulus will cause a reduction in contact area and hence, an increase in interfacial pressure. Despite this increase in pressure, higher modulus films also generally have higher yield strengths, allowing them to withstand higher pressures.

Poisson's Ratio: Poisson's ratio is a measure of the compressibility of the film; its value can range from 0.0 to 0.5, with 0.5 representing a perfectly incompressible material. Matthewson (33) has shown that stresses within the layer vary significantly with Poisson's ratio--the higher Poisson's ratio corresponding to a higher state of stress within the film. This can be explained by considering the two possible causes of film volume reduction within the contact zone: 1. compression; and 2. radial displacement out of the contact area. If the film material is incompressible ($\nu = 0.5$) the volume will have to be removed by radial displacement, resulting in higher radial and circumferential strains and therefore, higher stresses

Adhesive and Frictional Forces at the Sphere-Film Interface: Strong adhesive forces between the steel ball and polymer film would tend to cause an increase in contact area and therefore a decrease in contact pressure. Since adhesive forces act to pull both of the contacting bodies together, their effect would be similar to superimposing

a distributed normal load (acting over the contact area) in addition to the applied normal load.

Frictional or traction forces (during normal loading only) acting tangentially to both of the contacting surfaces at the sphere-film interface will have an opposite effect. By opposing radial displacement of the film, and hence slip between the sphere and film, contact area would be less than that expected without frictional interaction. Frictional resistance to radial displacement of the layer out of the contact zone could also cause significant shear stresses to develop in the film, possibly resulting in debonding of the film from the substrate.

Viscoelastic Behavior

If the polymer coating behaves in a viscoelastic manner (as most polymers do), the time-dependent relationship between stress and strain must be considered. In order to formulate expressions for contact stresses, the relationship between stress and strain must be assumed to be linear, strains must remain small and the principle of superposition must be valid (46). In expressing the stress-strain relationships for viscoelastic materials, one of two types of functions is generally used: the creep compliance or the relaxation function. The creep compliance function describes the strain response to a step input of stress, while the relaxation function depicts the stress resonse to a step input of strain. To formulate an isotropic material's response to both shear and volumetric deformation, two independent functions must be determined--one corresponding to shear deformation and the other to volumetric deformation.

To date, a formulation of the contact between a sphere and a layered substrate which considers the layer to behave in a viscoelastic fashion has not appeared in the literature. If we consider the problem at hand, however, it is not difficult to see what effect viscoelasticity would have on the normal loading process. Since the relationships between stress and strain are time-dependent, the penetration of the steel sphere into the layer would also be a function of time, increasing with increasing time to some unknown value. It is for this reason that care was taken to begin each fretting test a specified time (30 seconds) after normal loading, so that the initial penetration depth would remain constant for all of the tests run on a given polymer type at a given load.

Plastic-Elastic Behavior

Once the yield point of the layer has been exceeded by a small amount as predicted by an appropriate failure theory, regions of material undergoing a plastic state of stress will be formed in the layer. In plastic-elastic behavior these regions are effectively contained by surrounding elastic regions which, in effect, cause the strains within the plastic material to be on the order of those in the elastically deformed material (47). This behavior, also known as contained plasticity, generally occurs between one and three times the yield strength of the softer material. A plastic-elastic development of sphere-on-layered flat contact does not presently exist; however, some work has been done by Hardy (48) on the indentation of a plastic-elastic half-space by a sphere utilizing Finite Element Methods.

Plastic Behavior

Plastic behavior is differentiated from plastic-elastic behavior by large strains within the deformed bodies as compared to those predicted by elastic theory. In this type of behavior, elastic effects can be neglected and the deformed material is considered to be comprised of perfectly rigid areas (where no deformation takes place) and regions of plastic flow. Within the plastic regions, flow occurs at a constant stress in shear, tension and compression. In this mode of deformation, stresses in the contacting bodies are described by a slip line field. These slip lines are parallel to the direction of the principle shearing stress at every point in the body (49). Application of Slip Line Theory to contact between a sphere and a perfectly plastic half-space has been formulated by Richmond (50) allowing for no interfacial slip. Richmond finds that the mean contact pressure is independent of penetration and that it is approximately equal to six times the shear strength of the half-space. No consideration of a layered half-space appears in the literature.

Considering the sphere-on-layered-flat geometry and the range of polymeric materials used in this investigation, two types of behavior could be expected once stresses within the polymer film exceed the yield limit. For ductile materials (those with a long elongation at break), it is conceivable that the polymer could simply flow out of the contact in response to the high stresses. For brittle materials (those with a short elongation at break), one would expect the film to fracture in response to the stress.

5.1.2 Tangential Motion

Tangential motion of the ball can be accommodated in two ways: 1. slip at the sphere-film or film-substrate interface; or 2. shear (or tangential) deformation of the film. Obviously, these are the two extreme cases and expected behavior would probably be a combination of both. Several factors will be important in determining which behavior is predominant:

1. The amount of penetration of the ball into the film layer caused by normal loading.

2. Adhesion between the ball and film.

3. The response of the coating material to tangential displacement at a given frequency.

4. The influence of the coating which is exterior to the contact area.

The degree of ball penetration into the film causes two primary effects. Penetration determines the amount of film material that must be "plowed" by the sphere once tangential motion is introduced, and it causes a reduction in the thickness of the film beneath the sphere. For a given film, the resistance produced by plowing could be sufficient to prevent gross sliding between the ball and film, depending on the shear properties of the polymer and the effective thickness of the film under the ball. One would expect a ductile film with a low shear modulus and an effective thickness (after normal loading) which is greater than the tangential displacement to behave in this fashion. Excessive plowing could also result in separation of the substrate-film interface by

generating tangential forces which are greater than the bond strength of the film to the underlying disk.

Adhesive forces between the steel ball and polymer film could have a similar effect. By increasing the "bond" strength between the ball and film, the applied tangential motion might not be sufficient to overcome these adhesive forces, resulting in no slip between the polymer and the ball. Delamination of the film from the substrate could also occur.

The dynamic response of the film to the tangential motion must also be considered. Due to the visocelastic nature of polymeric materials, some films may not be able to respond to the frequency of the tangential reciprocating motion which would result in slippage between the ball and film.

The film which is exterior to the contact zone will also have an effect on the sliding system. By containing the film within the contact area, the exterior film would tend to "stiffen" the response of the film in the contact, possibly resulting in slip between the ball and coating.

Effect of Sliding and Tangential Deformation

The effect of tangential loading upon a normally-loaded sphere in contact with a layered substrate has received no attention in the literature. One would tend to suspect that an increase in the state of stress would occur, especially with respect to the shear stresses within the layer. If the film was in a plastic state of stress prior to tangential motion of the ball, plastic behavior would probably be maintained and the motion of the ball could cause the polymer to flow out of the contact area at the ends of the sliding path, or promote brittle

fracture (depending on the polymer's response to stresses which exceed yield). It is also possible that tangential motion of the ball could cause a change in behavior. For example, if the layer behaves in an elastic fashion under normal load, tangential forces could increase the stress state of the film resulting in plastic behavior. In any case, high stresses exceeding the yield point of the polymer are undesirable and would allow polymer to be removed from the contact area by flow or fracture.

Once reciprocating sliding and tangential deformation begin, a wide range of behavior can occur. One of the most obvious results of the sliding and deformation would be heat generation by frictional processes within the film and at the sliding interface. An increase in temperature could then have a significant effect on the behavior of the polymer film, possibly leading to melting and flow out of the interface or at least a significant reduction in yield strength; either of these effects could result in film failure.

In a dynamic sliding situation, we must also consider the possibility of wear which can occur on either of the contacting surfaces: the steel ball or polymer film. Wear of the polymer film would generally be considered as unwanted behavior, since it would reduce the effective amount of film to prevent contact. However, it is possible that through a "wearing-in" process stresses at the interface could be reduced, in turn, resulting in a reduction in wear rate and a more conforming geometry. If fretting damage occurs to the steel surface (which is obviously undesirable since the purpose of the film is to prevent fretting), abra-

sive fragments of metal and metallic oxides trapped in the interface could also accelerate film failure.

5.2 General Findings

The results of this work show that there are two important considerations in using polymeric films to prevent fretting corrosion. First, the film must be able to prevent metallic contact for an extended period of time. Second, the film itself must not fret the steel countersurface. In the sections that follow, the general findings of this work with respect to these two criteria will be summarized and discussed.

5.2.1 Polymer Film Life

In this study, two observations were made with respect to polymer film life:

1. Polymer film life varies greatly with polymer type and is not solely a function of film thickness.

2. Polymer film life tends to decrease with increasing normal load.

Table 5-3 summarizes the life of the various polymer films tested at the 22.3 N normal load. The values in parenthesis are the mean thicknesses of the specimens tested for each polymer type. As can be seen, there is a large range of life from 8 seconds (with PVDC) to over 3600 seconds (for PS and HDPE); after 3600 seconds run time, both PS and HDPE had not failed and the test was terminated. Table 5-3 also shows that there is an overall trend for thicker films to last longer. However, there are a few exceptions. PI coatings had average lives which were signficantly longer or equal to films five times as thick, while

TABLE 5-3 Summary of Average Polymer Film Life and Thickness

(22.3 N Normal Load)

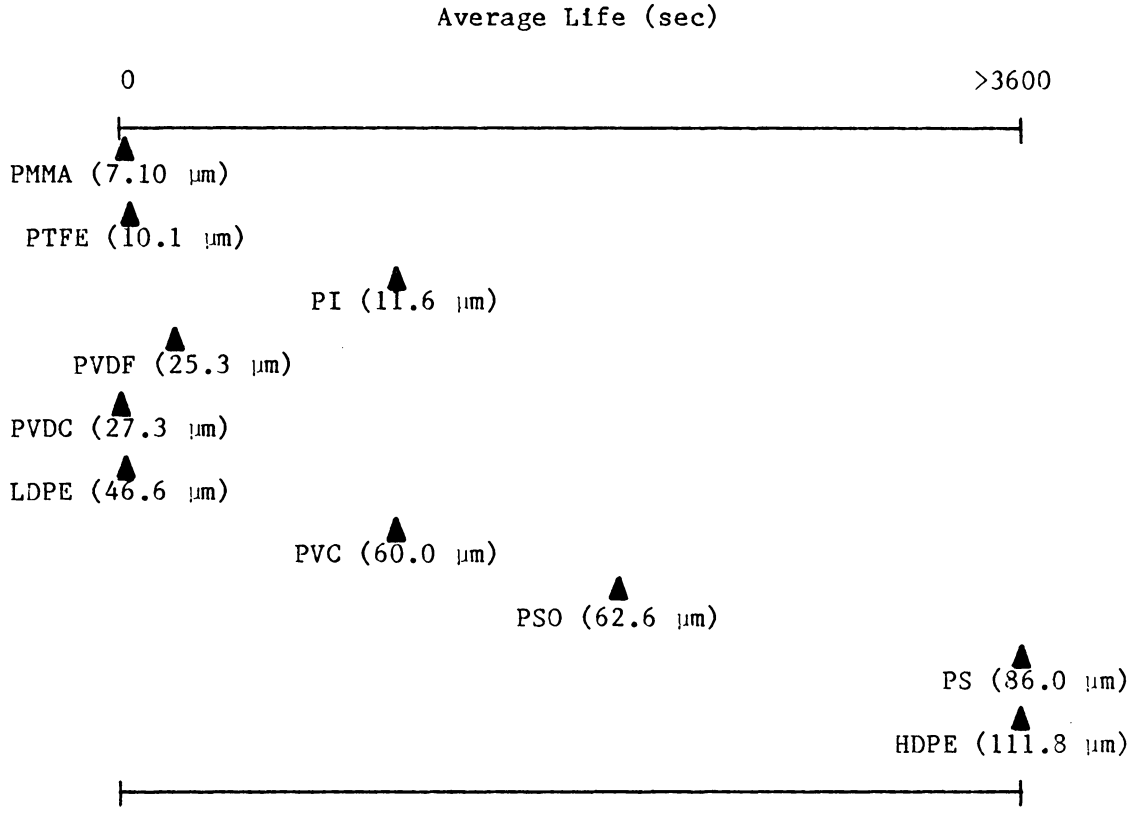

PVDC and LDPE had short lives compared to films of equivalent and lesser thicknesses. Since the interaction between film thickness and polymer type is not known, it is difficult to determine why certain films lasted longer than others. To overcome this problem, comparisons will be made within the four designated groups which are based on similar film thickness. All comparisons are based on data obtained at 22.3 N normal load.

Group I Films: PMMA, PTFE and PI

Table 5-4 compares some of the observed behavior (life and friction) along with several physical properties of the Group I films. As can be seen, there is an increase in average life (which is statistically significant) with polymer type in the order of PMMA, PTFE and PI. It is also interesting to note that PI had an average life 1100 seconds greater than PMMA and PTFE.

A comparison of the calculated maximum Hertzian contact pressure to the compressive yield strength for each polymer may explain this behavior. As can be seen for PMMA and PTFE, the Hertzian pressure is either in the range of or exceeds the compressive strength of the polymer film. Since the Hertzian contact pressure neglects the film substrate interaction (which has been shown to be significant for all of the films tested) and the effect of tangential loading caused by the motion of the steel ball, it is probably a conservative estimate of contact pressure. This would then tend to indicate that for both PMMA and PTFE, their response to a plastic state of stress would govern their life during fretting. Examination of the photographic data obtained for PMMA and PTFE shows that the fretting action removed the polymer film from the contact zone (and therefore led to film failure) by a different

TABLE 5-4 Properties of Group I Films

Property	Polymer Type PMMA	PTFE	PI
Average Thickness (μm)	7.10	10.1	11.6
Thickness Range (μm)	6.10-8.13	8.64-12.7	10.9-12.7
Average Life[a] (sec)	15	81	1223
Maximum Coefficient[a] of Friction (Mean Final)	0.68	0.11	0.77
Maximum Hertzian[a] Pressure (MPa)	85.1	26.2	71.9
Compressive Yield Strength[b] (MPa)	72.4-124.1	11.7	206.8-275.8
Shear Strength[b] (MPa)	27.6-43.4	8.3-20.0	49.7
Young's Modulus[b] (GPa)	2.2-3.1	0.40	2.1
Elongation at Break[b] (%)	2-10	200-400	8-10
Transition or Melt[b] Temperature (^{o}C)	90-105	327	310-365

(a) At 22.3 N Normal Load
(b) Source: Reference (38).

mechanism for each film. This might be expected since the structure of each is different. PMMA was believed to be removed from the interface by plastic flow and cracks or tears which developed in the polymer perpendicular to the sliding direction. PTFE was removed from the interface by the shear of thin layers from the film. This was believed to be caused by plowing action since scanning electron micrographs revealed almost 100% penetration of the ball into the film early during the fretting process.

For polyimide films, no conclusion can be made as to whether the contact stress exceeded the yield stress of the polymer since the calculated Hertzian pressure is less than the compressive yield strength. If we examine the photographic data for PI, we see no evidence of plastic flow. This might be expected since PI tends to behave in a brittle fashion (as evidenced by an elongation at break of 8-10%) in a state of stress which exceeds yield. PI films do show definite evidence of failure in shear due to the tangential motion of the ball, since a thick layer of the polymer film was observed to transfer to the steel ball during fretting. The adhesive forces between the polymer and the steel countersurface are thought (by the author) to be resonsible for this effect. Adhesive forces may play some role in the long life of the coating by keeping the sheared layer in the contact zone, resulting in a polymer-polymer sliding system.

If one examines the glass transition or melt temperatures of the three polymers, an obvious difference between PMMA and the other two polymers can be seen. The glass transition temperature of PMMA is less that that of PTFE and PI by more than a factor of three. PMMA also has

a relatively high coefficient of friction, similar to PI and over six times that of PTFE. Although no definite evidence exists, it is possible that frictional interaction between the steel ball and PMMA films could have led to interfacial temperatures higher than the glass transition temperature of the polymer. This, in turn, could lead to softening and a decrease in yield strength. The possible softening of PMMA could also account for its ability to flow out of the contact zone. This was unexpected since the polymer should behave in a brittle fashion as indicated by its short elongation at break (2-10%).

Group II Films: PVDF and PVDC

The Group II films, PVDF and PVDC, allow an excellent basis for comparison due to their similar structure and film thickness. Table 5-5 illustrates the thickness, life, and frictional data along with some physical properties of these two polymers. As can be seen, the average life of PVDF coatings was greater than PVDC, by over a factor of thirty. Also note that for both films, the estimate of contact pressure by Hertzian theory either exceeds the compressive yield strength of the polymer or lies within its range. The response of each film to this high state of stress will then need to be considered to try to understand the large difference in average life for the two polymers.

The photographic evidence obtained for each polymer shows a large difference in behavior, despite the similarity in structure. Some of the PVDC coatings tested did not even support the 22.3 N normal load without preventing metallic contact. It appeared that the cause of failure was plastic flow of the film out of the interface. PVDF coatings, in contrast, behaved in a manner similar to PTFE by shearing in

TABLE 5-5 Properties of Group II Films

Property	Polymer Type PVDF	PVDC
Average Thickness (μm)	25.3	27.3
Thickness (μm)	20.3-30.5	22.9-33.0
Average Life[a] (sec)	308	8
Maximum Coefficient[a] of Friction (Mean Final)	0.51	0.72
Maximum Hertzian[a] Pressure (MPa)	68.7	26.1
Compressive Yield Strength[b] (MPa)	36.5-95.1	13.8-18.6
Shear Strength[b] (MPa)	14.5-29.0	11.0
Young's Modulus[b] (GPa)	1.0-2.9	0.34-0.55
Elongation at Break[b] (%)	12-400	350-400
Transition or Melt[b] Temperature (°C)	164-178	160

(a) At 22.3 N Normal Load.
(b) Source: Reference (38).

thin layers which were then removed from the contact zone by the reciprocating action of the steel ball. The continuous removal of polymer from the contact area eventually resulted in metal-metal contact, and hence, the failure of PVDF films. Comparison of PVDF to PVDC adds support to the hypothesis that stronger films (those with higher yield strengths) will last longer, barring the influence of any secondary effects such as melting or thermal decomposition.

Group III Films: LDPE, PVC and PSO

Table 5-6 summarizes the thickness, life and properties of the Group III films. As can be seen, the LDPE coatings had a very short average life, at least a factor of 25 less than PVC and PSO. LDPE also has lower shear strength and modulus, which may explain its short life. LDPE films failed by a wear process called roll formation (51) in which layers of the coating are sheared by the motion of the ball and the plowing caused by excessive penetration. These layers are then rolled into cylindrical fibers and plowed out of the contact zone, resulting in eventual failure of the film. The low modulus of LDPE could account for large penetration on initial contact, resulting in excessive plowing once tangential motion is introduced. The low shear strength of the polymer could result in the shear of layers of the film during fretting.

While the average life of PVC is numerically less than that of PSO (i.e., 1212 vs. 2020 seconds, respectively), there is no significant difference between the two means because of the large range of life values obtained for each polymer. Despite the lack of statistical difference, it is interesting to note that the calculated Hertzian

TABLE 5-6 Properties of Group III Films

Property	Polymer Type LDPE	PVC	PSO
Average Thickness (μm)	46.6	60.0	62.6
Thickness Range (μm)	33.0-63.5	50.8-71.1	61.0-67.3
Average Life[a] (sec)	46	1212	2020
Maximum Coefficient[a] of Friction (Mean Final)	0.40	1.1	0.81
Maximum Hertzian[a] Pressure (MPa)	17.8	97.3	81.9
Compressive Yield Strength[b] (MPa)	-	55.2-89.6	275.8
Shear Strength[b] (MPa)	4.8-17.9	24.1-29.7	40.7
Young's Modulus[b] (GPa)	0.17-0.28	2.4-4.1	2.5
Elongation at Break[b] (%)	100-650	40-80	50-100
Transition or Melt[b] Temperature (°C)	106-115	75-105	190

(a) At 22.3 N Normal Load.
(b) Source: Reference (38).

pressure for PVC (the film with shorter life) exceeds the compressive yield limit whereas for PSO it does not.

In the initial stages of fretting, both PVC and PSO show some similar behavior. On initial contact, when the contact area is smallest, the stresses within the film will be their highest allowing the tangential motion of the ball to cause the top surface of the film to plastically flow out of the sliding path. This results in an increase in contact area. Once the contact area is enlarged, there is a corresponding drop in stress at the interface and both films behave in a brittle fashion. During this phase of behavior, cracks (which are oriented perpendicular to the sliding direction) form in the surface of the polymer. PSO continues to behave in a brittle fashion by the formation of cracks in the polymer coating, eventually resulting in failure. A different type of behavior is noted with PVC. The scanning electron micrographs taken after 45 minutes of run time for PVC show a definite change in the surface structure of the polymer; this is believed to be due to thermal softening. Note that both polymers had very high coefficients of friction, over 0.8, but that there is a marked difference in glass transition temperature. This difference (almost 100°C) may be responsible for the variation in behavior.

Group IV Films: PS and HDPE

Table 5-7 presents the thickness, life and friction data for polystyrene and high-density polyethylene. Physical properties of both polymers are also tabulated. As can be seen, PS and HDPE each had lives of over one hour. There is a significant difference in film thickness, PS being the thinner of the two by over 25%. A comparison of PS and

TABLE 5-7 Properties of Group IV Films

Property	Polymer Type PS	HDPE
Average Thickness (μm)	86.0	111.8
Thickness Range (μm)	81.3-91.4	99.1-132.1
Average Life (sec)	>3600	>3600
Maximum Coefficient[a] of Friction (Mean Final)	0.79	0.21
Maximum Hertzian[a] Pressure (MPa)	87.2	50.2
Compressive Yield Strength[b] (MPa)	82.7-89.6	18.6-24.8
Shear Strength[b] (MPa)	20.7-29.7	12.4-17.9
Young's Modulus[b] (GPa)	2.3-3.3	1.1
Elongation at Break[b] (%)	1.2-1.5	10-1200
Transition or Melt[b] Temperature (°C)	100-105	130-137

[a] At 22.3 N Normal Load.
[b] Source: Reference (38).

HDPE illustrates the contrast in behavior of a brittle polymer versus a ductile one.

Examination of the Hertzian contact pressure reveals that for both polymers the state of stress within the contact was probably sufficient to cause yielding. However, the response of each polymer is completely different. Large cracks, oriented perpendicular to the direction of sliding, form in the surface of PS films. This process also results in the formation of irregularly shaped debris particles.

HDPE behaves in a completely different fashion. Photomacrographs obtained from HDPE experiments reveal a plastic region in the center of the scar which appears to be effectively contained by the film surrounding the contact zone. HDPE films also respond to the tangential motion of the steel ball differently than polystyrene films. With PS, it is evident that the tangential motion of the ball results in sliding between the ball and film, since the scar has an elongated shape in the direction of motion. HDPE scars are almost completely circular in shape, indicating that little relative motion occurred between the ball and film, and the tangential displacement of the ball was accommodated by elastic deformation of the coating.

Effect of Normal Load on Polymer Film Life

An increase in normal load generally caused a decrease in average polymer film life. An increase in normal load can have several effects on the polymer film. As was previously discussed, the response of a film to normal loading will be determined by the state of stress within the film and the film itself. An increase in normal load could cause a change in behavior such as a transition from elastic behavior to either

elastic-plastic or plastic behavior. This could cause the film to either fracture or flow out of the contact zone. If the film was already in a state of plastic stress, the increase in load could lead to more extensive plastic flow or cracking of the polymer.

An increase in normal load will also cause the steel ball to penetrate more deeply into the polymer coating on initial contact. The increase in penetration will cause an increase in the plowing component of friction, causing higher shear stresses to be developed in the film once tangential motion occurs. For films in a plastic state of stress, this could cause the polymer to be plowed out of the interface once tangential motion is applied to the system. For elastic films the shear stresses within the film would increase, possibly resulting in shear failure or debonding from the substrate, either of which could lead to film failure.

The excessive plowing and deformation, either plastic or elastic could also lead to heat generation and therefore higher interfacial temperatures. As was previously mentioned, an increase in contact temperature could lead to melting or softening of the polymer film.

In this investigation, the effect of normal load on polymer film life was not documented by scanning electron microscopy or photomacroscopy, so it is not possible to describe the behavior of each film. However, it is important to note that an increase in normal load from 11.1 N to 44.5 N caused a dramatic decrease in the average life of most of the polymers studied. Table 5-8 presents the average lives of the polymers tested at the low and high loads. As can be seen for several of the polymers, the increase in load caused a decrease in life from

TABLE 5-8 Average Polymer Film Life at 11.1 and 44.5 N (sec)

Polymer Type	Average Life (11.1 N)	Average Life (44.5 N)
PMMA	76	4
PTFE	232	14
PI	2664	289
PVDF	1615	72
PVDC	1329	8
LDPE	138	35
PVC	>3600	18
PSO	>3600	15
PS	>3600	230
HDPE	>3600	>3600

over one hour to less than one hundred seconds. This observation is particularly interesting in that it shows the range of normal loads for which each polymer/thickness combination will be effective in preventing metallic contact (with the contact geometry studied). For example: PMMA, PTFE and LDPE had short lives at all of the three test loads which would tend to indicate that they are not effective barriers against contact. All of the other films had average lives over 1300 seconds at 11.1 N and might find application within and below the range of loads tested. HDPE films may be useful with higher normal loads since they lasted over one hour at all three of the test loads studied.

Two interesting observations were made with respect to the effect of normal load on polymer film life. Two of the polymers studied, polyvinylidene chloride and polystyrene, exhibited completely different behavior in response to an increase in normal load. For PVDC, a dramatic decrease in mean life (from 1300 to 8 seconds) was noted when normal load was increased from 11.1 to 22.3 N. Examination of the macroscope and SEM photographic data obtained from PVDC experiments at the higher load indicated that the polymer plastically flowed from the interface under the high contact stress and excessive plowing caused by deep penetration. For polystyrene, a large decrease in average life from greater than 3600 seconds to 230 seconds was noted when normal load was increased from 22.3 to 44.5 N, the result of gross brittle fracture at the higher load.

5.2.2 Frictional Behavior

Frictional forces can arise from two primary sources. The first is plowing of the film during the reciprocating motion of the steel ball

and the second is adhesion between the ball and film. As has been previously mentioned, if the frictional resistance is large compared to the ability of the film to deform in shear (e.g., films with low shear modulus), relative motion between the sphere and the steel substrate will be accommodated by tangential deformation of the film. If the film behaves in a rigid manner in response to the tangential forces, sliding would be expected to occur between the ball and film.

If one examines the frictional data recorded in fretting experiments for the ten different polymer types, three general observations can be made:

1. The coefficient of friction varies significantly with polymer type.

2. For all but two of the polymers (PTFE and HDPE), the coefficient of friction varies with run time, generally increasing from an initial value to some final value before film failure. For PTFE and HDPE, friction remained constant throughout a test.

3. The coefficient of friction does not correlate with average polymer film life.

Table 5-9 shows the mean initial and final coefficients of friction for the ten polymer/thickness combinations prior to film failure. As can be seen, a ten-fold variation of mean final coefficient of friction was observed with the ten polymers. Although the precise mechanisms by which each of the ten polymers resisted the tangential motion of the ball are not known, the photographic data obtained may provide some insight as to what is happening. The low friction of PTFE may be due to its highly linear crystalline structure which easily permits layers of

TABLE 5-9 Mean Initial Final Coefficient of Friction Prior to Film Failure (22.3 N Normal Load)

Polymer Type	Mean Initial Coefficient of Friction	Mean Final Coefficient of Friction
PMMA	0.51	0.68
PTFE	0.11	0.11
PI	0.34	0.77
PVDF	0.30	0.51
PVDC	0.65	0.72
LDPE	0.24	0.40
PVC	0.66	1.1
PSO	0.68	0.81
PS	0.62	0.79
HDPE	0.21	0.21

the polymer to be sheared by the reciprocating action of the ball. HDPE coatings also exhibited low friction. The frictional resistance of HDPE to the tangential motion of the steel ball is attributed to be caused by elastic deformation of the film. The almost circular scars observed in HDPE experiments support this view, indicating that slip at the sphere-film interface was limited. It is also interesting to note that several of the polymers had high coefficients of friction. PMMA, PI, PVDC, PVC, PSO and PS all had mean final coefficients of friction greater than 0.6. PMMA and PVDC were both plowed out of the contact zone; therefore, plowing is probably a factor governing their frictional behavior. The high coefficient of friction observed with polyimide films may be due to strong adhesive forces between the ball and film. These forces are thought to be responsible for the thick layer of transfer (to the steel ball) during polyimide experiments. The behavior of PVC, PSO and PS is less understood. Both PVC and PSO show evidence of plowing during the early stages of the test (less than 900 seconds), but not in the later stages. Polystyrene coatings show no signs of plowing or transfer (which might indicate strong adhesive forces), but only brittle fracture.

A second observation based on the frictional behavior of the polymers studied is that the coefficient of friction generally varies during a fretting test. For all of the films but PTFE and HDPE, the coefficient of friction increased from some initial value to a final value before film failure. This behavior is not fully understood; however, several factors could have played a role in the process:

1. Sliding between the ball and film could have acted to "clean" the contacting surfaces, possibly promoting stronger adhesive forces.

2. The increase in penetration of the steel ball during the test could have led to an increase in the plowing component of friction.

3. During the removal process of the film from the interface, the ball may have been forced to "ride" up on the polymer being displaced from the contact zone.

4. The increase in penetration of the ball may have caused an increase in the real area of contact. Since the adhesive component of friction is equal to the product of the shear strength of the junction and the real area of contact, an increase in contact area could cause an increase in friction.

Figure 5-2 is a plot of the mean final coefficient of friction versus average polymer film life. As can be seen, average life in no way correlates with the friction coefficient. As an example, four of the films which had coefficients of friction of about 0.8--PVDC, PI, PSO and PS--show a large range of life. PVDC coatings had an average life of eight seconds while PS coatings lasted over one hour.

It is important to consider what effect friction could have on the polymer film and the entire process. An obvious result of high friction previously discussed is heat generation, which could lead to softening or melting of the film. This effect would depend on the melting or glass transition temperature of the polymer, the amount of heat generated and the ability of the film to release or transmit heat through conduction, convection or radiation. Thermal processes (heat generation) are suspected to play a role in the life of two of the polymers

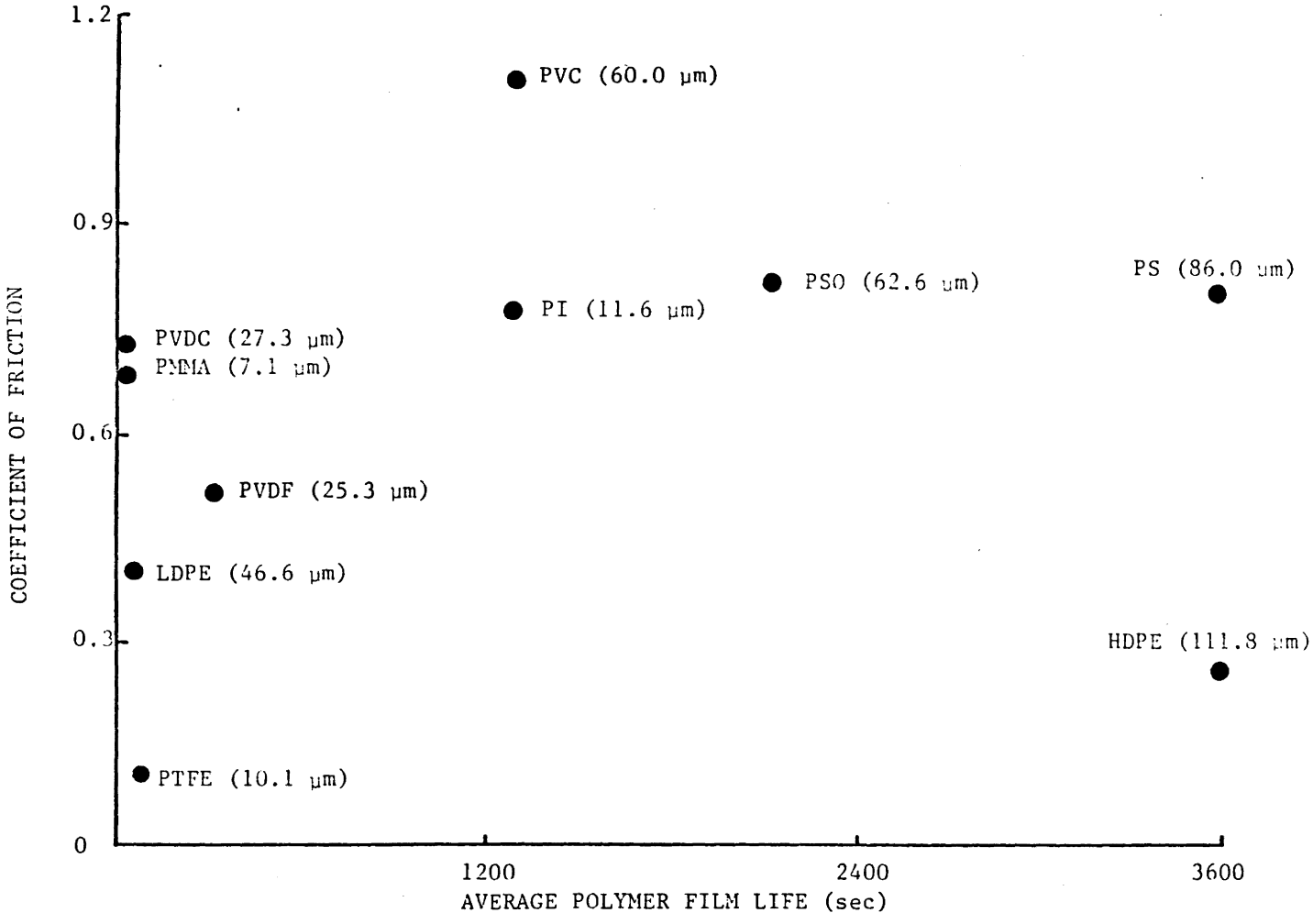

FIGURE 5-2. Plot of Mean Final Coefficient of Friction Prior to Film Failure Versus Average Polymer Film Life. (Numbers in Parentheses Refer to Average Film Thickness. All Values at 22.3 N Normal Load.)

studied in this investigation: PMMA and PVC. Although the evidence is not conclusive, both polymers have relatively high coefficients of friction and low glass transition temperatures; there is also photographic evidence of softening and flow.

5.2.3 Fretting of Steel by Polymer Films

Table 5-10 shows those films which caused fretting damage to the steel countersurface and their average lives. The photographic data obtained in phase 2 of the experimental work at 22.3 N normal load was used to make this determination. In the examination of the photographic data, two criteria were used to determine if the film caused steel damage: 1. the presence of obvious grooves or pits in the steel ball; and 2. the presence of fine reddish-brown to orange particulate debris. This debris is believed to be iron oxide since it was always present after metallic contact.

In examining Table 5-10, we must consider the life of each film and its behavior with respect to damage caused to the steel countersurface. As can be seen, three of the polymers which had relatively long lives (PVC, PSO and HDPE) also caused damage to the steel ball. Two of the polymers tested, PVDC and PMMA, could not be evaluated for fretting damage because of their very short lives. LDPE, PTFE and PVDF all prevented fretting corrosion. However, they had relatively short lives of less than 400 seconds. The two films which stand out in Table 5-10 are polyimide and polystyrene; both had average lives of greater than 1200 seconds (PS coatings had lives that exceeded the one hour test limit) while effectively preventing fretting corrosion.

TABLE 5-10 A Summary of Fretting Damage to the Steel Countersurface by Polymer Films

Polymer Type	Avg. Life[a] (sec)	Fretting of Steel by Polymer Film? YES	UNDETERMINED	NO
PVDC	8		X	
PMMA	15		X	
LDPE	46			X
PTFE	81			X
PVDF	308			X
PVC	1212	X		
PI	1223			X
PSO	2020	X		
PS	>3600			X
HDPE	>3600	X		

[a]At 22.3 N Normal Load.

Several of the polymer films studied in this investigation have been evaluated in bulk form by other investigators (see Chapter 2.0, Section 2.2) for fretting damage to steel. These polymers are: polymethylmethacrylate, polytetrafluorethylene, polyvinylidene fluoride, polyvinyl chloride, polysulfone and polyethylene. Higham, Bethune and Stott (24,25) find that polymethylmethacrylate, polyvinyl chloride, polysulfone and polyethylene (they do not state whether high or low density was used) all cause damage to a steel countersurface. The authors also found that PTFE and PVDF did not cause fretting damage to steel. As can be seen from Table 5-10, the conclusions of these investigators agree with the behavior observed in this work.

If we examine the group of films which prevented fretting corrosion prior to their failure (LDPE, PTFE, PVDF, PI and PS), we note that there is a wide variety in chemical structure, PTFE and PVDF being the most similar. The behavior of these five films during fretting is also quite different. Thin films of PTFE and PVDF were transferred to the steel ball; this may have played a role in their ability to prevent steel damage. A thick layer of polyimide coatings transferred to the steel countersurface which resulted in a polymer-polymer sliding system, possibly protecting the steel ball. Both LDPE and PS prevented fretting corrosion and in these tests no polymer transfer was observed on the steel ball within the contact region.

The films which did cause steel damage: PVC, PSO, and HDPE also have very different chemical structures. The nature of the steel damage caused by each is also different. PVC films caused extensive grooving throughout the contact region, apparently caused by metallic oxide

particles which were trapped in the interface. The process by which these oxides were formed is unknown. However, examination of the photomacrographs suggests that PVC produced more metallic oxide debris than PSO or HDPE in a given period of time. PSO also caused grooves in the steel countersurface, but not to the extent that PVC did. In contrast to PVC, PSO coatings were capable of removing large volumes of metal from the steel ball in less than 30 minutes run time. Since no large particles of metal were observed in the photographs of PSO scars, the process of metal removal is assumed to occur continuously over a period of time and not abruptly. Again, the mechanism by which this process begins is unknown. HDPE films also caused damage to the steel ball during fretting. However, it was much less severe than that caused by PVC and PSO. HDPE coatings form a series of randomly spaced grooves in the center of the contact region on the ball. As is the case with PVC and PSO, these grooves are oriented in the sliding direction. HDPE ball scars also show streaks of a brown material which are approximately the same size and shape of the grooves in the steel ball. Although the nature of these "streaks" is unknown, it is possible that they could be metallic oxides forming on the surface of ball and responsible for the grooves seen on the ball surface.

The differences in chemical structure and mechanical properties within the groups of polymers that prevented and caused fretting damage suggest that there may be numerous mechanisms for both prevention and initiation of fretting corrosion by polymer films. By either chemical or mechanical processes, the film may behave in a manner which eliminates the possibility of fretting corrosion. Since no chemical analysis

was done in this work, it is difficult to make any definite conclusions as to chemical processes which possibly could have prevented or caused fretting damage. However, two physical mechanisms by which a polymer film can prevent fretting corrosion are evident. The first is the transfer of polymer to the steel countersurface which results in a polymer-polymer sliding system, eliminating slip at the steel-polymer interface. Polyimide coatings were an excellent example of this type of behavior. The second mechanism of protection is that the polymer film may be able to deform elastically in response to the tangential motion of the ball, again resulting in no relative motion between the ball and film. Although this behavior was only observed to a limited extent with HDPE (which caused fretting damage), it is thought to be a plausible prevention mechanism and should be the subject of future investigation, possibly by the use of elastomeric films.

In order to gain further understanding of the behavior of the ten polymer films studied, it is necessary to consider each on an individual basis. This will be presented in the following sections.

5.3 Specific Findings: Behavior of Each Polymer Type

One of the most striking results of this investigation was the wide variety of behavior that was photographed with the ten polymer types studied. In this section, the photographic data for each polymer film at 22.3 N normal load will be discussed.

5.3.1 General Comments on the Photographic Data

Before proceeding with a discussion of each polymer, some general comments need to be made concerning the photographic data. Although

each polymer had its own particular response in fretting contact, all of the behavior observed can be grouped into seven different types which are presented in Table 5-11. A question mark next to a polymer type indicates that although the behavior is not directly confirmed by the photographic data, it is hypothesized to occur on the basis of indirect evidence.

It is important to note from Table 5-11 that several of the polymers are listed as showing several different types of behavior. For example, PMMA exhibited plastic flow, brittle fracture, transfer to the steel ball within the contact zone and possible softening (which may have caused it to plastically flow out of the interface). It is felt that the interrelationship of these types of behavior is important in studying the response of polymer films to fretting contact.

It is also important to note that each behavior listed in Table 5-11 did not occur in the same fashion with each polymer film. As an example, if we consider plastic flow, five polymers showed this type of response to fretting contact. For four of these--PMMA, PVDC, PVC and PSO--plastic flow resulted in removal of polymer film from the contact area and is attributed to be the major cause of failure of PMMA and PVDC. Plastic flow only occurs in the early stages of fretting for PVC and PSO, resulting in a larger contact area. For HDPE, plastic behavior occurs in a central region of the film in the contact zone. This central region appears to be effectively contained by the surrounding polymer film which prevents removal of polymer from the interface.

Another general observation made on close examination of the macroscope and SEM photographs is the difference in shape of the scars for

TABLE 5-11 Summary of Polymer Film Behavior

Type of Behavior	Polymer Films which Exhibit Such Behavior
Plastic flow or deformation	PMMA, PVDC, PVC, PSO, and HDPE
Brittle fracture	PMMA, PI, PVC, PSO, and PS
Shear in thin layers	PTFE and PVDF
Shear in thick layers	PI
Roll formation	PVDF and LDPE
Transfer to steel countersurface	PMMA, PTFE, PI, PVDF, PVDC, and PVC
Thermal softening	PMMA (?) and PVC (?)

each polymer type. Four different types of shapes: elliptical, circular, rhombic and rectangular were noted and are summarized in Figure 5-3 along with the polymers that developed each shape. The difference in scar shapes suggest complex physical phenomena--a definite source for future study. It is also believed that these shapes could provide valuable insight as to the behavior of the films studied.

An elliptical shape implies that the penetration depth of the ball as it slides across the polymer surface is not constant, but less at the ends of the sliding path than at the center. It is interesting to note that the polymers with low modulus and compressive yield strength show this type of behavior. Both properties could result in deep penetration of the ball into the film on initial contact, either by elastic or plastic deformation, which would then result in plowing, causing the ball to "ride" up on the plowed polymer at both ends of the sliding path once tangential motion occurs.

The circular scar, only observed with HDPE, indicates that instead of gross sliding between the ball and film, the tangential motion of the ball was accommodated by tangential deformation of the film in the direction of sliding. The low shear modulus of HDPE along with its thickness (HDPE was the thickest film tested) may account for this behavior.

Of all of the shapes, the rhombic or "diamond-shaped" scar is the most unusual. The formation of this scar only occurs with PVC and PSO. Both of these polymers plastically flow in the early stages of fretting, followed by brittle fracture and cracking.

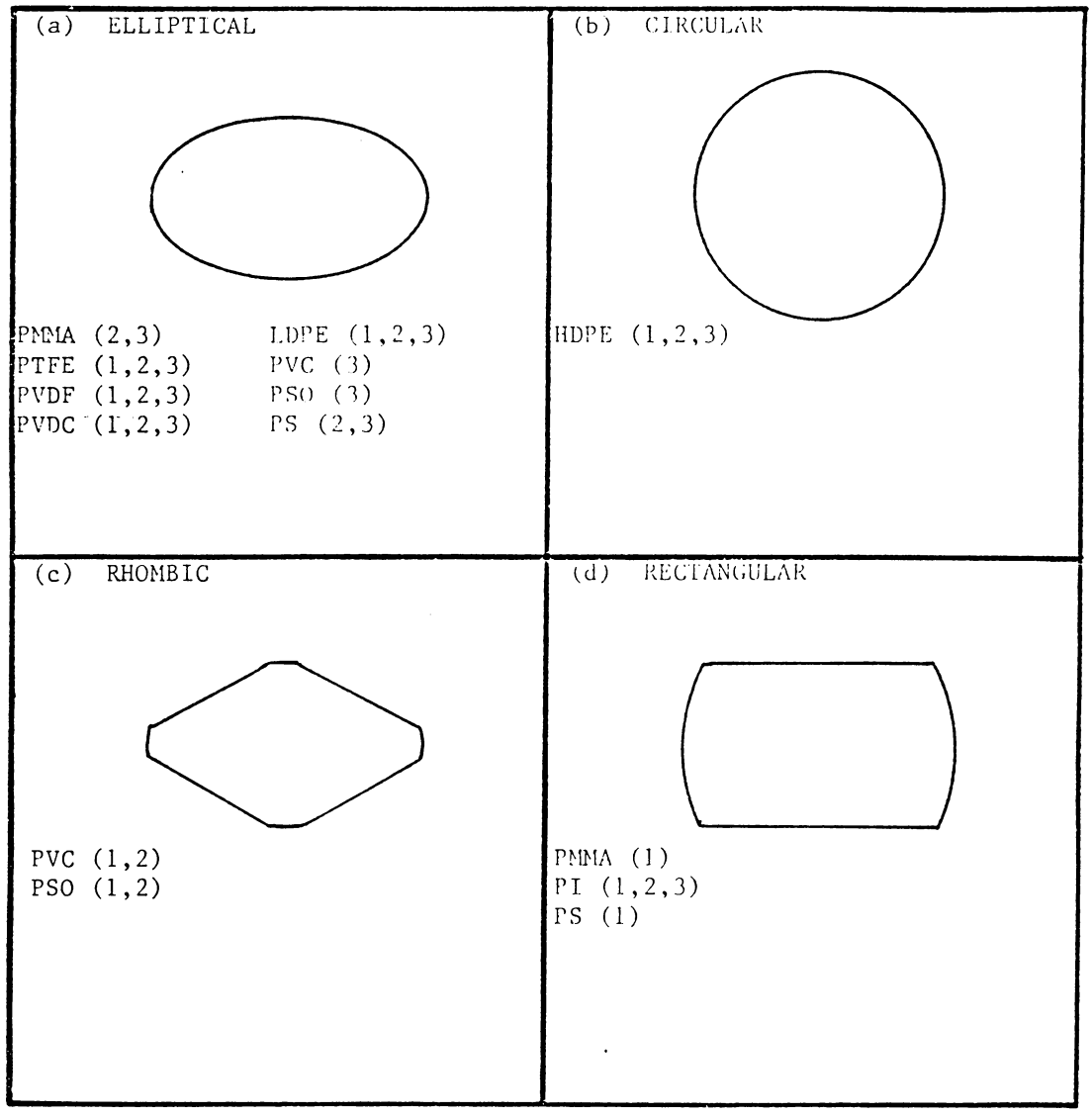

FIGURE 5-3. Various Scar Shapes Observed on Polymer-Coated Disks in Fretting Tests Run at 22.3 N Normal Load. (Test Numbers in Parentheses Refer to Fretting Behavior Test Run Times Presented in Table 4-2).

The almost rectangular shape tends to occur only with the rigid, brittle polymers, namely those with a low elongation at break and high modulus. The straight edges of this type of scar indicate a constant depth of ball penetration during each cycle of motion. This would be expected of a more rigid, high modulus material in which plowing is not a significant factor in the sliding process.

It is also important to note that the scar shape is a function of run time. Examination of Figure 5-3 shows that for several of the polymers, the shape of the scar changed with increasing run time. For example, PMMA Test 1 scars (5 seconds run time) were rectangular in shape while the Test 2 and Test 3 scars (33 and 60 seconds run time, respectively) were elliptical in shape. This effect may be explained by the fact that penetration of the ball into the polymer film is not constant throughout a test for these polymers. As penetration increases, leading to film failure, the pattern of the scar will change.

5.3.2 Behavior of Each Polymer Type

In the following sections, the behavior of each polymer type will be discussed on an individual basis.

Polymethylmethacrylate

PMMA films were not successful in preventing metallic contact (mean life = 8 sec.). The major cause of their failure seems to be plastic flow. Close examination of the photographs reveals that early in the fretting process (less than 1200 cycles), a large portion of the polymer film was forced to one end of the contact zone. Cracks or tears in the polymer surface running perpendicular to the sliding direction then facilitated the formation of debris. The plastic flow of PMMA is con-

sidered to be a surprising effect, since it was expected to behave in a purely brittle fashion (elongation at break of 2-10%). It is possible that the occurrence of plastic flow could be caused by softening of the polymer film by frictional heat generation. PMMA films had a relatively high coefficient of friction (0.68) along with a comparatively low glass transition temperature (90-105°C).

No conclusion could be made as to whether PMMA coatings caused fretting damage.

Polytetrafluoroethylene

PTFE coatings were unable to prevent metallic contact for over two minutes. The behavior of PTFE is consistent with its highly crystalline structure which allows slippage of molecular layers due to the absence of any crosslinking or branching. Due to the relatively low modulus of PTFE (about 0.5 GPa) and low compressive strength (11.7 MPa), penetration (due to static normal loading) of the ball with respect to the thickness was probably large. Measurements taken from the SEM photographs (after 30 seconds run time) indicate that penetration was almost 100% of the film thickness. This, in turn, caused significant plowing once tangential motion was applied. Thin layers of the film were then sheared from the coating and removed from the contact zone. These thin films also transferred to the steel countersurface, but were not of sufficient thickness or strength to provide protection from metallic contact.

PTFE coatings caused no damage to the steel ball during their short lives. However, as soon as all of the film was removed from the interface, gross fretting damage occurred to the contacting steel surfaces.

Polyimide

The polyimide films tested were relatively thin and had surprisingly long life values, i.e., up to 2800 seconds. The reason for this may be due to the transfer of a thick layer of the polyimide film to the steel ball during fretting. Strong adhesive forces between the film and the steel ball presumedly caused shear within the film layer and at the film-substrate interface once tangential motion occurred. This causes some interesting changes in the sliding system. Instead of the steel ball sliding on the polyimide film, the transferred layer (on the ball) slides on the remaining layer of film on the steel disk and the exposed metal substrate. This opens up the possibility of fretting of the exposed metal substrate by the transferred layer, although no such behavior was observed. Under the phase two test conditions, thicker films may eliminate the shear failure at the film-substrate interface while still permitting adhesive transfer of a layer of the film, resulting in a polymer-polymer sliding system. This protective mechanism could be externally imposed on any sliding system by coating both of the contacting bodies with polymer film.

Consistent with the brittle nature of polyimides, both the transferred film and that remaining bonded to the substrate begin to fracture after a significant number of cycles of fretting, producing large irregular shaped debris particles and eventual metallic contact. After film failure, the process resembles that of a steel-on-steel system with fretting damage to both surfaces and production of metallic oxides.

Polyvinylidene fluoride

PVDF coatings were able to prevent damage to the steel countersurface prior to metallic contact. During the fretting process, thin layers of the film were sheared from the coating and removed from the interface at both ends of the sliding path; this is similar to the behavior observed with PTFE. These thin layers were also transferred to the steel countersurface, but proved to be ineffective in preventing metallic contact. Small fibers of PVDF were also formed in the process by a mechanism known as roll formation (51). In this process, shear first occurs within the polymer layer. Then, due to the reciprocating nature of the sliding system, the removed layers are rolled into cylindrical fibers. After film breakthrough, damage occurs on both steel surfaces.

Polyvinylidene chloride

PVDC coatings were not capable of preventing metallic contact, often even under static loading, resulting in a range of life values from zero to twelve seconds at the 22.3 N normal load. Due to: (a) the fact that the stresses within the polymer exceeded the yield limit; and (b) the ductile nature of the polymer (elongation at break over 350%), the film plastically flowed out of the interface at both ends of the sliding path. This process was also accompanied by the formation of large rolls of polymeric material which were evidently plowed out of the contact zone during the first few cycles of fretting action.

PVDC coatings also produced one of the most striking and peculiar patterns of transfer to the steel ball. The nature of the brown transfer is unknown; however, it obviously has little beneficial effect on

life. Due to the short lives of PVDC, coatings no conclusion could be made as to their ability to prevent fretting corrosion.

Low-density polyethylene

LDPE coatings, while not causing any damage to the steel countersurface, did not last over 90 seconds. The primary mechanism of polymer removal from the interface appears to be roll formation (51), as is evident from the nature of the polymer debris. Deep penetration of the ball into the film as a result of the low modulus of the material along with its low shear strength facilitated the formation of debris. Once tangential motion was applied to the system, plowing and possibly adhesion caused small "areas" of polymer to be torn out of the film surface which were in turn trapped in the interface and rolled into cylindrical fibers. This accounts for both the nature of the debris and the rough texture of the polymer within the contact zone prior to film breakthrough. Eventually this rolling process resulted in the removal of these fibers from the interface, leading to film failure.

Polyvinyl chloride

PVC films lasted up to 1700 seconds while causing significant damage to the steel countersurface in less than 900 seconds. In all three of the phase two test runs (900 sec, 1800 sec, and 2700 sec), reddish brown metallic oxides are present and the steel surface appears to be grooved and polished. Apparently the oxide particles are responsible for the grooving of the steel ball, acting as third body abrasives trapped within the interface. As the oxide particles migrate out of the interface, they apparently cause damage to the entire contact are of the ball. The formation of these oxides is not understood. However, the

thermal instability of PVC along with its tendency to release HCl may play a significant role in the process.

Three stages of behavior were observed with PVC coatings. In the first stage, a layer of the polymer was removed by plastic flow. At the initiation of a test, the contact area will be the smallest; hence stresses will be at their highest values causing the polymer to flow to the ends of the sliding path. This process causes an increase in contact area resulting in lower stresses within the remaining polymer film. In the second stage, the polymer behaves in a brittle fashion with large cracks forming in the polymer surface running perpendicular to the sliding direction. The surface also has areas containing large amounts of broken up polymer fragments. In the third stage, the surface is completely different, having a smooth but irregular texture which appears to be the result of softening. Frictional heat generation may have been responsible for this behavior since PVC coatings were shown to have maximum coefficients of friction greater than 1.0 and the lowest glass transition temperature of any of the polymers tested (i.e., 75°C).

Another peculiar behavior of PVC was the formation of a light-colored annulus around the contact zone. This behavior was observed in both static (no tangential displacement) and dynamic situations. The observed annulus may be the result of high shear stresses within the polymer film which may cause the film to delaminate from the disk substrate; this could change the optical properties of the system. These high shear stresses are believed (by the author) to be caused by strong adhesion between the steel ball and polymer. Adhesive forces are thought to be a significant component of the frictional force for PVC

primarily since plowing only appeared to be significant in the initial stages of the fretting process.

Polysulfone

Polysulfone caused damage to the steel ball in less than 900 seconds. Grooving of the steel in the sliding direction, presumedly caused by abrasive oxide particles trapped within the contact zone, is present. However, the steel surface has a deformed appearance and large areas of metal have been removed. Since no large metal particles were found in any of the debris, it is possible that the removal of metal may have occurred over a period of time, possibly being initiated by the abrasion of metallic oxide particles in the interface.

Polysulfone coatings show two distinct types of behavior during the fretting process. The first is plastic flow, undoubtedly initiated by the small contact area at the beginning of each test. After the contact area has been enlarged by plastic flow, the polymer behaves in a purely brittle fashion. Cracks form in the polymer running perpendicular to the sliding direction. This results in the formation of a peculiar ridge structure in the film. That these ridges support the load of the steel ball can be easily seen since their surfaces have a smooth, worn appearance. These ridges also explain the deformed appearance of the ball scars in polysulfone experiments. In order for wear to occur in this system there must be contact, and since contact is confined to the tops of these ridges, the wear pattern on the ball matches the pattern of the ridges; this results in an uneven, worn ball surface.

The light annular region observed with PVC is also seen surrounding the contact area in PSO coatings. Again, high shear stresses within the

polymer layer are believed to be the cause of this effect, since PSO films also had high coefficients of friction (often greater than 0.8).

Continuous formation of cracks within the load-supporting ridges is suggested as the primary mechanism of failure of polysulfone films. Further crack propagation results in the formation of loose polymer debris particles which are removed from the interface. Eventually a point is reached where only loose polymer debris particles remain in the interface; these are not capable of preventing metallic contact.

Polystyrene

Polystyrene coatings were capable of preventing fretting corrosion while having lives that exceeded one hour. The behavior of polystyrene contrasts to several of the other polymers (PTFE, PI, and PVDF) which prevented fretting corrosion in that no transfer of polymer (PS) was observed on the steel countersurface.

Polystyrene films exhibited a "wearing in" process that may be responsible for their long life. In the initial part of the fretting process, large particles of the polymer were fractured from the coating; this resulted in a very rough surface and an irregularly shaped contact area. Similar to the behavior of PVC and PSO, cracks running perpendicular to the sliding direction were also formed in the film. As this initial stage proceeds, the contact area becomes larger and more clearly defined, eventually obtaining an almost perfectly elliptical shape with a smoother surface. The combination of increased contact area and a more conforming contact may reduce stresses within the coating and cause a significant change in the wear process. This change is a dramatic

decrease in the size of the wear particles and possibly a lower wear rate (actual wear volumes were not measured).

High-density polyethylene

HDPE films had lives which exceeded one hour while causing damage to the steel countersurface. HDPE coatings caused a series of grooves in the steel ball which were confined to a central region of the ball scar, extending across its width. The mechanism by which these grooves were formed is unknown. However, there is some evidence to suggest third-body abrasion since grooves corresponding to those seen on the ball are also present in the film and streaks of brown material--possibly iron oxides--can be seen on the ball surface.

The behavior of HDPE coatings is quite unique. Two obvious differences should be noted: 1. the almost perfectly circular scar; and 2. no evidence of wear debris, only permanent deformation. The circular shape of the scar implies that gross sliding did not occur at the ball-film interface. Therefore, the tangential motion must have been accommodated by elastic deformations within the film. Two possible mechanisms could explain this behavior. Measurements of scar width made from scanning electron micrographs show that the ball penetrated into the film up to 50% of the original coating thickness. The depth of penetration determines the amount of material that must be displaced by the tangential motion of the ball. Since HDPE has a relatively low shear modulus and high elongation at break, this volume of polymer film may have been sufficient to prevent gross sliding between the ball and film. Another possibility is that adhesive forces between the steel ball and coating could have been large enough to prevent gross sliding.

Since sliding between the ball and film was limited and most of the tangential displacement was taken up by deformation of the film, HDPE coatings did not show significant wear. In fact, the behavior of HDPE is essentially constant throughout a test. No polymer wear debris was seen in any of the photomacrographs or SEM micrographs, only grooves in the polymer film. The nature of these grooves is not fully understood. However, it is possible that they were formed by metallic oxide particles migrating out of the interface.

6.0 CONCLUSIONS

In this work, ten different polymer coatings were investigated as to their ability to prevent metallic contact and fretting corrosion in steel-on-steel systems. The ten polymer types were: polymethylmethacrylate (PMMA), polytetrafluoroethylene (PTFE), polyimide (PI), polyvinylidene fluoride (PVDF), polyvinylidene chloride (PVDC), low-density polyethylene (LDPE), polyvinyl chloride (PVC), polysulfone (PSO), polystyrene (PS), and high-density polyethylene (HDPE). The ten types represent a wide variety of mechanical and structural properties and were applied to 1045 steel disks in the form of thin coatings which were fretted by a 52100 steel ball.

The experiment consisted of two phases. In the first phase of experimentation, the life (which is a measure of durability) of these films was evaluated at three normal loads: 11.1, 22.3, and 44.5 N; constant sliding amplitude (300 μm); and constant frequency (20 Hz). Life data from the first phase was used to select a 22.3 N normal load for the second phase of experimentation. In the second phase, optical and scanning electron microscopy were used to study the fretting interface in detail as function of run time.

The following major conclusions can be drawn from this study:

1. The techniques and methods developed for this study were found to work satisfactorily, providing valuable information concerning polymer film wear and durability, physical changes, friction, and fretting corrosion.

2. The results of this study reveal two important requirements for a "good" film, namely (a) the film must have a long life and (b) not

cause damage to the steel countersurface.

3. Average polymer film life varies greatly with the polymer/thickness combination. For example, at 22.3 N normal load, average life can range from as low as 8 seconds for polyvinylidene chloride coatings to over one hour for polystyrene and high-density polyethylene.

4. Low-density polyethylene, polytetrafluoroethylene, polyvinylidene fluoride, polyimide and polystyrene all prevented fretting corrosion to the steel countersurface prior to film failure at 22.3 N normal load. PS films prevented fretting corrosion for one hour, after which the test was terminated and the film had not failed. The mechanism (or mechanisms) by which these films prevented steel damage is unknown. However, transfer to the steel countersurface during fretting may have played a role in the protective capabilities of PTFE, PVDF and PI. Polymethylmethacrylate and polyvinylidene chloride had such short lives that no conclusion could be made as to their ability to prevent fretting corrosion.

5. Three of the polymers studied--polyvinyl chloride, polysulfone and high-density polyethylene--were found to cause damage to the steel countersurface at 22.3 N normal load. The precise mechanism (or mechanisms) by which PVC, PSO and HDPE cause damage to the steel countersurface is unknown. However, photographic data suggests that metallic oxide particles trapped in the interface are responsible for a significant part of the damage.

6. A wide variety of physical behavior was observed with the ten polymer types. Several different types of behavior were noted, i.e., plastic flow or deformation, brittle fracture and cracking, shear in

thin layers, shear in thick layers, roll formation, transfer to the steel countersurface, and possible thermal softening or melting. Each of the films exhibited at least two types of behavior, and each behavior often did not occur in the same manner with each film. Four different patterns of "wear" scars were also observed: elliptical, circular, rhombic and rectangular. The elliptical and circular shapes occurred with the more ductile polymers--those with low modulus and long elongation at break. The rhombic and rectangular shapes were observed with the brittle polymers--those with high modulus and short elongation at break.

7. After film failure, the fretting process proceeds with gross fretting damage occurring on both contacting surfaces.

8. In general, normal load had a large effect on polymer film life. For all of the films but one (HDPE), there was a decrease in average polymer life by at least 75% as normal load was increased from 11.1 to 44.5 N. HDPE coatings had lives of over one hour at all three of the test loads.

9. A large variation of frictional behavior was also observed among the ten polymer types. For example, at 22.3 N, there was a tenfold variation in the mean final coefficient of friction prior to film failure. PTFE coatings had the lowest coefficient of friction (0.11) and PVC the highest (1.1). The coefficient of friction also increased somewhat with run time, the extent of this variation depending on the polymer/thickness combination.

10. There is no correlation between polymer film life and friction.

11. There is some evidence to support the hypothesis that for a given thickness, stronger (higher yield strength) and more rigid (higher modulus) polymer films will have a longer life, barring secondary effects such as melting or softening.

12. It would appear that the processes occurring in this fretting system--steel sphere on polymer-coated steel flat--are complex, involving a combination of physical, mechanical, thermal and chemical effects; more research is needed to understand these phenomena.

7.0 RECOMMENDATIONS

Recommendations from this work fall into two categories, namely (a) suggested changes or modifications in experimental method or apparatus and (b) possible areas for future investigation and study. These will now be presented.

1. Upgrade the current data recording system. The use of a microcomputer-based data acquisition system would make the process more efficient and developed software could ease data manipulation and analysis.

2. Modify the Mark IIIB fretting corrosion device to run five sphere-on-flat setups at one time, thus providing more data in a given period of operation.

3. Incorporating a macroscope into the Mark IIIB system would allow immediate photographic documentation of wear scars after testing without removing the ball or disk specimens from their holders. This would require some modifications to the ball-holders and would eliminate the possibility of damage to the specimens in transport to the macroscope.

4. The vibration amplitude of the moving test specimen (in this work, the steel ball) should be monitored on a continuous basis throughout the experiment as opposed to only static adjustment prior to testing.

5. The test start-up procedure (see Section 3.2.2) should be fully automated in order to eliminate variation from test to test.

6. Better and more repeatable methods need to be developed for preparing and characterizing a wide variety of polymer coated specimens.

7. Further work needs to be done on the characterization of debris generated in fretting experiments along with possible structural and chemical changes in the polymer-steel system.

8. Methods need to be developed to determine the mechanical properties (e.g., shear strength, hardness, compressive strength, etc.) of polymeric films on rigid substrates.

9. Three of the polymers studied in this investigation: polyimide, polyvinylidene fluoride and polystyrene are suggested for further study. Polyimides not only prevented fretting corrosion but had relatively long life values while being one of the thinnest films tested. Polyvinylidene fluoride, while not having very long life, also did not cause steel damage and might find an application in a more conforming geometry. Polystyrene had life values exceeding one hour for the 11.1 and 22.3 N test loads while causing no damage to the steel counterface.

10. Work should be done to study the effect of film thickness on polymer film life with a wide variety of polymer types. Obvious suggestions include those recommended for future study above.

11. Polymeric films should be evaluated under fretting conditions in a variety of contact geometries (e.g., cylinder-in-cylinder, flat-on-flat, etc.). Coating of both metal surfaces in contact should also be tried since several of the polymers in this work showed the ability to transfer to the steel countersurface while preventing fretting corrosion.

12. More types of polymeric materials need to be evaluated. A selection could be elastomers such as natural and synthetic rubbers.

13. Further work on the measurement of contact area surface temperatures applied to fretting conditions is suggested. The infrared microscope device developed by Furey (52) could be easily adapted for this work.

14. Theoretical development of the sphere (or any type of indentor) on a flat layered substrate contact problem with normal and tangentially applied loads should be investigated. The ability to calculate stresses in the layer might provide a basis for a model and would provide a means for selecting different polymer types. Both elastic and plastic behavior should be considered.

REFERENCES

1. Frantz, R. D., "An Experimental study of Fretting Corrosion at a Bearing/Cartridge Interface," Masters Thesis, Mechanical Engineering, Virginia Polytechnic Institute and State University, February 1983.

2. Furey, M. J., N. S. Eiss, Jr., and H. H. Mabie, "Fundamental Studies on the Effects of Thin Polymeric Surface Films in Reducing Fretting Corrosion and Wear," Research Proposal, U. S. Army Research Office, Mechanical Engineering Department, VPI&SU, Blacksburg, Virginia, August 1983.

3. Sweitzer, K. A., "The Effects of Thin Polymeric Surface Films on Fretting Corrosion," Masters Thesis, Mechanical Engineering, Virginia Polytechnic Institute and State University, September 1984.

4. Furey, M. J., N. S. Eiss, H. H. Mabie, and K. A. Sweitzer, "The Effects of Thin Polymeric Surface Films on Fretting Corrosion and Wear," Proceedings XIth International Conference in Organic Coatings Science and Technology, Athens, Greece, 8-12 July 1985, pp. 29-45.

5. Puzio, D., "A Study of Chlorinated Polymer Coatings in a Fretting Interface," Masters Thesis, Mechanical Engineering, Virginia Polytechnic Institute and State University, November 1985.

6. Rorrer, R. A. L., "The Effects of Load, Frequency, Slip Amplitude, Humidity and Film Thickness of Polyvinyl Chloride on Fretting Corrosion," Masters Thesis, Mechanical Engineering, Virginia Polytechnic Institute and State University, December 1985.

7. Glossary of Terms and Definitions in the Field of Friction, Wear and Lubrication--Tribology, OECD, 1969, p. 35.

8. Hurricks, P. L., "The Mechanism of Fretting - A Review," Wear, 15, 1970, pp. 387-409.

9. Waterhouse, R. B., "Fretting," Treatise on Materials, 13, 1979, pp. 259-286.

10. Tomlinson, G. A., "The Rusting of Steel Surfaces in Contact," Proceedings of the Royal Society, Series A, 115, 1927, pp. 472-486.

11. Feng, I. M., and B. G. Rightmire, "The Mechanism of Fretting," Lubrication Engineering, 9, 1953, pp. 134-136.

12. Uhlig, H. H., "Mechanism of Fretting Corrosion," Journal of Applied Mechanics, 21, 1954, pp. 401-407.

13. Johnson, K. L., and J. J. O'Connor, "Mechanics of Fretting," Proceedings, Institute of Mechanical Engineers, 178, part 3J, 1964, pp. 7-12.

14. Bethune, B., and R. B. Waterhouse, "Electro-chemical Studies of Fretting Corrosion," Wear, 12, 1968, pp. 27-34.

15. Stowers, I. F., and E. Rabinowicz, "The Mechanism of Fretting Wear," Journal of Lubrication Technology, Transactions of ASME, 95, (1), 1973, pp. 65-70.

16. Archard, J. F., "Wear Theory and Mechanisms," Wear Control Handbook, edited by M. B. Peterson and W. O. Winer, ASME, New York, NY, 1980, pp. 35-80.

17. Waterhouse, R. B., and D. E. Taylor, "Fretting Debris and the Delamination Theory of Wear," Wear, 29, 1974, pp. 337-344.

18. Suh, N. P., "The Delamination Theory of Wear," Wear, 25, 1973, pp. 111-124.

19. Waterhouse, R. B., "The Role of Adhesion and Delamination in the Fretting Wear of Metallic Materials," Wear, 45, 1973, pp. 355-364.

20. Sproles, E. S., Jr., and D. J. Duquette, "The Mechanism of Material Removal in Fretting," Wear, 49, 1978, pp. 339-352.

21. Bill, R. C., "The Role of Oxidation in the Fretting Wear Process," Wear of Materials, ASME, New York, NY, 1981, pp. 229-237.

22. Johnson and O'Connor, op. cit., pp. 7-21.

23. Ohmae, N., K. Kobayashi, and T. Tsukizo, "Characteristics of Fretting of Carbon Fibre Reinforced Plastics," Wear, 29, 1974, pp. 345-353.

24. Higham, P. A., F. H. Stott, and B. Bethune, "The Influence of Polymer Composition on the Wear of the Metal Surface During Fretting of Steel on Polymer," Wear, 47, 1978, pp. 71-80.

25. Stott, F. H., B. Bethune, and P. A. Higham, "Fretting-Induced Damage Between Contacting Steel-Polymer Surfaces," Tribology International, 10, (4), 1977, pp. 211-215.

26. Higham, P. A., B. Bethune, and F. H. Stott, "The Influence of Experimental Conditions on the Wear of the Metal Surface During Fretting of Steel on Polycarbonate," Wear, 46, 1978, pp. 335-350.

27. Higham, P. A., B. Bethune, and F. H. Stott, "Mechanisms of Wear of the Metal Surface During Fretting Corrosion of Steel on Polymer," Corrosion Science, 18, 1978, pp. 3-13.

28. Amuzu, J. K. A., B. J. Briscoe, and D. Tabor, "Friction and Shear Strength of Polymers," American Society of Lubrication Engineers, Transactions, 20, (4), 1977, pp. 354-358.

29. Briscoe, B. J. and A. C. Smith, "The Effect of Periodic Loading on the Shear Strength Properties of Thin Organic Polymeric Films," American Society of Lubrication Engineers, Transactions, 23, (3), pp. 232-236.

30. Briscoe, B. J. and A. C. Smith, "The Influence of Solvent and Thermal History on the Friction of Polymeric Films," Friction and Traction, edited by D. Dowson, Westbury House, Guildford, England, 1980, pp. 99-104.

31. Aleksandrov, V. M., "Some Contact Problems for the Elastic Layer," Physics and Mechanics of Materials, 27, (4), 1963, pp. 758-764.

32. Aleksandrov, V. M. and I. I. Vorvich, "The Action of a Die on an Elastic Layer of Finite Thickness," Physics and Mechanics of Materials, 24, (2), 1960, pp. 323-333.

33. Matthewson, M. J., "Axi-Symmetric Contact on Thin Compliant Coatings," Journal of Mechanics and Physics of Solids, 29, (2), 1981, pp. 89-113.

34. Conway, H. D. and P. A. Engel, "Contact Stresses in Slabs Due to Round Rough Indentors," International Journal of Mechanical Sciences, 11, 1969, pp. 709-722.

35. Billmeyer, F. W., Textbook of Polymer Science, John Wiley and Sons, New York, NY, 1982.

36. Plastics, Polymer Science and Technology, edited by M. D. Baijal, John Wiley and Sons, New York, NY, 1982.

37. Jones, J. W., "The Correlation of Chemical Structure to Tribological Properties of Polyimide Thin Films," Masters Thesis, Mechanical Engineering, Virginia Polytechnic Institute and State University, May 1983.

38. Modern Plastics Encyclopedia, edited by J. Agranof, 60, (10A), Oct. 1983.

39. Billmeyer, op. cit., pp. 400-403.

40. Billmeyer, op. cit., pp. 419-424.

41. Fusaro, R. L., "Tribological Properties and Thermal Stability of Various Types of Polyimide Films," NASA-TM-81765, pp. 1-23.

42. Billmeyer, op. cit., p. 412-414.

43. Billmeyer, op. cit., pp. 363-371.

44. Billmeyer, op. cit., pp. 394-399.

45. Furey, M. J., "Metallic Contact and Friction Between Sliding Surfaces," American Society of Lubrication Engineers, Transactions, 4, 1961, pp. 1-11.

46. Johnson, K. L., Contact Mechanics, Cambridge University Press, 1985, pp. 184-196.

47. Johnson, op. cit., pp. 171-179.

48. Hardy, C., C. N. Baronet, and G. V. Tordion, "Elastoplastic Indentation of a Half-Space by a Rigid Sphere," Journal of Numerical Methods in Engineering, 3, 1971, pp. 172-183.

49. Johnson, op. cit., pp. 157-160.

50. Richmond, O., H. L. Morrison, and M. L. Devenpeck, "Sphere Indentation with Application to Brinell Hardness Test," International Journal of Mechanical Sciences, 16, 1974, pp. 170-200.

51. Aharon, M., "Wear of Polymers by Roll-Formation," Wear, 25, 1973, pp. 309-327.

52. Furey, M. J., "Infrared Measurements of Surface Temperatures Produced in Tribological Processes," Proceedings, 3rd International Tribology Congress, Warsaw, Poland, September 21-24, 1981, Vol. I, pp. 118-139.

APPENDIX A

LIST OF INSTRUMENTS

1. Shaker Table

   Manufacturer: All American Tool & Mfg. Co.

   Model No.: 10-VA-T

2. Cycle Counter

   Manufacturer: Hewlett-Packard

   Model No.: 5326B

   Serial No.: 1612A03614

3. Bridge Amplifier, Test Position A

   Manufacturer: Vishay Instruments

   Model No.: Vishay/Ellis-11

   Serial No.: 032461

4. Bridge Amplifer, Test Position B

   Manufacturer: Vishay Instruments

   Model No.: Vishay/Ellis-11

   Serial No.: 032457

5. Strip Chart Recorder, Test Position A

   Manufacturer: Gould Inc.

   Model No.: 15-6327-57

   Serial No.: 15840

6. Strip Chart Recorder, Test Position B

   Manufacturer: Gould Inc.

   Model No.: 15-6327-57

   Serial No.: 15846

7. Photomacroscope

   Manufacturer: Wild Heerbrugg Ltd.

   Model No.: 420

   Serial No.: 189759

8. Scanning Electron Microscope

   Manufacturer: Amray

   Model No.: AMR-900-J3

9. Ultrasonic Cleaner

   Manufacturer: Fisher Scientific

   Model No.: B-92

   Serial No.: 0131

10. Coating Thickness Gauge

    Manufacturer: Elektro Physik

    Model No.: F102

11. Profilometer Electronic Unit

    Manufacturer: Rank Precision Industries, Ltd.

    Model No.: 112

    Serial No.: 1000-F-3113

12. Profilometer Rectilinear Recorder

    Manufacturer: Rank Precision Indsutries, Ltd.

    Model No.: 112

    Serial No.: 1005-2775

13. Profilometer Rectilinear Recorder

    Manufacturer: Rank Precision Industries, Ltd.

    Model No.: 112

    Serial No.: 1002-2436

APPENDIX B

APPLICATION OF POLYMER COATINGS

This appendix will present the various sources and methods of application for the ten polymers studied. Table B-1 summarizes the sources for the ten polymer types. As has been previously mentioned, four of the polymer types--PVDC, PVC, PSO and PS--were coated by the author at VPI&SU. The remaining six were prepared at Boyd Coatings Research in Hudson, Massachusetts. After all the surface preparation work was completed (see Section 3.1.2) the disks were heated to ca. 370°C for thirty minutes in a gas fired convection oven (in air) at Boyd Coatings. The polymers were then applied to the steel disks in the following ways:

PVDC, PVC, PSO, and PS

PVDC, PVC, PSO and PS were all coated by a solvent deposition technique at VPI&SU. This method is illustrated in Figure B-1. The disks were held by a magnetic holder and repeatedly dipped into a polymer-solvent solution. The original lay of the grind marks on the disks prior to sandblasting was oriented parallel to the surface of the polymer solution. For PVDC a 5% solution (by weight) in THF was used, each disk being dipped five times, allowing fifteen minutes between each dip. For PVC a 7% solution (by weight) in THF was used. The disks were then dipped four times, allowing fifteen minutes between each dip. PSO coatings were prepared from a 7% solution (by weight) in chloroform, each disk being dipped three times, allowing a fifteen minute interval between each dip. PS coatings were prepared from a 9% solution (by weight) in chloroform. The disks were dipped two times with fifteen minutes between each dip. After coating, each of the polymer-coated disks was placed in vacuum for twenty-four hours.

TABLE B-1 Polymer Types and Sources

Polymer Type	Source
PMMA	VPI&SU[a]
PTFE	DuPont Water Dispersion[a]
PI	DuPont Pyre-MLRK-692 and Normal Pyrollidone[a] Formulation
PVDF	DuPont
PVDC	Dow Chemical Type F-278 Resin
LDPE	VPI&SU, Dr. D. G. Baird (Chem. Eng.)
PVC	B. F. Goodrich Company (70,000 MW)
PSO	VPI&SU, Dr. J. E. McGrath (Chemistry)
PS	VPI&SU, Dr. T. C. Ward (Chemistry)
HDPE	VPI&SU, Dr. T. C. Ward (Chemistry)

[a]Information obtained from personal conversation with Dr. Pedro Diaz, Boyd Coatings Research Incorporated.

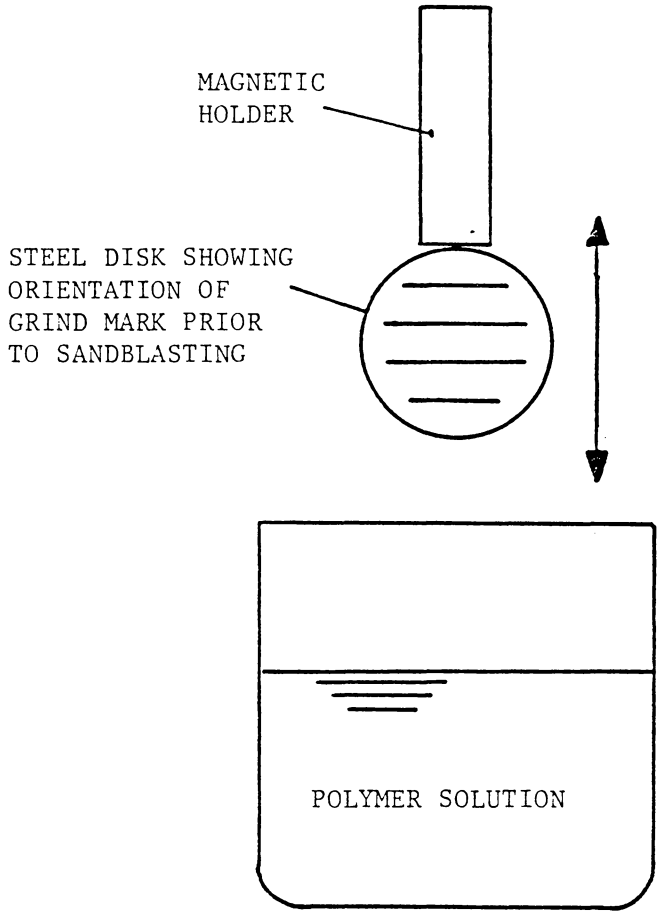

FIGURE B-1. Solvent Deposition Method Used at VPI&SU.

The coated disks were then stored in a desiccator until they were used in fretting experiments.

PMMA and PI

PMMA and PI films were solvent cast at Boyd Coatings. PMMA was dissolved in MEK and then sprayed on the steel disks. The PMMA coated disks were then heated (in air) to ca. 150°C for fifteen minutes. PI films were also sprayed, using a polymer solution formulated by DuPont (see Table B-1). The PI coated disks were then baked at ca. 315°C for fifteen minutes in air.

PTFE

PTFE coatings were prepared (at Boyd Coatings) from a water dispersion obtained from DuPont. After coating, the disks were heated to ca. 330°C for fifteen minutes in air.

PVDF, LDPE, and HDPE

PVDF, LDPE and HDPE films were all prepared by electrostatic powder deposition at Boyd Coatings. After deposition, all three coatings were heated in air. PVDF coatings were heated to ca. 260°C for five minutes in air. LDPE and HDPE coatings were heated to ca. 150°C for five minutes in air.

APPENDIX C

POLYMER COATING THICKNESS DATA

TABLE C-1 PMMA Coating Thicknesses

Specimen #	Thickness Measurements (μm) 1	2	3	4	5	Mean
1	7.11	7.11	6.86	6.35	6.60	6.81
2	6.60	6.60	7.37	7.11	7.11	6.96
3	7.11	7.62	8.13	6.10	6.10	7.01
6	7.11	7.62	8.13	6.60	7.87	7.47

Mean of all Measurements: 7.06 μm
Range of all Measurements: 6.10-8.13 μm

TABLE C-2 PTFE Coating Thicknesses

Specimen #	Thickness Measurements (μm) 1	2	3	4	5	Mean
1	10.2	9.91	9.91	10.2	9.65	9.97
2	9.65	9.14	10.9	12.7	9.14	10.3
3	9.65	10.2	10.4	9.65	10.2	10.0
4	9.91	12.7	9.65	8.64	9.14	10.0

Mean of all Measurements: 10.1 μm
Range of all Measurements: 8.64-12.7 μm

TABLE C-3 PI Coating Thicknesses

Specimen #	Thickness Measurements (μm) 1	2	3	4	5	Mean
1	11.4	10.9	11.9	12.7	11.9	11.8
2	12.2	11.7	11.7	11.4	12.2	11.8
3	10.9	12.2	11.7	11.4	10.9	11.4
4	10.9	12.2	11.7	11.4	10.9	11.4

Mean of all Measurements: 11.6 μm
Range of all Measurements: 10.9-12.2 μm

TABLE C-4 PVDF Coating Thicknesses

Specimen #	Thickness Measurements (μm) 1	2	3	4	5	Mean
1	30.5	27.9	30.5	30.5	30.5	30.0
2	27.9	21.6	25.4	25.4	27.9	25.6
3	22.9	20.3	21.6	20.3	24.1	21.8
4	25.4	22.9	21.6	24.1	25.4	23.9

Mean of all Measurements: 25.3 μm
Range of all Measurements: 20.3-30.5 μm

TABLE C-5 PVDC Coating Thickness Measurements

Specimen #	Thickness Measurements (μm) 1	2	3	4	5	Mean
1	26.7	33.0	29.2	27.9	29.2	29.2
2	22.9	26.7	25.4	25.4	29.2	25.9
3	22.9	30.5	22.9	31.8	27.9	27.2
4	25.4	27.9	26.7	27.9	26.7	26.9

Mean of all Measurements: 27.3 μm
Range of all Measurements: 22.9-33.0 μm

TABLE C-6 LDPE Coating Thicknesses

Specimen #	Thickness Measurements (μm) 1	2	3	4	5	Mean
2	40.6	40.6	45.7	58.4	33.0	43.6
3	43.2	50.8	55.9	43.2	55.9	49.8
4	63.5	45.7	33.0	40.6	45.7	45.7
7	55.9	48.3	38.1	48.3	44.5	47.0

Mean of all Measurements: 46.5 μm
Range of all Measurements: 33.0-63.5 μm

TABLE C-7 PVC Coating Thicknesses

Specimen #	Thickness Measurements (μm) 1	2	3	4	5	Mean
1	50.8	58.4	57.2	57.2	57.2	56.2
2	59.7	58.4	58.4	53.3	57.2	57.4
3	69.9	71.1	66.0	63.5	63.5	66.8
4	58.4	59.7	58.4	61.0	61.0	59.7

Mean of all Measurements: 60.0 μm
Range of all Measurements: 50.8-71.1 μm

TABLE C-8 PSO Coating Thicknesses

Specimen #	Thickness Measurements (μm) 1	2	3	4	5	Mean
1	61.0	63.5	61.0	61.0	63.5	62.0
2	61.0	66.0	66.0	62.2	67.3	64.5
3	61.0	62.2	61.0	61.0	61.0	61.2
4	61.0	62.2	66.0	63.5	61.0	62.7

Mean of all Measurements: 62.6 μm
Range of all Measurements: 61.0-67.3 μm

TABLE C-9 PS Coating Thicknesses

Specimen #	Thickness Measurement (μm) 1	2	3	4	5	Mean
1	85.1	85.6	85.1	82.6	86.4	85.0
2	86.4	88.9	82.6	81.3	82.6	84.4
3	82.6	85.1	86.4	82.6	87.6	84.9
4	85.1	91.4	91.4	90.2	90.2	89.7

Mean of all Measurements: 86.0 μm
Range of all Measurements: 81.3-91.4 μm

TABLE C-10 HDPE Coating Thicknesses

Specimen #	Thickness Measurement (μm) 1	2	3	4	5	Mean
1	119.4	132.1	121.9	121.9	121.9	123.4
2	111.8	114.3	109.2	101.6	99.1	107.2
3	116.8	106.7	99.1	111.8	104.1	107.7
4	106.7	104.1	111.8	104.1	116.8	108.7

Mean of all Measurements: 111.8 μm
Range of all Measurements: 99.1-132.1 μm

APPENDIX D

POLYMER COATING LIFE DATA

TABLE D-1 Test Run Dates

Polymer	Date	Tdb(°C)	R.H.(%)	Specimen #	Test #	Position	Load(N)
PMMA	7/25/85	21.7	54.1	1	1	A	11.1
PMMA	7/25/85	21.7	54.1	2	1	B	11.1
PMMA	7/31/85	21.5	54.0	1	2	A	11.1
PMMA	7/31/85	21.5	54.0	2	2	B	11.1
PMMA	7/25/85	21.7	54.1	1	1	A	22.3
PMMA	7/25/85	21.7	54.1	2	1	B	22.3
PMMA	7/27/85	21.6	60.1	3	2	A	22.3
PMMA	7/27/85	21.6	60.1	6	2	B	22.3
PMMA	7/27/85	21.6	60.1	3	3	A	22.3
PMMA	7/27/85	21.6	60.1	6	3	B	22.3
PMMA	7/27/85	21.6	60.1	3	4	A	22.3
PMMA	7/27/85	21.6	60.1	6	4	B	22.3
PMMA	7/25/85	21.7	54.1	1	1	A	44.5
PMMA	7/25/85	21.7	54.1	2	1	B	44.5
PMMA	7/25/85	21.7	54.1	1	2	A	44.5
PMMA	7/25/85	21.7	54.1	2	2	B	44.5
PTFE	7/24/85	21.9	51.7	3	1	A	11.1
PTFE	7/31/85	21.9	51.7	4	1	B	11.1
PTFE	7/31/85	21.6	51.6	3	2	A	11.1
PTFE	7/31/85	21.6	51.6	4	2	B	11.1
PTFE	7/24/85	21.9	52.0	3	1	A	22.3
PTFE	7/24/85	21.9	52.0	4	1	B	22.3
PTFE	7/27/85	21.7	61.4	1	2	A	22.3
PTFE	7/27/85	21.7	61.4	2	2	B	22.3
PTFE	7/27/85	21.7	61.4	1	3	A	22.3
PTFE	7/27/85	21.7	61.4	2	3	B	22.3
PTFE	7/27/85	21.7	61.4	1	4	A	22.3
PTFE	7/27/85	21.7	61.4	2	4	B	22.3
PTFE	7/24/85	21.8	52.9	3	1	A	44.5
PTFE	7/24/85	21.8	52.9	4	1	B	44.5
PTFE	7/31/85	21.6	52.1	3	2	A	44.5
PTFE	7/31/85	21.6	52.1	4	2	B	44.5

TABLE D-1 (Continued)

Polymer	Date	Tdb(°C)	R.H.(%)	Specimen #	Test #	Position	Load(N)
PI	7/24/85	21.3	54.7	1	1	A	11.1
PI	7/24/85	21.3	54.7	2	1	B	11.1
PI	7/31/85	21.5	53.1	1	2	A	11.1
PI	7/31/85	21.5	53.1	2	2	B	11.1
PI	7/24/85	22.1	52.7	1	1	A	22.3
PI	7/24/85	22.1	52.7	2	1	B	22.3
PI	7/27/85	21.7	61.4	3	2	A	22.3
PI	7/27/85	21.7	61.4	4	2	B	22.3
PI	7/27/85	21.7	61.4	3	3	A	22.3
PI	7/27/85	21.7	61.4	4	3	B	22.3
PI	7/27/85	21.5	60.4	3	4	A	22.3
PI	7/27/85	21.5	60.4	4	4	B	22.3
PI	7/25/85	21.5	54.1	1	1	A	44.5
PI	7/25/85	21.5	54.1	2	1	B	44.5
PI	7/31/85	21.5	53.1	1	2	A	44.5
PI	7/31/85	21.5	53.1	2	2	B	44.5
PVDF	7/24/85	21.2	53.2	1	1	A	11.1
PVDF	7/24/85	21.2	53.2	2	1	B	11.1
PVDF	7/30/85	22.4	53.1	1	2	A	11.1
PVDF	7/30/85	22.4	53.1	2	2	B	11.1
PVDF	7/24/85	21.7	49.6	1	1	A	22.3
PVDF	7/24/85	21.7	49.6	2	1	B	22.3
PVDF	7/27/85	21.5	60.4	3	2	A	22.3
PVDF	7/27/85	21.5	60.4	4	2	B	22.3
PVDF	7/27/85	21.6	60.4	3	3	A	22.3
PVDF	7/27/85	21.6	60.4	4	3	B	22.3
PVDF	7/27/85	21.6	60.4	3	4	A	22.3
PVDF	7/27/85	21.6	60.4	4	4	B	22.3
PVDF	7/24/85	22.3	51.9	1	1	A	44.5
PVDF	7/24/85	22.3	51.9	2	1	B	44.5
PVDF	7/31/85	22.5	52.8	1	2	A	44.5
PVDF	7/31/85	22.5	52.8	2	2	B	44.5

TABLE D-1 (Continued)

Polymer	Date	Tdb(°C)	R.H.(%)	Specimen #	Test #	Position	Load(N)
PVDC	8/16/85	21.9	56.7	1	1	A	11.1
PVDC	8/16/85	21.9	56.7	4	1	B	11.1
PVDC	8/16/85	21.9	56/7	1	2	A	11.1
PVDC	8/16/85	21.9	56.7	4	2	B	11.1
PVDC	8/16/85	21.9	56.7	1	1	A	22.3
PVDC	8/16/85	21.9	56.7	4	1	B	22.3
PVDC	8/16/85	21.6	54.1	2	2	A	22.3
PVDC	8/16/85	21.6	54.1	3	2	B	22.3
PVDC	8/16/85	21.6	54.1	2	3	A	22.3
PVDC	8/16/85	21.6	54.1	3	3	B	22.3
PVDC	8/16/85	21.6	54.1	2	4	A	22.3
PVDC	8/16/85	21.6	54.1	3	4	B	22.3
PVDC	8/16/85	21.7	54.0	1	1	A	44.5
PVDC	8/16/85	21.7	54.0	4	1	B	44.5
PVDC	8/16/85	21.7	54.0	1	2	A	44.5
PVDC	8/16/85	21.7	54.0	4	2	B	44.5
LDPE	7/24/85	22.0	54.4	3	1	A	11.1
LDPE	7/24/85	22.0	54.4	7	1	B	11.1
LDPE	7/31/85	21.6	54.0	3	2	A	11.1
LDPE	7/31/85	21.6	54.0	7	2	B	11.1
LDPE	7/24/85	22.2	54.3	3	1	A	22.3
LDPE	7/24/85	22.2	54.3	7	1	B	22.3
LDPE	7/27/85	21.6	60.6	2	2	A	22.3
LDPE	7/24/85	21.6	60.6	4	2	B	22.3
LDPE	7/27/85	21.6	60.6	2	3	A	22.3
LDPE	7/24/85	21.6	60.6	4	3	B	22.3
LDPE	7/27/85	21.6	60.6	2	4	A	22.3
LDPE	7/24/85	21.6	60.6	4	4	B	22.3
LDPE	7/25/85	21.9	55.3	3	1	A	44.5
LDPE	7/25/85	21.9	55.3	7	1	B	44.5
LDPE	7/31/85	21.6	54.0	3	2	A	44.5
LDPE	7/31/85	21.6	54.0	7	2	B	44.5

TABLE D-1 (Continued)

Polymer	Date	Tdb(°C)	R.H.(%)	Specimen #	Test #	Position	Load(N)
PVC	7/24/85	21.6	56.9	1	1	A	11.1
PVC	7/24/85	21.6	56.9	2	1	B	11.1
PVC	7/30/85	22.3	56.9	1	2	A	11.1
PVC	7/30/85	22.3	56.9	2	2	B	11.1
PVC	7/24/85	22.2	52.8	1	1	A	22.3
PVC	7/24/85	22.2	52.8	2	1	B	22.3
PVC	7/27/85	21.8	59.2	3	2	A	22.3
PVC	7/27/85	21.8	59.2	4	2	B	22.3
PVC	7/27/85	21.6	62.1	3	3	A	22.3
PVC	7/27/85	21.6	62.1	4	3	B	22.3
PVC	7/27/85	21.8	59.2	3	4	A	22.3
PVC	7/27/85	21.8	59.2	4	4	B	22.3
PVC	7/25/85	21.7	54.1	1	1	A	44.5
PVC	7/25/85	21.7	54.1	2	1	B	44.5
PVC	7/30/85	22.5	53.1	1	2	A	44.5
PVC	7/30/85	22.5	53.1	2	2	B	44.5
PSO	8/13/85	21.7	61.0	1	1	A	11.1
PSO	8/13/85	21.7	61.0	2	1	B	11.1
PSO	8/13/85	21.8	59.6	1	1	A	22.3
PSO	8/13/85	21.8	59.6	2	1	B	22.3
PSO	8/13/85	21.7	60.6	3	2	A	22.3
PSO	8/13/85	21.7	60.6	4	2	B	22.3
PSO	8/13/85	21.7	59.8	3	3	A	22.3
PSO	8/13/85	21.7	59.8	4	3	B	22.3
PSO	8/13/85	21.7	59.8	3	4	A	22.3
PSO	8/13/85	21.7	59.8	4	4	B	22.3
PSO	8/13/85	21.8	58.8	1	1	A	44.5
PSO	8/13/85	21.8	58.8	2	1	B	44.5
PSO	8/13/85	21.8	58.8	1	2	A	44.5
PSO	8/13/85	21.8	58.8	2	2	B	44.5

TABLE D-1 (Continued)

Polymer	Date	Tdb(^{o}C)	R.H.(%)	Specimen #	Test #	Position	Load(N)
PS	8/10/85	21.3	60.0	1	1	A	11.1
PS	8/10/85	21.3	60.0	3	1	B	11.1
PS	8/10/85	21.6	59.0	1	1	A	22.3
PS	8/10/85	21.6	59.0	3	1	B	22.3
PS	8/13/85	21.9	59.4	2	2	A	22.3
PS	8/13/85	21.9	59.4	4	2	B	22.3
PS	8/13/85	21.7	59.6	2	3	A	22.3
PS	8/13/85	21.7	59.6	4	3	B	22.3
PS	8/13/85	21.6	58.7	2	4	A	22.3
PS	8/13/85	21.6	58.7	4	4	B	22.3
PS	8/13/85	21.8	58.8	1	1	A	44.5
PS	8/13/85	21.8	58.8	3	1	B	44.5
PS	8/13/85	21.8	58.8	1	2	A	44.5
PS	8/13/85	21.8	58.8	3	2	B	44.5
HDPE	7/25/85	22.0	55.7	2	1	A	11.1
HDPE	7/25/85	22.0	55.7	3	1	B	11.1
HDPE	7/25/85	21.4	54.2	2	1	A	22.3
HDPE	7/25/85	21.4	54.2	3	1	B	22.3
HDPE	7/27/85	21.5	60.6	1	2	A	22.3
HDPE	7/27/85	21.5	60.6	4	2	B	22.3
HDPE	7/27/85	21.6	60.4	1	3	A	22.3
HDPE	7/27/85	21.6	60.4	4	3	B	22.3
HDPE	7/27/85	21.4	60.5	1	4	A	22.3
HDPE	7/27/85	21.4	60.5	4	4	B	22.3
HDPE	7/25/85	22.7	53.1	2	1	A	44.5
HDPE	7/25/85	22.7	53.1	3	1	B	44.5

TABLE D-2 Polymer Life Data at 11.1 N
(sec)

Polymer	Test #1 Test Position A	Test #1 Test Position B	Test #2 Test Position A	Test #2 Test Position B
PMMA	5	110	0	188
PTFE	219	174	364	171
PI	2071	3149	2573	2862
PVDF	1857	983	2069	1551
PVDC	1284	1848	1020	1164
LDPE	156	71	171	155
PVC	>3600	>3600	>3600	>3600
PSO	>3600	>3600	----	----
PS	>3600	>3600	----	----
HDPE	>3600	>3600	----	----

TABLE D-2 (Continued)

Polymer	Average Life	95% Confidence Range		
PMMA	76	0	-	220
PTFE	232	88	-	376
PI	2664	1932	-	3395
PVDF	1615	864	-	2366
PVDC	1329	752	-	1906
LDPE	138	66	-	211
PVC	>3600		----	
PSO	>3600		----	
PS	>3600		----	
HDPE	>3600		----	

TABLE D-3 Polymer Life Data at 22.3 N
(sec)

Polymer	Test #1 Test Position A	Test #1 Test Position B	Test #2 Test Position A	Test #2 Test Position B
PMMA	0	19	0	0
PTFE	95	50	140	123
PI	2784	1764	768	422
PVDF	587	189	202	325
PVDC	12	12	1	12
LDPE	90	86	32	36
PVC	1188	1721	1478	463
PSO	2364	1368	2328	----
PS	>3600	>3600	----	----
HDPE	>3600	>3600	----	----

TABLE D-3 (Continued)

Polymer	Test #3 Test Position A	Test #3 Test Position B	Test #4 Test Position A	Test #4 Test Position B
PMMA	31	9	33	----
PTFE	33	43	----	----
PI	631	1092	1101	----
PVDF	321	221	----	----
PVDC	4	5	----	----
LDPE	28	20	30	----
PVC	----	----	----	----
PSO	----	----	----	----
PS	----	----	----	----
HDPE	----	----	----	----

TABLE D-3 (Continued)

Polymer	Average Life	95% Confidence Range		
PMMA	15	1	-	28
PTFE	81	33	-	128
PI	1223	472	-	1975
PVDF	308	151	-	464
PVDC	8	3	-	13
LDPE	46	19	-	73
PVC	1212	345	-	2080
PSO	2020	616	-	3424
PS	>3600			----
HDPE	>3600		----	

TABLE D-4 Polymer Life Data at 44.5 N
(sec)

Polymer	Test #1 Test Position A	Test #1 Test Position B	Test #2 Test Position A	Test #2 Test Position B
PMMA	0	8	5	1
PTFE	13	16	8	17
PI	302	316	162	375
PVDF	104	57	84	43
PVDC	0	12	6	12
LDPE	32	39	28	42
PVC	14	15	25	18
PSO	12	24	12	12
PS	312	186	180	240
HDPE	>3600	>3600	----	----

TABLE D-4 (Continued)

Polymer	Average Life	95% Confidence Range		
PMMA	4	0	-	9
PTFE	14	7	-	20
PI	289	145	-	432
PVDF	72	29	-	115
PVDC	8	0	-	17
LDPE	35	25	-	45
PVC	18	10	-	26
PSO	15	5	-	25
PS	230	132	-	327
HDPE	>3600		----	

APPENDIX E

FRICTION DATA

TABLE E-1 Initial Coefficient of Friction Prior to Film Failure at 11.1 N

Polymer	Test #1 Test Position A	Test #1 Test Position B	Test #2 Test Position A	Test #2 Test Position B
PMMA	----	0.64	0.56	0.56
PTFE	0.16	0.08	0.12	0.12
PI	0.16	0.32	0.32	0.24
PVDF	0.27	0.27	0.24	0.24
PVDC	0.72	0.40	0.64	0.56
LDPE	0.32	0.32	0.32	0.24
PVC	0.53	0.53	0.72	0.56
PSO	0.40	0.56	----	----
PS	0.75	0.72	----	----
HDPE	0.27	0.27	----	----

TABLE E-1 (Continued)

Polymer	Mean	95% Confidence Range		
PMMA	0.61	0.50	-	0.73
PTFE	0.12	0.068	-	0.17
PI	0.26	0.14	-	0.38
PVDF	0.26	0.24	-	0.36
PVDC	0.58	0.36	-	0.80
LDPE	0.30	0.24	-	0.36
PVC	0.59	0.44	-	0.73
PSO	0.48	0.0	-	1.5
PS	0.74	0.54	-	0.93
HDPE	0.27	0.27	-	0.27

TABLE E-2 Initial Coefficent of Friction Prior to Film Failure at 22.3 N

Polymer	Test #1 Test Position A	Test #1 Test Position B	Test #2 Test Position A	Test #2 Test Position B
PMMA	----	0.48	0.48	0.56
PTFE	0.11	0.11	0.11	0.11
PI	0.40	0.40	0.27	0.27
PVDF	0.27	0.37	0.27	0.29
PVDC	0.96	0.80	0.48	0.35
LDPE	0.26	0.21	0.21	0.27
PVC	0.80	0.80	0.51	0.51
PSO	0.88	0.76	0.53	0.53
PS	0.88	0.60	0.53	0.48
HDPE	0.21	0.21	----	----

TABLE E-2 (Continued)

Polymer	Mean	95% Confidence Range		
PMMA	0.51	0.39	-	0.62
PTFE	0.11	0.11	-	0.11
PI	0.34	0.22	-	0.45
PVDF	0.30	0.22	-	0.37
PVDC	0.65	0.20	-	1.1
LDPE	0.24	0.19	-	0.29
PVC	0.66	0.39	-	0.92
PSO	0.68	0.40	-	0.95
PS	0.51	0.34	-	0.91
HDPE	0.21	0.21	-	0.21

TABLE E-3 Initial Coefficient of Friction Prior to Film Failure at 44.5 N

Polymer	Test #1 Test Position A	Test #1 Test Position B	Test #2 Test Position A	Test #2 Test Position B
PMMA	----	0.25	0.40	0.40
PTFE	0.08	0.06	0.08	0.08
PI	0.25	0.19	0.24	0.20
PVDF	0.24	0.21	0.22	0.28
PVDC	0.70	0.60	0.44	0.46
LDPE	0.24	0.27	0.28	0.24
PVC	0.44	0.50	0.36	0.36
PSO	1.0	1.0	0.8	0.82
PS	0.66	0.62	0.84	0.74
HDPE	0.17	0.24	----	----

TABLE E-3 (Continued)

Polymer	Mean	95% Confidence Range		
PMMA	0.61	0.13	-	0.57
PTFE	0.51	0.06	-	0.09
PI	0.22	0.17	-	0.27
PVDF	0.24	0.18	-	0.29
PVDC	0.55	0.35	-	0.75
LDPE	0.26	0.22	-	0.29
PVC	0.42	0.31	-	0.52
PSO	0.91	0.73	-	1.1
PS	0.72	0.56	-	0.87
HDPE	0.21	0.0	-	0.65

TABLE E-4 Final Coefficient of Friction Prior to Film Failure at 11.1 N

Polymer	Test #1 Test Position A	Test #1 Test Position B	Test #2 Test Position A	Test #2 Test Position B
PMMA	0.72	0.88	---	0.96
PTFE	0.16	0.12	0.12	0.12
PI	0.80	0.74	0.88	0.72
PVDF	0.69	0.64	0.72	0.56
PVDC	1.28	1.12	1.12	0.88
LDPE	0.48	0.48	0.43	0.48
PVC	1.17	1.28	1.20	1.04
PSO	1.28	1.20	---	---
PS	1.05	0.96	---	---
HDPE	0.27	0.27	---	---

TABLE E-4 (Continued)

Polymer	Mean	95% Confidence Range
PMMA	0.85	0.55 - 1.2
PTFE	0.13	0.10 - 0.16
PI	0.79	0.67 - 0.90
PVDF	0.65	0.54 - 0.76
PVDC	1.1	0.84 - 1.4
LDPE	0.47	0.43 - 0.51
PVC	1.2	1.0 - 1.3
PSO	1.2	0.73 - 1.7
PS	1.0	0.43 - 1.6
HDPE	0.27	0.27 - 0.27

TABLE E-5 Final Coefficient of Friction Prior to Film Failure at 22.3 N

Polymer	Test #1 Test Position A	Test #1 Test Position B	Test #2 Test Position A	Test #2 Test Position B
PMMA	---	0.53	0.67	0.83
PTFE	0.11	0.11	0.11	0.11
PI	0.61	0.83	0.83	0.75
PVDF	0.56	0.43	0.53	0.51
PVDC	0.96	0.80	0.59	0.53
LDPE	0.37	0.32	0.32	0.43
PVC	1.12	1.08	1.07	1.15
PSO	0.96	0.92	0.69	0.67
PS	0.99	0.88	0.64	0.64
HDPE	0.21	0.21	----	-----

TABLE E-5 (Continued)

Polymer	Mean	95% Confidence Range
PMMA	0.68	0.30 - 1.0
PTFE	0.11	0.11 - 0.11
PI	0.79	0.58 - 0.96
PVDF	0.65	0.42 - 0.60
PVDC	1.1	0.41 - 1.0
LDPE	0.47	0.28 - 0.44
PVC	1.1	1.0 - 1.2
PSO	0.81	0.57 - 1.1
PS	0.79	0.51 - 1.1
HDPE	0.21	0.21 - 0.21

TABLE E-6 Final Coefficient of Friction Prior to Film Failure at 44.5 N

Polymer	Test #1 Test Position A	Test #1 Test Position B	Test #2 Test Position A	Test #2 Test Position B
PMMA	----	0.56	0.52	0.40
PTFE	0.10	0.06	0.12	0.16
PI	0.50	0.50	0.52	0.52
PVDF	0.45	0.45	0.48	0.40
PVDC	0.70	0.60	0.62	0.56
LDPE	0.39	0.37	0.44	0.34
PVC	0.89	0.94	0.86	0.72
PSO	1.0	1.0	0.80	0.72
PS	0.92	0.90	0.92	0.86
HDPE	0.17	0.24	----	----

TABLE E-6 (Continued)

Polymer	Mean	95% Confidence Range		
PMMA	0.49	0.27	-	0.70
PTFE	0.11	0.044	-	0.18
PI	0.51	0.49	-	0.53
PVDF	0.45	0.39	-	0.50
PVDC	0.62	0.53	-	0.71
LDPE	0.39	0.32	-	0.45
PVC	0.85	0.70	-	1.0
PSO	0.91	0.73	-	1.1
PS	0.90	0.86	-	0.94
HDPE	0.21	0.0	-	0.65

APPENDIX F

STATISTICAL ANALYSIS OF LIFE DATA

TABLE F-1 ANOVA Table for One-Way Classification of PMMA Life Means at 11.1, 22.3 and 44.5 N

Source	Sum of Squares	D.O.F.	Mean Square	Ftest
Between Sample	12783.5	2	50778.2	3.0
Within Sample	25843.4	12	2153.6	
Totals	38626.9	14		

TABLE F-2 ANOVA Table for One-Way Classification of PTFE Life Means at 11.1, 22.3 and 44.5 N

Source	Sum of Squares	D.O.F.	Mean Square	Ftest
Between Sample	101556.0	2	50778.2	16.0
Within Sample	34876.2	11	3179.6	
Totals	136433.0	13		

TABLE F-3 ANOVA Table for One-Way Classification of PI Life Means at 11.1, 22.3 and 44.5 N

Source	Sum of Squares	D.O.F.	Mean Square	Ftest
Between Sample	1.152 E+07	2	5.76 E+06	15.0
Within Sample	4.619 E+06	12	3848948.0	
Totals	1.614 E+07	14		

TABLE F-4 ANOVA Table for One-Way Classification of PVDF Life Means at 11.1, 22.3 and 44.5 N

Source	Sum of Squares	D.O.F.	Mean Square	Ftest
Between Sample	5.747 E+06	2	2.873 E+06	40.4
Within Sample	781702.0	11	71063.8	
Totals	6.528 E+06	13		

TABLE F-5 ANOVA Table for One-Way Classification of PVDC Life Means at 11.1, 22.3 and 44.5 N

Source	Sum of Squares	D.O.F.	Mean Square	Ftest
Between Sample	4.989 E+06	2	2.494 E+06	69.6
Within Sample	394317.0	11	35847.0	
Totals	5.383 E+06	13		

TABLE F-6 ANOVA Table for One-Way Classification of LDPE Life Means at 11.1, 22.3 and 44.5 N

Source	Sum of Squares	D.O.F.	Mean Square	Ftest
Between Sample	27417.4	2	13708.7	14.4
Within Sample	11401.5	12	950.1	
Totals	38818.9	14		

TABLE F-7 ANOVA Table for One-Way Classification of PMMA Life Means at 11.1, 22.3 and 44.5 N (LOG DATA)[a]

Source	Sum of Squares	D.O.F.	Mean Square	Ftest
Between Sample	8.59	2	4.30	0.52
Within Sample	100.1	12	8.34	
Totals	108.7	14		

[a]Natural Logarithm of Life Data Taken Prior to Analysis.

TABLE F-8 ANOVA Table for One-Way Classification of PTFE Life Means at 11.1, 22.3 and 44.5 N (LOG DATA)[a]

Source	Sum of Squares	D.O.F.	Mean Square	Ftest
Between Sample	16.31	2	8.15	35.45
Within Sample	2.53	11	0.23	
Totals	18.84	13		

[a]Natural Logarithm of Life Data Taken Prior to Analysis.

TABLE F-9 ANOVA Table for One-Way Classification of PI Life Means at 11.1, 22.3 and 44.5 N (LOG DATA)[a]

Source	Sum of Squares	D.O.F.	Mean Square	Ftest
Between Sample	10.30	2	5.15	21.2
Within Sample	2.91	12	0.24	
Totals	13.21	14		

[a]Natural Logarithm of Life Data Taken Prior to Analysis

TABLE F-10 ANOVA Table for One-Way Classification of LDPE Life Means at 11.1, 22.3 and 44.5 N (LOG DATA)[a]

Source	Sum of Squares	D.O.F.	Mean Square	Ftest
Between Sample	4.58	2	2.29	10.57
Within Sample	2.60	12	0.22	
Totals	7.18	14		

[a]Natural Logarithm of Life Data Taken Prior to Analysis

TABLE F-11 T-Test of 22.3 N and 44.5 N Life Data for PVC

Source	Mean	Variance	D.O.F.	Pooled Variance	Ttest
22.3 Life	1212.0	297141.0	4	385.5	4.38
44.5 Life	18.0	24.6	4		

TABLE F-12 T-Test of 22.3 N and 44.5 N Life Data for PSO

Source	Mean	Variance	D.O.F.	Pooled Variance	Ttest
22.25 Life	2020.0	319152.0	3	357.0	7.35
44.50 Life	15.0	36.0	4		

TABLE F-13 Summary of ANOVA and TTEST Results of Life Data
(95% Confidence Limit)

Polymer	ANOVA	ANOVA-LOG	TTEST	Result
PMMA	N	N	----	N
PTFE	N	Y	----	Y
PI	N	Y	----	Y
PVDF	Y	----	----	Y
PVDC	Y	----	----	Y
LDPE	N	N	----	N
PVC	----	----	Y	Y
PSO	----	----	Y	Y
PS	----	----	----	----
HDPE	----	----	----	----

N: No significant decrease in polymer film life.

Y: Significant decrease in polymer film life.

The vita has been removed from the scanned document